A Nonholonomic Parallel Mechanism and Body Motion-Based Leader-Follower Operation Methods for Mobile Manipulators

YAO QIANG

2023

Doctoral Thesis

A Nonholonomic Parallel Mechanism and Body Motion-Based Leader-Follower Operation Methods for Mobile Manipulators

YAO QIANG

Department of Mechanical Engineering and Science
Graduate School of Engineering, Kyoto University

A Thesis submitted for the degree of
Doctor of Engineering

2023

Acknowledgment

First of all, I would like to express my sincere gratitude to my supervisor, Professor Dr. Masaharu Komori, for his professional guidance and invaluable instructions. He not only helped me carry out the research, but also inspired my academic thinking of robotics, mechatronics, and ergonomics. Also, my hearty appreciations go to Assistant Professor Dr. Tatsuro Terakawa, whose suggestions and encouragement have given me much insight into this research. I cannot imagine how to achieve the degree of doctor without their supporting and supervising.

My warm gratitude should also go to all faculty members of the Department of Mechanical Engineering and Science, Kyoto University, especially Professor Fumitoshi Matsuno and Professor Atsushi Matsubara, for their comments and instructions during the thesis review. They gave me substantial supports and helped me to improve the academic value of this thesis.

I am deeply grateful to all the members of the Mechanism and Motion Engineering Laboratory, Kyoto University. Assistant Professor Tetsuya Nonaka offered me much advice of research and daily life. This thesis owes a debt to the coauthors, Mr. Yuya Morita, Mr. Hirotaka Fujita, Mr. Ikko Yasuda, Mr. Riku Higashide, and Mr. Toshiki Watanabe who helped me construct the experimental setup and complete the experiments. I would like to thank all the students in this laboratory for giving me a perfect laboratory life full of fun and surprise.

No words can express the full measure of my gratitude to my family and friends. I owe my father and mother the greatest debt of thankfulness. Without their love and care, I would never be able to come to Kyoto University and finish my doctor program. This thesis is dedicated to all the people who love me and whom I love.

"A gentleman is not a utensil (君子は器ならず)." The degree of doctor proves my achievements in a small domain, and also encourages me to explore a larger world in the future.

Abbreviations and Acronyms

Abbreviations & Acronyms	Specifications
2WD	Two-Wheeled Drive
CI	Confidence Interval
CP	Center Point
DOF	Degree Of Freedom
EOM	Equation Of Motion
FSPP	Four-Step Path Planning
IRH	Imaginary Robotic Hand
LEM	Lead Elongation Mechanism
MPM	Mobile Parallel Manipulator
MSM	Mobile Serial Manipulator
ROM	Range Of Motion
SLPTM	Single-Loop Parallel Transmission Mechanism
TP	Teaching Pendant
VAS	Visual Analogue Scale
VEMOPAM	VErsatile MObile PArallel Manipulator
VOS	Virtual Operation Space

Notations and Symbols

Notations & Symbols	Specifications	Units
c	Motion scale of operator's hand to IRH (constant)	
G	A matrix representing nonholonomic constraints	
i	$i = 1, 2$ represents carts A1 and A2 of VEMOPAM	
J	Jacobian matrix of VEMOPAM	
K_x, K_y, K_ϕ	Constants in Kanayama's control rule	
K_p, K_i	Gains of proportional-integral controller used in A1 and A2	
l_1, l_2, l_3, l_s	Lengths of linkages used in VEMOPAM	[mm]
l_{s1}	Value of l_s after first step of FSPP method, given by Eq. (2.16)	[mm]
l_{scon}	Constant	[mm]
$O{-}XYZ$	Fixed reference frame	
$O_a{-}X_aY_aZ_a$	VOS reference frame	
$O_A{-}X_AY_AZ_A$	Operator reference frame	
$O_{c,i}{-}X_{c,i}Y_{c,i}Z_{c,i}$	Cart reference frame	
$O_h{-}X_hY_hZ_h$	IRH reference frame	
$O_H{-}X_HY_HZ_H$	Hand reference frame	
$O_p{-}X_pY_pZ_p$	Platform reference frame	
p	Pose vector of A1 and A2, $p = \{x_1, y_1, \phi_1, x_2, y_2, \phi_2\}^T$	
p_1	Lead of screw pairs B1-C1 and B2-C2 of VEMOPAM	[mm/r]
p_2	Lead of screw pair B3-C3 of VEMOPAM	[mm/r]
$p_{a,i}$	Actual pose of A1 and A2, $p_{a,i} = \{x_{a,i}, y_{a,i}, \phi_{a,i}\}^T$	
p_i	Planned pose of A1 and A2, $p_i = \{x_i, y_i, \phi_i\}^T$	
p_{ini}	Initial pose vector of A1 and A2, $p_{\text{ini}} = \{x_{10}, y_{10}, \phi_{10}, x_{20}, y_{20}, \phi_{20}\}^T$	
p_{tar}	Target pose vector of A1 and A2, $p_{\text{tar}} = \{x_{1t}, y_{1t}, \phi_{1t}, x_{2t}, y_{2t}, \phi_{2t}\}^T$	
q	Pose vector of platform of VEMOPAM, $q = \{x, y, z, \phi_x, \phi_y, \phi_z\}^T$	
${}^aq$	Position vector of IRH with respect to $O_a{-}X_aY_aZ_a$, ${}^aq = \{{}^ax, {}^ay, {}^az\}^T$	
${}^aq_t$	Position vector of target with respect to $O_a{-}X_aY_aZ_a$, ${}^aq_t = \{{}^ax_t, {}^ay_t, {}^az_t\}^T$	
${}^Aq$	Position vector of operator's hand with respect to $O_A{-}X_AY_AZ_A$	

$\boldsymbol{q}_{\text{ini}}$	Initial pose vector of platform of VEMOPAM, $\boldsymbol{q}_{\text{ini}} = \left\{ x_0, y_0, z_0, \phi_{x0}, \phi_{y0}, \phi_{z0} \right\}^T$	
$\boldsymbol{q}_{\text{tar}}$	Target pose vector of platform of VEMOPAM, $\boldsymbol{q}_{\text{tar}} = \left\{ x_t, y_t, z_t, \phi_{xt}, \phi_{yt}, \phi_{zt} \right\}^T$	
r	Radius of drive wheels of A1 and A2	[mm]
${}^a\boldsymbol{r}_h$	Posture matrix of IRH with respect to $O_a{-}X_aY_aZ_a$, ${}^a\boldsymbol{r}_h = \left\{ {}^a\boldsymbol{r}_x, {}^a\boldsymbol{r}_y, {}^a\boldsymbol{r}_z \right\}^T$	
${}^a\boldsymbol{r}_{ht}$	Posture matrix of target with respect to $O_a{-}X_aY_aZ_a$, ${}^a\boldsymbol{r}_{ht} = \left\{ {}^a\boldsymbol{r}_{xt}, {}^a\boldsymbol{r}_{yt}, {}^a\boldsymbol{r}_{zt} \right\}^T$	
${}^A\boldsymbol{r}_H$	Posture matrix of operator's hand with respect to $O_A{-}X_AY_AZ_A$	
r_c	Radius of sector path generated in second step of FSPP method	[mm]
$\boldsymbol{T}_q, \boldsymbol{T}_r$	Matrices for reference frame transformation, given by Eq. (3.2)	
v_0	Rated translational velocity of A1 and A2	[mm/s]
v_1, v_2	Translational velocities of A1 and A2	[mm/s]
w	Distance between CP of A1 or A2 and touchdown point of its drive wheel	[mm]
$\{x, y, z\}$	Position of platform of VEMOPAM with respect to $O{-}XYZ$	[mm]
$\{x_{a,i}, y_{a,i}\}$	Actual positions of A1 and A2 with respect to $O{-}XYZ$	[mm]
$\{x_{e,i}, y_{e,i}\}$	Differences between planned and actual positions of A1 and A2 with respect to $O_{c,i}{-}X_{c,i}Y_{c,i}Z_{c,i}$	[mm]
$\{x_i, y_i\}$	Planned positions of A1 and A2 of VEMOPAM with respect to $O{-}XYZ$	[mm]
z_{con}	Constant	[mm]
α	Viewpoint angle	[rad]
$\Delta\phi_1, \Delta\phi_2$	Turnabout angles of A1 and A2 before first step of FSPP method	[rad]
$\Delta\phi_3$	Turnabout angle of A1 and A2 before second step of FSPP method	[rad]
$\Delta\phi_4$	Central angle of sector path generated in second step of FSPP method	[rad]
$\Delta\phi_5$	Turnabout angle of A1 and A2 before third step of FSPP method	[rad]
$\Delta\phi_6$	Angle of rotation of A1 in third step of FSPP method	[rad]
$\Delta\phi_7, \Delta\phi_8$	Angles of rotation of A1 and A2 in fourth step of FSPP method	[rad]

ϕ_{10}, ϕ_{20}	Initial angles of rotation of A1 and A2, given by Eq. (2.13)	[rad]
$\phi_{a,i}$	Actual angles of rotation of A1 and A2 of VEMOPAM with respect to $O-XYZ$	[rad]
$\phi_{e,i}$	Differences between planned and actual angles of rotation of A1 and A2 with respect to $O_{c,i}-X_{c,i}Y_{c,i}Z_{c,i}$	[rad]
ϕ_i	Planned angles of rotation of A1 and A2 of VEMOPAM with respect to $O-XYZ$	[rad]
$\{\phi_x, \phi_y, \phi_z\}$	Orientation angles (yaw, pitch, and roll) of platform of VEMOPAM with respect to $O-XYZ$ (defined in section 2.2.II)	[rad]
ω_0	Rated rotational velocity of A1 and A2	[rad/s]
ω_1, ω_2	Rotational velocities of A1 and A2	[rad/s]
$\omega_{l,i}, \omega_{r,i}$	Rotational speeds of left and right drive wheels of A1 and A2	[rad/s]

Contents

CHAPTER 1
General Introduction

1.1   BACKGROUND AND MOTIVATION

With declining birthrates and aging populations, labor shortages are becoming serious in many countries. In recent decades, a variety of robots have been introduced into factories and warehouses to replace repetitive manual labor. **Fig. 1.1** shows a diagrammatic sketch of a conventional automated production line. This production line has many objects (i.e., the parts, products, and jigs) transported using a transportation system with a belt or roller conveyor, and processed using several fixed robots. However, some problems in such a production line have not yet been solved: i) with each upgrade of the products, in response to changes in the sizes, shapes, and weights of the parts and products, the production line must be frequently redesigned and reassembled, including changing the positions of the robots, adjusting the parameters of the transportation system; ii) even if only one robot on the production line fails, the whole line must be paused to repair it; iii) the layout of the production line is necessary to be properly arranged to adapt itself to the complicated factory environment, especially if the production line is long.

Modularized automated production lines consisting of multiple mobile robots can effectively avoid the above problems. Manipulators mounted on a mobile base, called mobile manipulators (see **Fig. 1.2**), have a high degree of freedom (DOF) and a wide working range [5, 6], and therefore they

Parts from feeders

SCARA robot
(YK-XE Series, Yamaha Motor Co., Ltd.)

Gantry robot
(TT Series, IAI Robot Co., Ltd.)

Vertical articulated robot
(YA Series, Yamaha Motor Co., Ltd.)

Conveyor system
(VBL, Okura Yusoki Co., Ltd.)

Parts, products and jigs

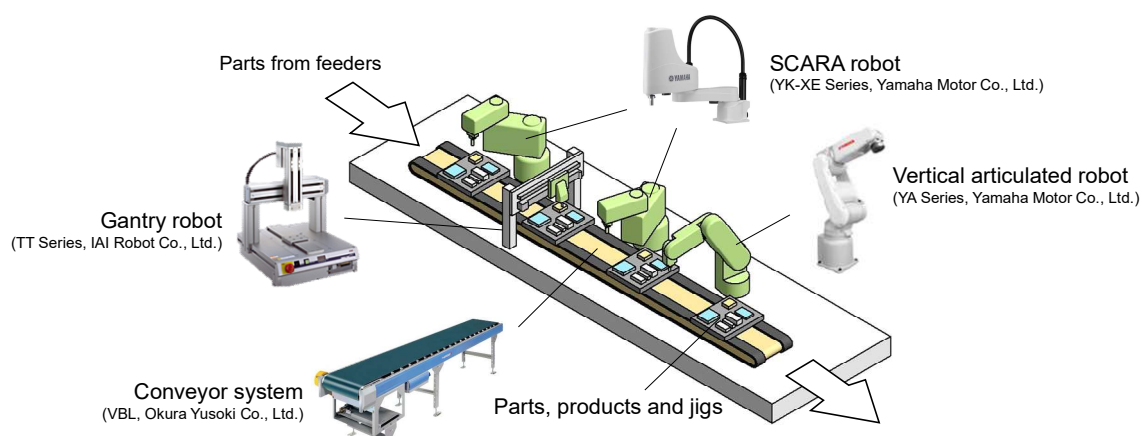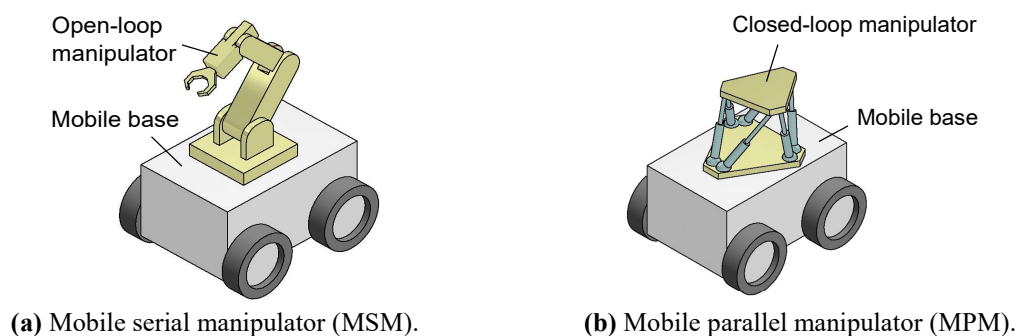**Fig. 1.1** Example of an automated production line with several fixed robots and a belt conveyor system [1–4].

Open-loop manipulator

Mobile base

Closed-loop manipulator

Mobile base

(a) Mobile serial manipulator (MSM).   **(b)** Mobile parallel manipulator (MPM).
Fig. 1.2 Mobile manipulators.
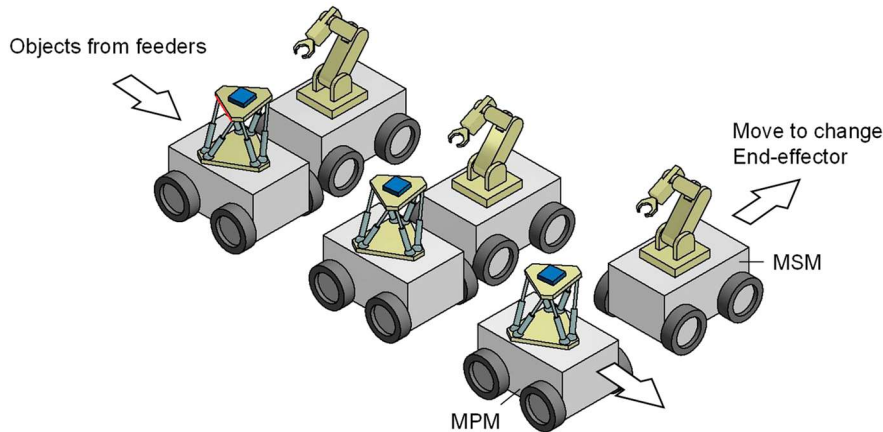
Fig. 1.3 Modularized automated production line.

	Current topics	Future topics
Robot	**1. Cost reduction of robots** Reducing motors in a mobile manipulator without reducing its DOFs	
Operation	**2. Easy robot operation** Easy operation methods of mobile manipulators when viewpoint changes occur	**3. Other body parts used for robot operation** The use of lower limbs in body motion-based Leader-Follower operations

Fig. 1.4 Topics for further popularization of mobile manipulators.

are expected to be applied in modularized production lines. **Fig. 1.2(a)** shows a mobile base equipped with an open-loop manipulator, named mobile serial manipulator (MSM). Many MSMs have been provided for various purposes [10–12], such as industrial production [7], education [8], human supporting [9], etc. Open-loop mechanisms have a large working range and high operational flexibility, and thus MSMs are expected to be used for complicated and dexterous tasks in industrial sites (e.g., screw tightening and soldering) or in daily life (e.g., loading and unloading of objects). On the other hand, **Fig. 1.2(b)** shows a mobile base equipped with a closed-loop manipulator, named mobile parallel manipulator (MPM). Since the stiffness and positioning accuracy of closed-loop mechanisms are known to be higher than those of open-loop mechanisms, MPMs are better at the tasks of transporting and positioning heavy objects.

Figure 1.3 shows an example of a modularized production line in which the above-described MSMs and MPMs are used. As shown in this figure, some MPMs move in a line formation to transport objects from a feeding system to specified workstations; each workstation has an MSM process and assemble the parts and products. The MSMs can move to a specified position to change its end-effector (e.g., pneumatic robotic hands, screw tightening and soldering machines) so that they can perform various tasks. Compared with the conventional production lines shown in **Fig. 1.1**, such a modularized production line has three advantages: i) even if the sizes, shapes, and weights of the transported objects are changed, the use of mobile manipulators makes complicated redevelopments of the production line unnecessary, which reduces the redevelopment and reassembly cost; ii) a faulty mobile manipulator can be immediately replaced by another one, the capacity utilization rate of the entire production line can be thus maintained high; iii) the layout of the whole production line can be flexibly arranged regardless of factory environment.

The mobile manipulators described above have some unsolved problems. First, if multiple mobile manipulators are used in a production line, the higher the cost of one mobile manipulator, the higher the manufacturing cost of the whole production line. Second, if mobile manipulators are used for complex tasks, the operations of them may be difficult. In the future, mobile manipulators are also expected to be used by ordinary people in daily life, it is therefore required that even novice operators can easily operate them. Hence, this thesis aims to further popularize mobile manipulators, and focuses on the cost reduction of mobile manipulators and simple operation methods for novice operators. Three research topics shown in **Fig. 1.4**, including two current topics and one future topic, are considered in this thesis:

1) Current research topic one: how to reduce the number of motors in a mobile manipulator without reducing its DOFs. Lower cost of mobile manipulators can be realized by reducing the number of motors used in them. This research proposes a novel MPM with fewer motors than the conventional MPMs, analyzes its kinematics, and presents a path planning method for it.

2) Current research topic two: in order to spread the use of mobile manipulators to more people, easier robot operation methods are needed for novice operators. Especially, operating a mobile manipulator is considered to be more difficult than operating a fixed robot, since the viewpoint from the operator relative to the robot may be frequently changed. This research proposes an evaluation system to investigate the influence of viewpoint change on different operation methods and clarifies the influence.

3) Future research topic: with the body motion-based leader-follower operation method, it is considered that the more body parts the operator uses, the more kinds of operations he/she can perform. This research focuses on human lower limbs, proposes an operation device, and evaluates the effectiveness and operability of the robot operation method using lower limbs.

1.2 CURRENT TOPIC ONE: HOW TO REDUCE MOTORS USED IN MOBILE MANIPULATORS WITHOUT REDUCING THEIR DOFS (A NOVEL MOBILE PARALLEL MANIPULATOR)

Current topic one discusses how to reduce motors used in an MPM without reducing its DOFs. To date, various sorts of parallel mechanisms that can be used in MPMs have been developed. Stewart presented a parallel flight simulator (see **Fig. 1.5**) in which a top platform was supported and moved using six linear actuators [13]. This mechanism, called the Stewart platform, is well known as one of the typical parallel mechanisms. Arai studied the isotropy of forces and moments occurred in the Stewart platform based on the statics [14]. When analyzing the dynamics of a Stewart platform using a Jacobian matrix, it is unnatural to deal with the forces and moments together since their dimensions are different. Kosuge *et al.* described how to separately deal with the forces and moments to eliminate this unnaturalness [15]. Lebert *et al.* derived an equation of motion (EOM) for a Stewart-platform-based manipulator used for milling process, and developed a stable control system for it [16]. Dasgupta and Mruthyunjaya formularized the EOM for a rigid Stewart platform using Newton-Euler method, and modelled all unknowns (e.g., inertia force, centripetal force, Coriolis force, gravity, and friction) [17, 18]. Liu *et al.* discussed how to derive a forward kinematic equation for a Stewart platform using Kane's method [19]. Such Stewart platforms have been fixed on a mobile robot to develop MPMs; and the dynamics [20] and acceleration compensation [21, 22] have been studied. Besides, MPMs with other types of parallel mechanisms have also been constructed. Yamawaki *et al.* proposed a MPM that could climb steps and lift objects upward by transformations of 4R or 5R parallel linkages [23].

Li *et al.* proposed a mobile robot on which a DELTA parallel manipulator was fixed [24]. However, as shown in **Fig. 1.6**, if an MPM has a parallel mechanism and an omnidirectional mobile base separately actuated, more than six motors must be used to realize the 6-DOF spatial motions of the platform and the 3-DOF planar motions of the mobile base, which may lead to kinematic redundancy. In addition, the more motors used in a mobile manipulator, the higher its cost of developing and deployment. It is therefore desired to reduce the number of motors.

An MPM that has fewer motors than the above-mentioned MPMs has been proposed [26, 28]. As shown in **Fig. 1.7(a)**, this MPM is composed of a platform and three limbs; one end of each limb is connected to a 2-DOF locomotion unit via a spherical joint, and the other end is connected to the platform via a revolute joint. With the screw theory, an instantaneous Jacobian matrix for such three-limb MPMs has been derived [27], and a type synthesis method for them has been discussed [32]. Ben-Horin *et al.* developed some three-limb MPMs shown in **Fig. 1.7(b)** and examined their kinematic and dynamic performance by several experiments [29–31]. Besides, Terakawa *et al.* proposed a novel slidable-wheeled mobile base which was also applicable for the three-limb MPMs [33, 34].

Although each locomotion unit in a three-limb MPM has only two kinematic DOFs under the nonholonomic constraint, it has three geometric DOFs. Therefore, it is theoretically possible to set the 6-DOF pose (i.e., the position and orientation) of the MPM with only two locomotion units. This thesis proposes a novel MPM with only two locomotion devices, named VErsatile MObile PArallel Manipulator (VEMOPAM). These two locomotion devices are connected to a platform through a parallel mechanism. Compared with the conventional three-limb MPMs, the proposed mechanism has a total of four motors, which makes it possible to further reduce the number of motors. In addition, whereas a three-limb MPM has multiple loops in its parallel structure, VEMOPAM has only one loop and thus occupies a smaller area. Therefore, VEMOPAM is considered to be more economical and practical than the conventional MPMs. Detailed descriptions and analyses of VEMOPAM will be given in the following chapters.

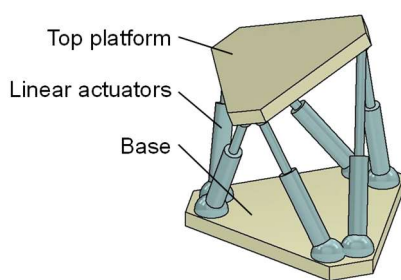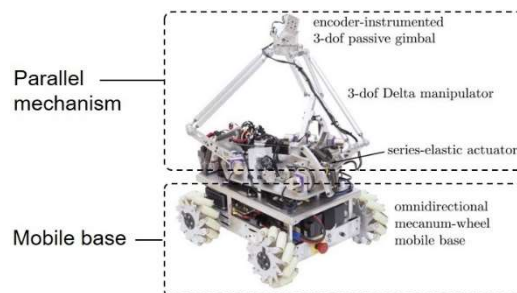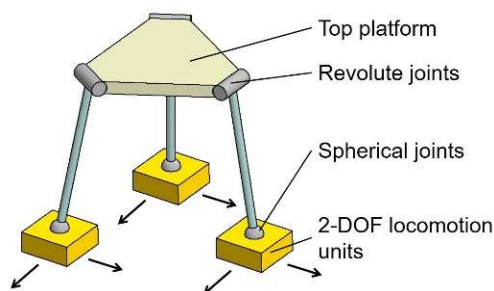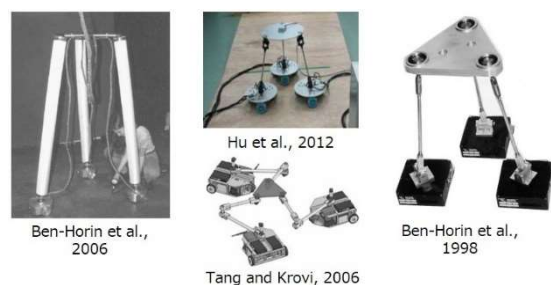**Fig. 1.5** Stewart platform.   **Fig. 1.6** MPM with a parallel mechanism fixed on a mobile base [25].

(a) Structure of a three-limb MPM.   **(b)** Some developed three-limb MPMs [29, 31, 35, 36].
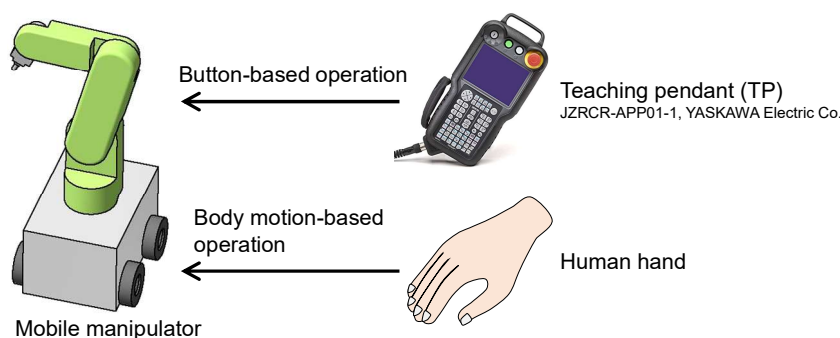
Fig. 1.7 Three-limb MPMs.

Fig. 1.8 Body motion- and button-based operation methods.

1.3 CURRENT TOPIC TWO: EASIER OPERATION METHODS OF MOBILE MANIPULATORS FOR NOVICE OPERATORS (VIEWPOINT CHANGES IN ROBOT OPERATION)

Before employing mobile manipulators, the desired motion commands must be taught to them [85]. Conventionally, as shown in **Fig. 1.8**, a teaching pendant (TP) with multiple buttons is used to conduct this teaching [86]. However, when teaching complicated movements to a multi-DOF mobile manipulator, it has been reported that the more complicated the movements, the longer the operation time of TP, and the less accurate the button operations tend to be [87]. Especially, as described previously, MSMs are generally used for complex and dexterous works, thus the button operations for MSMs are considered to be more difficult than those for MPMs. Moreover, as mobile manipulators will also be increasingly used as life-supporting devices in the future, it can be expected that they will frequently be operated by novices who are unfamiliar with the operation method, making easier operation methods essential [88].

As an alternative to the TP method, many methods in which the operation commands of robots and machines are taught based on the movement of the operator's upper limb have been studied [89–95]. Two main types of operation methods have been proposed in the previous research. One is to operate the robots by associating specific operation commands with recognized hand gestures. Hu *et al.*, for example, proposed a new teleoperation method in which seven kinds of commands respectively corresponded to seven kinds of hand gestures [96]. Miadlicki and Pajor considered a way to control various machines, e.g., CNC milling machines, by detecting specific hand gestures using Microsoft Kinect [97]. The second type, called "leader-follower" (formerly also called "master-slave") operation method (see **Fig. 1.8**), has the robot reproduce movements similar to human hand poses. Hameed *et al.* proposed a method utilizing Leap Motion to make a robotic hand imitate human hand postures [98]. Du *et al.* used Kinect to track movements of upper limbs and described how one could manipulate a robot using comfortable hand postures [99]. Leader-follower teleoperation systems and control methods have been presented for heavy construction machines [101–106]. Some other leader-follower operation methods, such as digital-twin-based [107] and virtual-reality-based [108] methods, have also been proposed.

Compared with the conventional robot operation method using a TP (button-based method), the above body motion-based leader-follower operation method (body motion-based method) can be used to implement intuitive implement intuitive operations, their operability are thus considered to be high, especially for novice operators. However, since many devices (motion capture systems, operation screens, etc.) are needed for the construction of the body motion-based operating
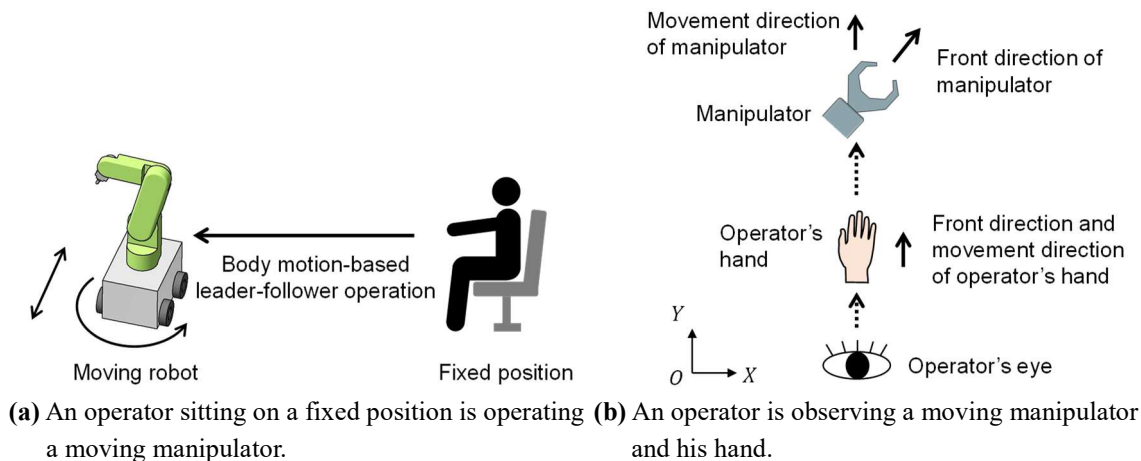
(a) An operator sitting on a fixed position is operating **(b)** An operator is observing a moving manipulator
a moving manipulator.   and his hand.

Fig. 1.9 Viewpoint change in mobile manipulator teleoperations

environment, the cost of the body motion-based interfaces is generally higher than that of the button-based interfaces. Komori *et al.* developed an operability evaluation system using a 3D motion capture system and compared the performance of the body motion- and button-based operation methods [100], by which the selection of the operation method based on the quantitative evaluation of cost performance becomes possible.

In the previous studies, it has been assumed that the operator's viewpoint relative to the operated robot was fixed during operating. Nevertheless, as shown in **Fig. 1.9(a)**, if an operator sitting on a fixed chair operates a mobile manipulator using a body motion-based operation device, due to the motions of this mobile manipulator, the operator may observe that the relative pose of the leader device fixed on his/her hand is often different from that of the manipulator (follower device), which can mean frequent changes in the operator's viewpoint. **Fig. 1.9(b)** exemplifies the effect of viewpoint changes. If the operator moves his/her hand in the front direction (Y direction), he/she can observe that the front and movement directions of his/her hand are the same. However, in the operator's eyes, since the reference frames respectively fixed on the hand and the robot are non-uniform, the front and movement directions of the manipulator become different. Such viewpoint changes can also occur when other kinds of operation methods, including the button-based method, are used. It is considered that viewpoint changes have different effects on different operation methods. Therefore, this thesis proposes an evaluation system which can be utilized to uniformly evaluate the influence of viewpoint changes on various robot operation methods, and investigates the differences between the body motion- and button-based methods using the proposed evaluation system.

1.4   FUTURE TOPIC: EXPANDING POSSIBILITIES OF BODY PARTS USED FOR ROBOT OPERATIONS (ROBOT OPERATION USING LOWER LIMBS)

Upper limbs in human (e.g., arms, hands, and fingers) are often used for manipulating objects. With the conventional leader-follower teleoperation devices, an operator can use his/her arms to change the 6-DOF pose of a mobile manipulator. Additionally, he/she can use his/her fingers to manipulate an end-effector (e.g. a gripper). That is, the more body parts the operator uses during the operation, the more kinds of robot operations he/she can perform. If the operator's body parts other than the upper limbs, such as the lower limbs, are also used, he/she is considered to be able to finish more complicated operations.

Lower limbs in human (e.g., legs, feet, and toes) are mainly employed for walking, kicking, and stepping; they are rarely used for complex manipulations. Although human lower limbs are often moved with a slower speed than upper limbs, they also have multiple DOFs similar to upper limbs. Therefore, lower limbs are expected to play a new role for the future operation methods of robots. Some studies have researched and developed operation devices that utilize lower limbs. Matsuda *et al.* developed a projection-type I/O interface in which the screen, which was projected onto the floor from a projector fixed on the operator's chest, could be operated by the feet [139]. Fukahori *et al.* developed an operation device using the pressure applied on some specific positions of the soles [140]. Yamamoto *et al.* proposed an operation device that tracked the foot movements of a jogger through sensors attached to the shoes and generated four different operation commands [141]. In recent years, several studies have been conducted on recognition methods for foot gestures, such as kicking and striking [142], and PC operation devices utilizing such gestures have been developed [143]. An operation method based on ankle angles which were measured by a motion capture system has also been proposed [144]. Komori *et al.* experimentally investigated the characteristics of foot movements during operation and proposed a method to compensate errors of foot motions [145]. Besides, Kume *et al.* presented a double-foot-type computer mouse and evaluated the accuracy and efficiency of pointing operations of human toes [146].

As described above, a variety of operation devices using the motions of legs and feet have been developed. However, operation devices using toes have rarely been proposed. And, the operability and movement characteristics of toes when they are used for robot operations have not yet been available. Therefore, this thesis proposes an operation device utilizing the flexions and extensions of toes, surveys the operability when one or two toes are used, and compares the operability of toes and fingers.

1.5 OVERVIEW OF THESIS

This thesis focuses on the above three topics and shows the research results in the following chapters. A brief overview of this thesis is given as follows:

Chapter 2 shows the structure of the proposed MPM. A Jacobian matrix is obtained based on the inverse kinematics of the proposed mechanism. A singularity analysis is also conducted using the derived Jacobian matrix. Then, a path planning method and a path tracking control method for this mechanism are presented. Moreover, an experimental prototype is constructed to experimentally verify the validity of the proposed mechanism and methods.

Chapter 3 includes the proposition of an evaluation system for evaluating the operability of the body motion- and button-based operation methods involving with viewpoint changes. Taking the operation times and the numbers of trial-and-errors as the main evaluation indices of these two methods, this chapter investigates their operability by several experiments.

Chapter 4 focuses on the development of an operation device which is operated by human toes. Several experiments are conducted to demonstrate the potential of this device in position operations. Based on the experimental results, the operation times of the toes and fingers, the great toes and long toes, and the one-toe/finger and two-toe/finger operations are compared.

Chapter 5 summarizes the conclusions in each chapter and discusses the future research.

CHAPTER 2
A Mobile Parallel Manipulator and Its Path Planning

2.1 INTRODUCTION

As have been explained, the more motors used in a mobile manipulator, the higher its cost. Some kinds of mobile manipulators, such as three-limb MPMs, have their work manipulator and mobile base driven by the mutual motors, which makes the number of the motors of these robots is smaller than that of the conventional MPMs. However, because of the movements of the three locomotion devices used in a three-limb mobile manipulator, the occupied area of this mobile manipulator may become very large.

This chapter proposes a novel MPM, named VEMOPAM, which is composed of two 2-DOF nonholonomic locomotion devices, a single-loop parallel transmission mechanism (SLPTM), and a top platform. By moving the two locomotion devices, VEMOPAM can change the 6-DOF pose of the top platform. The two locomotion devices are driven by a total of four motors, which makes the number of motors smaller than the DOF of the platform. This realizes the reduction of motors, leading to a lower development cost than the conventional MPMs. Moreover, compared with the three-limb MPMs, VEMOPAM has a smaller occupied area since it has only two locomotion devices connected with the SLPTM.

Figure 2.1 shows some kinds of 2-DOF locomotion devices, each of which has three geometric DOFs and two kinematic DOFs. In these devices, one of the three geometric DOFs is constrained by the nonholonomic constraint, and the other two are actuated by two motors. **Fig. 2.1(a)** shows a steerable cart with an active caster. Two driving motors are used to control the straight and steering movements of the caster wheel, respectively [37–39]. **Fig. 2.1(b)** shows a cart with an active omni wheel. One motor is used to rotate this wheel, and the other motor is used to rotate the rollers on the circumference of this wheel [40, 41]. Other types of vehicles, such as Mecanum-wheel-drive [42, 43] and spherical-wheel-drive [44] vehicles, have also been developed. Compared with these movement devices, two-wheel-drive (2WD) carts that are driven by two independent wheels [see **Fig. 2.1(c)**] have a simpler structure and can be easily controlled; two 2WD cats are thus utilized as the locomotion units of VEMOPAM.

The SLPTM in VEMOPAM, which consists of three screw pairs, some rigid rods and revolute joints, is used to transmit the 2-DOF planar motions of the 2WD carts to the top platform. Dynamic models based on the Euler-Lagrange equation have been proposed for the dynamic analyses of
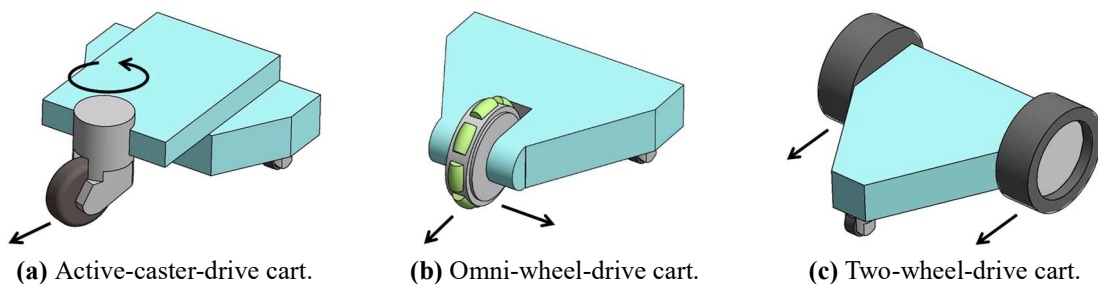

   (a) Active-caster-drive cart.   **(b)** Omni-wheel-drive cart.   **(c)** Two-wheel-drive cart.
Fig. 2.1 Examples of 2-DOF nonholonomic movement devices.

mobile robots [45–47] as well as parallel mechanisms [48, 49]. Previous studies have also proposed various dynamic models for screw mechanisms [50–52]. However, the dynamic model of VEMOPAM established by these modelling methods is quite complex, it thus complicates the movement analysis of VEMOPAM. And, dynamics is considered to be especially effective for high-velocity motions, whereas this chapter mainly studies low-velocity motions of VEMOPAM, which can also be validly analyzed by kinematics. Thus, in this chapter, a kinematic model based on the geometric relations between the parts of VEMOPAM is constructed. Using this model, the kinematic characteristics of VEMOPAM are investigated and analyzed. The detailed descriptions of the structure and kinematic analysis of VEMOPAM are given in the following sections.

To move the platform of VEMOPAM to any desired position and orientation, it is necessary to plan how to move the two 2WD carts. Since the 2WD carts are not movable in their lateral directions due to the nonholonomic constraints, an appropriate path planning method for such a nonholonomic mechanism is needed. To date, path planners for a mobile robot based on a variety of algorithms have been proposed [54–61]. For multi-mobile-robot systems, a coordinative path planning method based on a genetic algorithm has been presented [62, 63]. Applying and improving this coordinative path planning method, Kosuge *et al.* developed a decentralized coordinative transportation system with a nonholonomic mechanism [64–66]. Some other path planners and controllers, such as a path planner based on the recursive subdivision of the path [67] and a controller based on the decomposition of acceleration [68], have also been proposed. However, due to the complicated constraint conditions (e.g., the nonholonomic constraints and the strokes of the screw pairs) and unique structural characteristics (e.g., the singularities) of VEMOPAM, none of the above path planning methods can be used to optimize the paths of the two carts. In this chapter, a custom path planning method with four steps is presented for VEMOPAM. Although this method does not provide optimal paths for the carts, it can be easily realized with low computational cost because the paths can be planned without considering the complex constraint conditions of VEMOPAM. This chapter shows the features of this path planning method, and analyzes the motions of VEMOPAM in each step using simulations. Moreover, an experimental prototype of VEMOPAM is constructed to demonstrate the usefulness of the proposed mechanism and path planning method.

2.2   PROPOSED NOVEL MOBILE PARALLEL MANIPULATOR

This section shows the structure and motions of VEMOPAM.

I. Structure of Proposed Mobile Parallel Manipulator

Figure 2.2(a) shows the structure of VEMOPAM. As shown in this figure, VEMOPAM has two 2WD carts (A1 and A2), each of which has two drive wheels installed on the left and right sides, respectively, and two auxiliary wheels installed on the front and back sides, respectively, to maintain balance. The projected point of the midpoint between the two drive wheels on the floor is defined as the center point (CP) of the cart. Two screw shafts (B1 and B2) are respectively fixed on A1 and A2 so that they can move together. The center axes of B1 and B2 pass through the CPs of A1 and A2, respectively. Screw shafts B1, B2, and B3, and screw nuts C1, C2, and C3 form three screw pairs; revolute joints D1 and D2 form two revolute pairs of the linkages; and revolute joint D3 forms a revolute pair of the linkages and the platform. Therefore, the motions of A1 and A2 are transmitted to the platform via a parallel mechanism, i.e., the SLPTM, which is composed of f three screw pairs (B1-C1, B2-C2, and B3-C3), and three revolute joints (D1, D2, and D3).
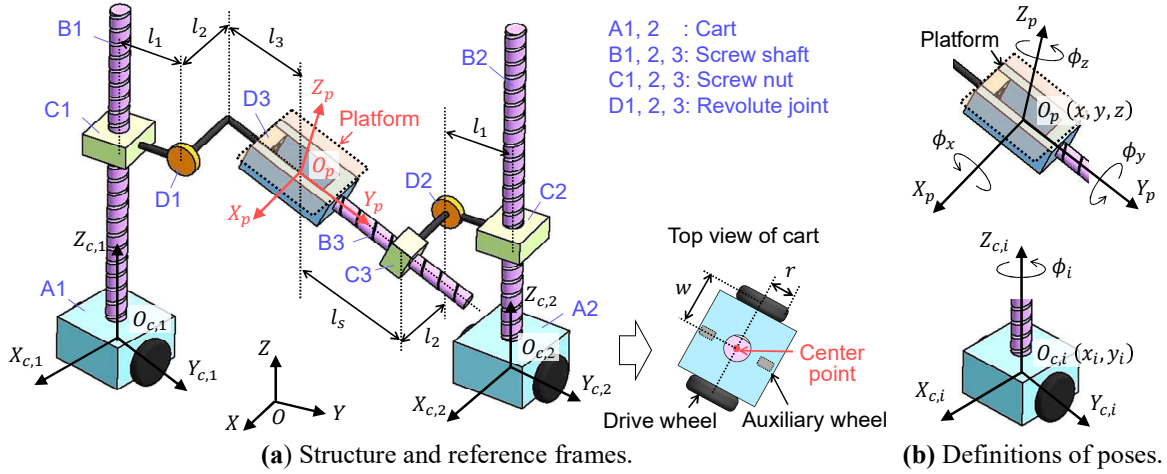
(a) Structure and reference frames.   (b) Definitions of poses.

Fig. 2.2 Proposed VEMOPAM.

The number of geometric DOFs of VEMOPAM N_{dof} is calculated by Gruebler's equation as follows:

$$N_{\text{dof}} = 6\left(N_{\text{link}} - N_{\text{joint}} - 1\right) + \sum_{j=1}^{N_{\text{joint}}} f_i, \tag{2.1}$$

where N_{link} is the total number of links, N_{joint} is the total number of joints, and f_i indicates the number of DOFs of each joint. The mechanism of VEMOPAM has eight links; each of the joints between carts A1 and A2 and the floor has three geometric DOFs, and each of the other joints has one DOF. Therefore, $N_{\text{link}} = 8$, $N_{\text{joint}} = 8$, and $\sum f_i = 2 \times 3 + 6 \times 1 = 12$. From Eq. (2.1), it can be confirmed that VEMOPAM has six geometric DOFs ($N_{\text{dof}} = 6$).

II.   Definitions of reference frames and pose

To describe the pose of VEMOPAM, some reference frames are defined as shown in **Fig. 2.2(b)**. $O-XYZ$ is defined as a fixed frame, and $O-XY$ is the floor on which the carts move. Platform frame $O_p-X_pY_pZ_p$ is fixed at the platform. Axis Y_p coincides with the center axis of screw shaft B3. Two cart frames $O_{c,i}-X_{c,i}Y_{c,i}Z_{c,i}$ are fixed to carts A1 and A2. Origins $O_{c,i}$ are the CPs and correspond to the center of rotation of the carts. Axes $X_{c,i}$ and $Y_{c,i}$ are respectively the forward and left lateral directions of the carts. Axes $Z_{c,1}$ and $Z_{c,2}$ coincide with the center axes of screw shafts B1 and B2, respectively. In this chapter, the subscript $i = 1$ and 2 is used to represent A1 and A2, respectively.

With respect to $O-XYZ$, the position of the platform is defined by the position $\{x, y, z\}$ of O_p. The orientation of the platform is represented using three angles of rotation around axes X_p, Y_p, and Z_p, i.e., yaw ϕ_x, pitch ϕ_y, and roll ϕ_z, respectively. We define the reference orientation of the platform to be $\phi_x = \phi_y = \phi_z = 0$ (i.e., the directions of X_p, Y_p, and Z_p are respectively the same as those of X, Y, and Z). After the platform is rotated about the three axes in the order of Z_p, X_p, and Y_p, it changes from the reference orientation to the current orientation, and ϕ_x, ϕ_y, and ϕ_z become the current values. On the other hand, with respect to the floor $O-XY$, the positions of carts A1 and A2 are defined by the positions of $O_{c,i}$ which are represented as $\{x_i, y_i\}$. And the angles of rotation of A1 and A2 with respect to $O-XY$ are represented as ϕ_i. Similarly, the subscript $i = 1$ and 2 is used to represent A1 and A2, respectively.
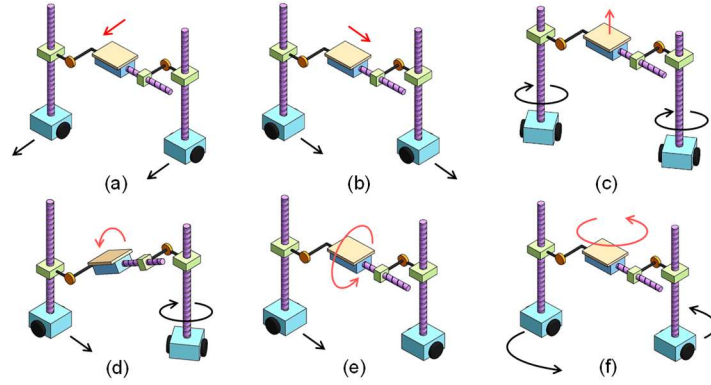
Fig. 2.3 Basic movements of VEMOPAM: (a−c) 3-DOF translational movements and (d−f) 3-DOF rotational movements of platform.

III. Movements of Carts and Platform

As shown in **Fig. 2.3**, the pose $\{x, y, z, \phi_x, \phi_y, \phi_z\}$ of the platform can be controlled by moving A1 and A2. **Fig. 2.3(a)−(c)** show that $\{x, y, z\}$ is changed if A1 and A2 translate or rotate with the same direction and velocity; **Fig. 2.3(d)** shows that ϕ_x is changed if nuts C1 and C2 move vertically with different velocities; **Fig. 2.3(e)** shows that ϕ_y is changed due to the screw motions of screw pair B3-C3; **Fig. 2.3(f)** shows that ϕ_z is changed if A1 and A2 revolve in concentric circles.

The movement shown in **Fig. 2.3(e)**, i.e., the change of ϕ_y, is considered to be extremely difficult if B3-C3 has a small lead. For example, if the lead of B3-C3 is 20 mm/r, even a small error of 1 mm in the linear motion of nut C3 in Y_p would cause an 18° deviation of ϕ_y. This is a drawback of this mechanism. This study addresses this problem by using a speed reducer when realizing a prototype of VEMOPAM. The details are described in Section 2.6-I.

2.3   KINEMATICS OF VEMOPAM

Prior to the discussion of the path planning method, this section analyzes the kinematics of VEMOPAM to clarify its motion conditions.

I. Inverse Kinematics

For parallel mechanisms, inverse kinematics is easier than forward kinematics [14]. VEMOPAM is treated as a movable parallel mechanism and its inverse kinematics is thus considered. Under the assumptions that: i) the floor is flat and smooth; and ii) no vibrations or deformations occur in the vertical rigid shafts B1 and B2 during low-velocity movements, the following equations based on the definitions of the poses of the platform and carts A1 and A2 (see Section 2.2-II) are established to represent the geometric relations among the parts of VEMOPAM:

$$
\begin{aligned}
x_1 &= x + l_1 \sin \phi_z + l_2 \cos \phi_z + l_3 \cos \phi_x \sin \phi_z , \\
y_1 &= y - l_1 \cos \phi_z + l_2 \sin \phi_z - l_3 \cos \phi_x \cos \phi_z , \\
\phi_1 &= \phi_z - 2\pi(z - z_{\mathrm{con}} - l_3 \sin \phi_x)/p_1 , \\
x_2 &= x - l_1 \sin \phi_z - l_2 \cos \phi_z - l_s \cos \phi_x \sin \phi_z , \\
y_2 &= y + l_1 \cos \phi_z - l_2 \sin \phi_z + l_s \cos \phi_x \cos \phi_z , \\
\phi_2 &= \phi_z - 2\pi(z - z_{\mathrm{con}} + l_s \sin \phi_x)/p_1,
\end{aligned}
\tag{2.2}
$$

where l_1, l_2, l_3, and l_s are the lengths of the linkages (see **Fig. 2.2**), p_1 is the lead of screw pairs

B1-C1 and B2-C2, and z_{con} is a constant. Appendix 1 shows the derivations of these equations. The value of l_s varies depending on the screw motions of screw pair B3-C3:

$$l_s = l_{scon} - \frac{p_2 \phi_y}{2\pi}, \tag{2.3}$$

where p_2 is the lead of B3-C3, and l_{scon} is a constant.

By rearranging Eq. (2.2), several equations describing the geometric features of VEMOPAM can be obtained. Eq. (2.4) can be derived by rearranging the first, second, fourth, and fifth equations of Eq. (2.2).

$$(x_1 - x_2) \cos \phi_z + (y_1 - y_2) \sin \phi_z = 2l_2. \tag{2.4}$$

Eq. (2.4) shows that the roll ϕ_z of the platform depends on only the relative position of the carts. The condition $x_1 - x_2 = y_1 - y_2 = 0$ (i.e., A1 and A2 collide with each other) is never satisfied as long as $l_2 > 0$. In addition, Eq. (2.5) can be derived by rearranging the third and sixth equations of Eq. (2.2).

$$\phi_1 - \phi_2 = \frac{2\pi}{p_1}(l_3 + l_s) \sin \phi_x. \tag{2.5}$$

Eq. (2.5) shows the relation between the difference in the angles of rotation of the carts $(\phi_1 - \phi_2)$ and the yaw ϕ_x and pitch ϕ_y of the platform.

Differentiating Eq. (2.2) with respect to time yields Eq. (2.6).

$$\dot{p} = J\dot{q}. \tag{2.6}$$

Here, p, q, and the Jacobian matrix J are given in Eq. (2.7).

$$p = \{x_1, y_1, \phi_1, x_2, y_2, \phi_2\}^T, q = \{x, y, z, \phi_x, \phi_y, \phi_z\}^T,$$

$$J = \begin{vmatrix} 1 & 0 & 0 \\ 0 & 1 & 0 \\ 0 & 0 & -2\pi/p_1 \\ 1 & 0 & 0 \\ 0 & 1 & 0 \\ 0 & 0 & -2\pi/p_1 \end{vmatrix}$$

$$\begin{vmatrix} -l_3 \sin \phi_x \sin \phi_z & 0 & (l_1 + l_3 \cos \phi_x) \cos \phi_z - l_2 \sin \phi_z \\ l_3 \sin \phi_x \cos \phi_z & 0 & (l_1 + l_3 \cos \phi_x) \sin \phi_z + l_2 \cos \phi_z \\ 2\pi l_3 \cos \phi_x/p_1 & 0 & 1 \\ l_s \sin \phi_x \sin \phi_z & p_2 \cos \phi_x \sin \phi_z/(2\pi) & -(l_1 + l_s \cos \phi_x) \cos \phi_z + l_2 \sin \phi_z \\ -l_s \sin \phi_x \cos \phi_z & -p_2 \cos \phi_x \cos \phi_z/(2\pi) & -(l_1 + l_s \cos \phi_x) \sin \phi_z - l_2 \cos \phi_z \\ -2\pi l_s \cos \phi_x/p_1 & p_2 \sin \phi_x/p_1 & 1 \end{vmatrix}. \tag{2.7}$$

With the rolling-without-slipping condition for the carts, the nonholonomic constraints are expressed using Eq. (2.8).

$$G\dot{p} = 0. \tag{2.8}$$

Here, G is given in Eq. (2.9).

$$G = \begin{bmatrix} -\sin\phi_1 & \cos\phi_1 & 0 & 0 & 0 & 0 \\ 0 & 0 & 0 & -\sin\phi_2 & \cos\phi_2 & 0 \end{bmatrix}. \tag{2.9}$$

Substituting Eq. (2.6) into Eq. (2.8) yields the following equation,

$$GJ\dot{q} = 0. \tag{2.10}$$

Eq. (2.10) shows the effect of the nonholonomic constraints on the movements of VEMOPAM.

II. Singular and Failure Configurations

Parallel mechanisms have two kinds of singularities [53]. The first kind occurs when $\det\left(J^{-1}\right) = 0$, and the second kind occurs when $\det(J) = 0$. An analysis based on the obtained J indicates that the first kind occurs when Eq. (2.11) is satisfied, and that the second kind does not exist for VEMOPAM.

$$\cos\phi_x = -\frac{2l_1}{l_3 + l_s}. \tag{2.11}$$

Fig. 2.4(a) shows that VEMOPAM falls into the second kind of singular configuration if the line of the CPs of the carts is normal to the projection of the center axis of screw shaft B3 on the floor. As shown in **Fig. 2.4(b)**, with this singular configuration, if carts A1 and A2 are commended to move far away from each other, because the direction of the screw motion of B3-C3 is no longer constrained, the platform has two possible poses (A and B) after moving. Because the right-hand side of Eq. (2.11) is negative, this singularity does not occur if $-\pi/2 \leq \phi_x \leq \pi/2$.

The above analysis was performed based on the premise that the axes of rotation of revolute joints D1 and D2 are always parallel due to the structural constraints of VEMOPAM. However, as shown in **Fig. 2.5**, when the center axis of screw shaft B3 becomes perpendicular to the floor (i.e.,
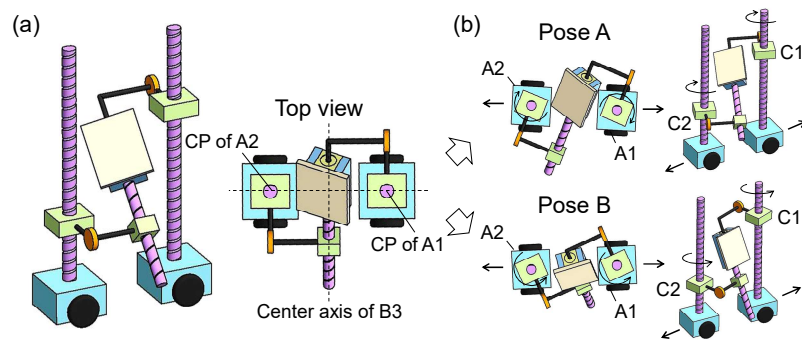

Fig. 2.4 Singularity analysis results for VEMOPAM: (a) singular configuration and (b) motions in this configuration.
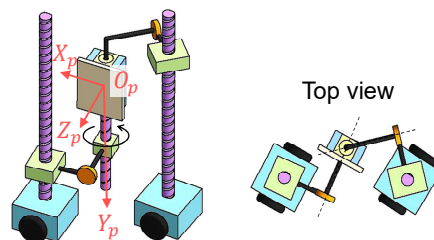

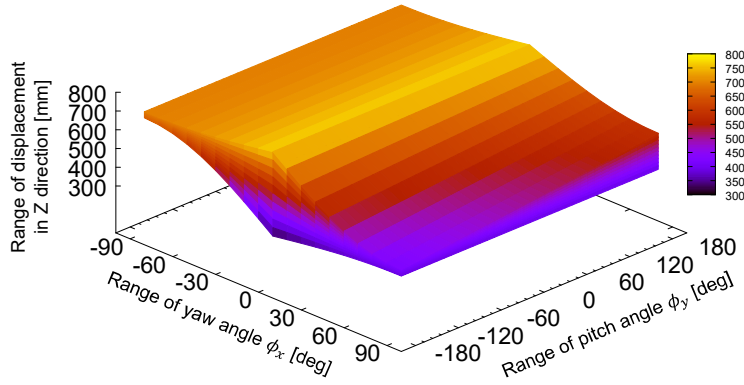**Fig. 2.5** Failure configuration for VEMOPAM.

Fig. 2.6 Paths of carts and motions of platform in first step of path planning.
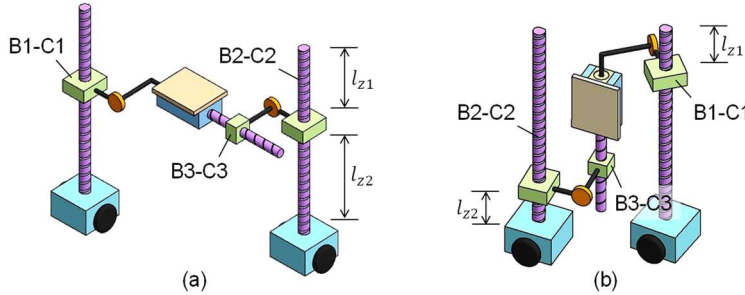
Fig. 2.7 Movable range of z if (a) $\phi_x = 0°$ and (b) $\phi_x = 90°$.

$\phi_x = \pm \pi/2$), the constraint condition for VEMOPAM changes. At this instant, if the carts revolve about the center axis of B3, the parallelism of D1 and D2 cannot be maintained, and the geometric relations represented by Eq. (2.2) no longer hold. In this chapter, this configuration is referred to as the failure configuration.

From the above analysis, it was confirmed that is ϕ_x is limited to be $-\pi/2 < \phi_x < \pi/2$, VEMOPAM can avoid the singular and failure configurations, and that the pose of the platform has a one-to-one correspondence with the poses of carts A1 and A2. On the other hand, since the workspace of the platform is limited due to the strokes of the screw pairs (as described below), the first kind of singular configuration may occur if the platform reaches the boundary of its workspace. Based on these analysis results, a path planning method is proposed for the two carts in the next section.

III. Workspace

Using the parameters of VEMOPAM given in **Table 2.1**, this section analyzes the workspace of its platform based on the above kinematic analysis. **Fig. 2.6** shows the analysis result of workspace. As shown in this figure, the platform can move freely in the axes X and Y, and can rotate about the axis Z, its displacements x, y, and ϕ_z can be moved without limitation. However, the changes

Table 2.1 Parameters for VEMOPAM.

Symbol	l_1	l_2	l_3	l_s	l_{scon}	z_{con}
Value	42	150	71.5	266±95	266	542.5
Unit	mm	mm	mm	mm	mm	mm
Symbol	p_1	p_2	r	w	v_0	ω_0
Value	20	160	62.5	99.5	75	0.38
Unit	mm/r	mm/r	mm	mm	mm/s	rad/s

of the other three DOFs of the platform, i.e., z, ϕ_x, and ϕ_y, are restricted due to the structural constraints of VEMOPAM (e.g., the strokes of the screw pairs). As shown in **Figs. 2.6** and **2.7**, the yaw ϕ_x of the platform has a significant effect on the movable range of its vertical displacement z. If ϕ_x is 0° [see **Fig. 2.7(a)**], the movable range of z, i.e., $l_{z1} + l_{z2}$, only depends on the stroke of screw pairs B1-C1 and B2-C2. However, if ϕ_x is close to 90° [see **Fig. 2.7(b)**], the movable range of z does not only depend on the stroke of B1-C1 and B2-C2, but also depends on the movement of B3-C3, which is determined by the value of ϕ_y.

2.4 PATH PLANNING FOR CARTS

In this section, a path planning method for carts A1 and A2 of VEMOPAM is presented. Vectors q_{ini} and q_{tar} are used to respectively represent the initial and target poses of the platform.

$$
\begin{aligned}
q_{\text{ini}} &= \left\{ x_0, y_0, z_0, \phi_{x0}, \phi_{y0}, \phi_{z0} \right\}^T, \\
q_{\text{tar}} &= \left\{ x_t, y_t, z_t, \phi_{xt}, \phi_{yt}, \phi_{zt} \right\}^T.
\end{aligned}
\tag{2.12}
$$

Substituting Eq. (2.12) into Eq. (2.2) yields vectors p_{ini} and p_{tar}, which respectively represent the initial and target poses of A1 and A2.

$$
\begin{aligned}
p_{\text{ini}} &= \{ x_{10}, y_{10}, \phi_{10}, x_{20}, y_{20}, \phi_{20} \}^T, \\
p_{\text{tar}} &= \{ x_{1t}, y_{1t}, \phi_{1t}, x_{2t}, y_{2t}, \phi_{2t} \}^T.
\end{aligned}
\tag{2.13}
$$

When A1 and A2 reach their target poses, the platform also reaches its target pose. However, with the nonholonomic constraints, the six outputs of VEMOPAM, i.e., the 6-DOF pose of the platform $\left\{ x, y, z, \phi_x, \phi_y, \phi_z \right\}$, cannot be simultaneously controlled by the four inputs, i.e., the speeds of the drive wheels of the carts. Our solution is to divide the path planning process into several steps. In each of the steps, fewer than four outputs are changed; the other outputs are fixed by the structural constraints. After the final step, all six outputs will have reached their target values. The following constraint conditions for VEMOPAM are considered in the design of the algorithm:

1) Due to the nonholonomic constraints, the motions of A1 and A2 in their lateral directions are restricted. As indicated in Eq. (2.10), these nonholonomic constraints for A1 and A2 may interact with each other via the SLPTM. Thus, the carts cannot move in a particular direction without some maneuvers, such as a turnabout.

2) For the miniaturization of VEMOPAM, screw pair B3-C3 should have a short stroke. This may increase the risk that nut C3 moves too far and hits at the end of the stroke of screw shaft B3. Therefore, the motions of the carts must be limited to ensure the safe use of B3-C3.

3) As described in Section 2.2-III, the pitch ϕ_y of the platform may be sensitive to the screw motions of B3-C3. To stabilize the motions of the platform, ϕ_y should not be changed for most of the movement time.

Such unique and complicated constraint conditions are not considered in conventional path planning methods. A custom path planning method that consists of four steps, named the Four-Step Path Planning (FSPP) method, is thus proposed for VEMOPAM. The first step is planned to move cart A1 to its target position, the second and third steps are planned to move cart A2 to its target position, and the fourth step is planned to rotate A1 and A2 until they reach the target angles of rotation. A detailed description of each step is given below.

I. First Step

Figure 2.8 shows the motions of A1 and A2 and the variation of the pose of the platform in the first step. A1 and A2 are expected to reach their target positions with a long-distance translation. If they directly move to their target positions, because of the screw movement of B3-C3, the pitch ϕ_y of the platform may greatly change, and C3 may hit at the end of the stroke, which is inconsistent with the path planning goals. To stabilize the motions of the platform, in the first step, a path is planned only for A1 to reach its target position; another path that is parallel to the path of A1 is planned for A2. In this step, two outputs, namely x and y, of the platform are changed.

A preliminary operation for this step, i.e., rotating A1 and A2, is necessary because of the nonholonomic constraints. The initial angles of rotation of A1 and A2, i.e., ϕ_{10} and ϕ_{20}, are represented in the following form:

$$
\begin{aligned}
\phi_{10} &= 2n_1\pi + \hat{\phi}_{10} \ \left(n_1 \in \mathbf{N}, -\pi < \hat{\phi}_{10} < \pi\right), \\
\phi_{20} &= 2n_2\pi + \hat{\phi}_{20} \ \left(n_2 \in \mathbf{N}, -\pi < \hat{\phi}_{20} < \pi\right).
\end{aligned}
\tag{2.14}
$$

Then, A1 is rotated at an angle of $\Delta\phi_1$ to set its forward or backward direction toward its target position. Simultaneously, A2 is rotated at angle of $\Delta\phi_2$ so that its forward direction is parallel to the forward direction of A1. The values of $\Delta\phi_1$ and $\Delta\phi_2$ are calculated using ϕ_{10} and ϕ_{20} as follows:

$$
\Delta\phi_i = \begin{cases}
\Delta\phi_i' & \left(\text{if } -\pi/2 \le \Delta\phi_i' < \pi/2\right), \\
\Delta\phi_i' - \pi & \left(\text{if } \Delta\phi_i' \ge \pi/2\right), \\
\Delta\phi_i' + \pi & \left(\text{if } \Delta\phi_i' < -\pi/2\right),
\end{cases}
\quad (i = 1, 2),
\tag{2.15}
$$

$$
\Delta\phi_1' = \tan^{-1}\frac{y_{1t} - y_{10}}{x_{1t} - x_{10}} - \hat{\phi}_{10}, \ \Delta\phi_2' = \tan^{-1}\frac{y_{1t} - y_{10}}{x_{1t} - x_{10}} - \hat{\phi}_{20}.
$$

Eqs. (2.14) and (2.15) guarantee that $|\Delta\phi_i| \le \pi/2 \ (i = 1, 2)$, which minimizes movement time. The rotational velocities of A1 and A2, which are respectively represented as ω_1 and ω_2, are set to $\omega_1 = \omega_2 = \omega_0$, where ω_0 is a rated rotational velocity. The angles of rotation for the carts after rotation are expressed in the following form:

$$
\begin{aligned}
\phi_{10} + \Delta\phi_1 &= 2n_1'\pi + \hat{\phi}_1, \\
\phi_{20} + \Delta\phi_2 &= 2n_2'\pi + \hat{\phi}_1, \left(n_1', n_2' \in \mathbf{N}, -\pi < \hat{\phi}_1 < \pi\right).
\end{aligned}
\tag{2.16}
$$

After the rotations of A1 and A2, if $\Delta\phi_1 \ne \Delta\phi_2$, the length of l_s may change from the initial value l_{s0} to l_{s1} due to the screw movement of B3-C3. The value of l_{s1} is expressed as follows:
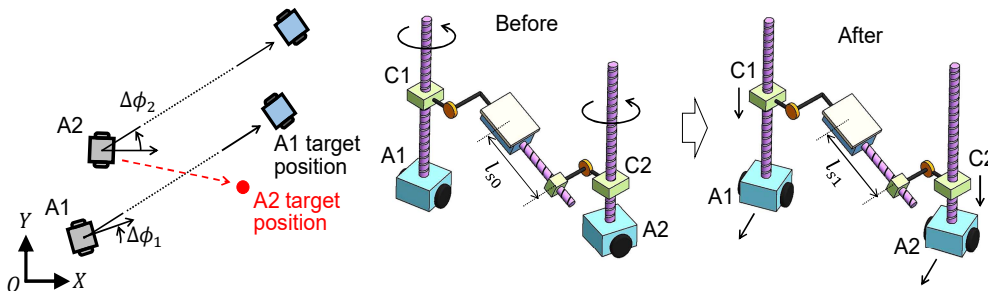

Fig. 2.8 Paths of carts and motions of platform in first step of path planning.

$$l_{s1} = -l_3 + \sqrt{a^2 + b^2},$$
$$a = -2l_1 + (x_{10} - x_{20})\sin\phi_{z0} - (y_{10} - y_{20})\cos\phi_{z0}, \tag{2.17}$$
$$b = p_1(\phi_{10} + \Delta\phi_1 - \phi_{20} - \Delta\phi_2)/(2\pi).$$

Because the difference between $\Delta\phi_1$ and $\Delta\phi_2$ is small, the change of l_s, i.e., $|l_{s1} - l_{s0}|$, is very small. By selecting a proper stroke for B3-C3, l_{s1} can be certainly limited within this stroke.

Next, A1 and A2 move at the same velocity until A1 reaches its target position. Their translational velocities, which are respectively represented as v_1 and v_2, are set to $v_1 = v_2 = v_0$, where v_0 is a rated translational velocity.

II. Second Step

Figure 2.9 shows the motions of A1 and A2 and the variation of the pose of the platform in the second step. After A1 is moved to its target position in the previous step, if A2 is also moved to its target position along the shortest path (red path in **Fig. 2.9**), due to the screw movements of B3-C3, ϕ_y would be greatly changed, and C3 may hit at the end of the stroke. To keep ϕ_y unchanged, A1 needs to be rotated to move nut C1 vertically. However, such a movement can greatly change the other five outputs, i.e., x, y, z, ϕ_x, and ϕ_z. Therefore, the second and third steps are designed so as to indirectly move A2 to its target position. The second step mainly changes three outputs, namely x, y, and ϕ_z, and sets ϕ_z to the target value ϕ_{zt}.

A preliminary operation, i.e., rotating A1 and A2 at the same angle of $\Delta\phi_3$, is necessary. To minimize the movement time, $\Delta\phi_3$ is calculated as follows:

$$\Delta\phi_3 = \begin{cases} \Delta\phi_3' & (\text{if } -\pi/2 \le \Delta\phi_3' < \pi/2), \\ \Delta\phi_3' - \pi & (\text{if } \Delta\phi_3' \ge \pi/2), \\ \Delta\phi_3' + \pi & (\text{if } \Delta\phi_3' < -\pi/2), \end{cases} \tag{2.18}$$

$$\Delta\phi_3' = \tan^{-1}\frac{y_{10} - y_{20}}{x_{10} - x_{20}} - \hat{\phi}_1 + \pi/2.$$

As done in the previous step, the rotational velocities of A1 and A2 are set to $\omega_1 = \omega_2 = \omega_0$. After rotation, the forward directions of A1 and A2 are both normal to the line of their CPs.

Then, a sector path for A2 is generated. The center of this path is the CP of A1, the radius r_c is the distance between the CPs of A1 and A2. The value of r_c is calculated using the initial positions of A1 and A2 as follows:
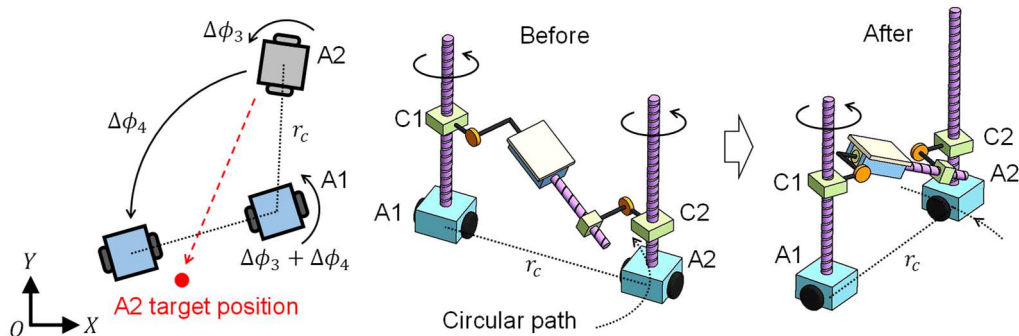

Fig. 2.9 Paths of carts and motions of platform in second step of path planning.

$$r_c = \sqrt{(x_{10} - x_{20})^2 + (y_{10} - y_{20})^2}. \tag{2.19}$$

The central angle $\Delta\phi_4$ of the sector path is set to

$$\Delta\phi_4 = \phi_{zt} - \phi_{z0}. \tag{2.20}$$

A2 moves on this path with a uniform velocity. Simultaneously, A1 rotates about its own CP in the same direction as that of the revolution of A2 to maintain the three outputs, i.e., z, ϕ_x, and ϕ_y, unchanged. The translational and rotational velocities of A1 and A2 are given as follows:

$$v_1 = 0, v_2 = v_0, \omega_1 = \omega_2 = v_0/r_c. \tag{2.21}$$

The angles of rotation for the carts after this step are expressed in the following form:

$$\begin{aligned}
\phi_{10} + \Delta\phi_1 + \Delta\phi_3 + \Delta\phi_4 &= 2n_1''\pi + \hat{\phi}_2, \\
\phi_{20} + \Delta\phi_2 + \Delta\phi_3 + \Delta\phi_4 &= 2n_2''\pi + \hat{\phi}_2, \left(n_1'', n_2'' \in \mathbf{N}, -\pi < \hat{\phi}_2 < \pi\right).
\end{aligned} \tag{2.22}$$

As indicated in Eq. (2.4), ϕ_z depends on only the relative positions of the carts. After the revolution of A2, ϕ_z changes from the initial value ϕ_{z0} to the target value ϕ_{zt}. In the next two steps, ϕ_z is kept unchanged.

III. Third Step

Figure 2.10 shows the motions of A1 and A2 and the variation of the pose of the platform in the
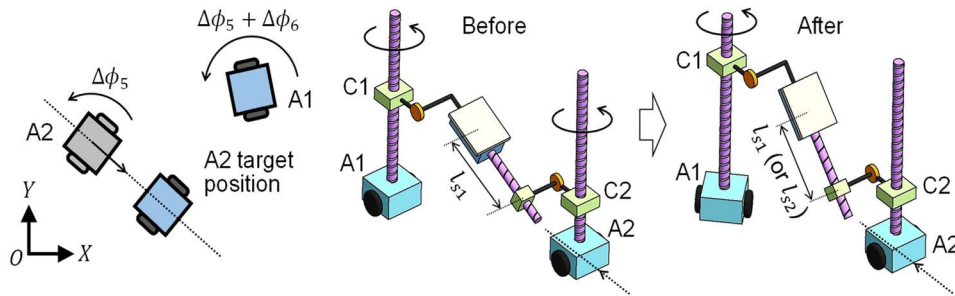

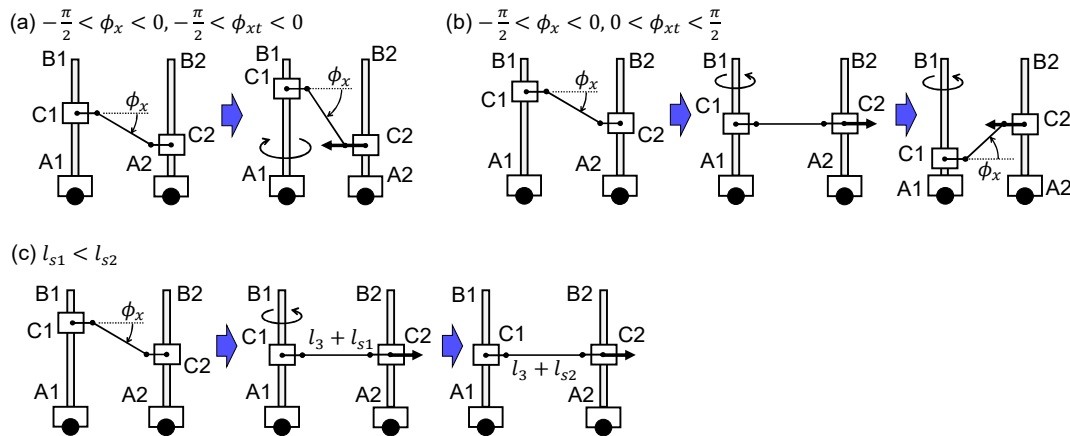Fig. 2.10 Paths of carts and motions of platform in third step of path planning.

Fig. 2.11 Examples of movements of nuts C1 and C2 in third step of path planning for (a) Case I, $-\pi/2 < \phi_x < 0$ and $-\pi/2 < \phi_{xt} < 0$; (b) Case II, $-\pi/2 < \phi_x < 0$ and $0 < \phi_{xt} < \pi/2$; and (c) Case III, $l_{s1} < l_{s2}$.

third step. This step is planned so as to move A2 to its target position. In this step, fewer than four outputs other than ϕ_z are simultaneously changed.

A1 and A2 rotated at the same angle of ϕ_5 before this step. The following equation, whose form is similar to Eq. (2.15), is used to calculate ϕ_5:

$$\Delta\phi_5 = \begin{cases} \Delta\phi_5' & \left(\text{if } -\pi/2 \leq \Delta\phi_5' < \pi/2\right), \\ \Delta\phi_5' - \pi & \left(\text{if } \Delta\phi_5' \geq \pi/2\right), \\ \Delta\phi_5' + \pi & \left(\text{if } \Delta\phi_5' < -\pi/2\right), \end{cases} \tag{2.23}$$

$$\Delta\phi_5' = \tan^{-1}\frac{y_{2t} - {}^3y_{20}}{x_{2t} - {}^3x_{20}} - \hat{\phi}_2,$$

where $\left({}^3x_{20}, {}^3y_{20}\right)$ indicates the position of A2 at the start of the third step and can be obtained from the previous two steps. As done in the previous steps, the rotational velocities of A1 and A2 are set to $\omega_1 = \omega_2 = \omega_0$. After rotation, the forward or backward direction of A2 is set toward its target position.

Then, a linear path for A2 is planned. By substituting the target position (x_{1t}, y_{1t}) of A1 and target roll ϕ_{zt} of the platform into Eq. (2.4), the following equation can be obtained,

$$(x_{1t} - x_2)\cos\phi_{zt} + (y_{1t} - y_2)\sin\phi_{zt} = 2l_2. \tag{2.24}$$

This equation is represented by the dotted lines shown in **Fig. 2.10**. If A1 is fixed at the target position and A2 is moved along this line, ϕ_z can be kept at the target value ϕ_{zt} due to the structural constraints of VEMOPAM. The movement direction of A2 is decided so as to limit the motions of B3-C3 within its stroke. The following three cases, shown in **Fig. 2.11**, are used to explain how to decide the motions of the carts.

1) Case I

As shown in **Fig. 2.11(a)**, at the start of the third step, if the yaw ϕ_x of the platform and its target value ϕ_{xt} satisfy the condition $\phi_x\phi_{xt} \geq 0$, A2 directly moves to its target position. At the same time, A1 is rotated to move nut C1 up or down to maintain length l_s at l_{s1}.

2) Case II

As shown in **Fig. 2.11(b)**, at the start of the third step, if ϕ_x and ϕ_{xt} satisfy the condition $\phi_x\phi_{xt} < 0$, A2 initially moves away from its target position until $\phi_x = 0$. A2 then moves in the opposite direction to approach its target position. At the same time, A1 is rotated to maintain length l_s at l_{s1}.

During the motions in Cases I and II, the two outputs ϕ_y and ϕ_z do not change. These motions are planned so as to make ϕ_x and ϕ_{xt} satisfy $\phi_x\phi_{xt} \geq 0$. The reason for this is explained in Section 2.4-IV.

3) Case III

As shown in **Fig. 2.11(c)**, when A2 reaches its target position, length l_s may increase. In this case, A2 initially moves toward its target position and A1 rotates to maintain l_s at l_{s1}. Similarly, ϕ_y and ϕ_z are not changed during the motion. When C1 reaches the height of C2 (i.e., the angles of rotation of the carts are the same, $\phi_1 = \phi_2$), A1 stops rotating but A2 continue moving, which changes l_s from l_{s1} to l_{s2} $(l_{s1} < l_{s2})$. The change in l_s can be limited within the stroke of B3-C3,

which is explained in Section 2.4-IV. Only ϕ_y is changed during this motion.

The displacements and velocities of A1 and A2 in the above three cases are now described in detail. By rearranging the first, second, fourth, and fifth equations of Eq. (2.2), the following equation can be obtained.

$$\cos\phi_x = \frac{(x_1 - x_2)\sin\phi_z - (y_1 - y_2)\cos\phi_z - 2l_1}{l_3 + l_s}. \tag{2.25}$$

After substituting the target positions of the carts, i.e., $\{x_{1t}, y_{1t}\}$ and $\{x_{2t}, y_{2t}\}$, the target roll $\phi_z = \phi_{zt}$, and $l_s = l_{s1}$ into Eq. (2.25), if the absolute value of the right-hand side of Eq. (2.25) is smaller than 1, i.e., $|(x_{1t} - x_{2t})\sin\phi_{zt} - (y_{1t} - y_{2t})\cos\phi_{zt} - 2l_1| \le l_3 + l_{s1}$, the methods described in Cases I and II are used to plan paths. In these cases, the rotational velocity of A1 is set to $\omega_1 = 4\omega_0$, based on which ϕ_1 at each moment and the total angle $\Delta\phi_6$ of rotation of A1 can be easily obtained. During the linear motion of A2, ϕ_2 does not change. Thus, we can substitute the values of ϕ_1 and ϕ_2 and $l_s = l_{s1}$ into Eq. (2.5) to calculate the time-varying value ϕ_x. Then, substituting the obtained ϕ_x, the target position $\{x_{1t}, y_{1t}\}$ of A1, the target roll ϕ_{zt}, and $l_s = l_{s1}$ into Eq. (2.25) yields the following equation.

$$\cos\phi_x = \frac{(x_{1t} - x_2)\sin\phi_{zt} - (y_{1t} - y_2)\cos\phi_{zt} - 2l_1}{l_3 + l_{s1}}. \tag{2.26}$$

By using Eqs. (2.24) and (2.26), the position $\{x_2, y_2\}$ of A2 at each moment can be planned.

On the other hand, the path planning method for the carts described in Case III is used if $|(x_{1t} - x_{2t})\sin\phi_{zt} - (y_{1t} - y_{2t})\cos\phi_{zt} - 2l_1| > l_3 + l_{s1}$. The position of A2 can be calculated using the same method used in Cases I and II until A1 stops rotating. When $\phi_1 = \phi_2$, A1 stops rotating and A2 continues moving with the velocity $v_2 = v_0$.

IV. Fourth Step

Figure 2.12 shows the motions of A1 and A2 and the variation of the pose of the platform in the fourth step. This step is planned so as to rotate A1 and A2 multiple times until they reach the target angles of rotation (ϕ_{1t} and ϕ_{2t}). The angles of rotation of A1 and A2 are represented by $\Delta\phi_7$ and $\Delta\phi_8$, respectively. After this final step, all six outputs will have reached their target values.

Here, an explanation for Cases I, II, and III of the third step (see above) is given. For example, if the value of ϕ_x before the fourth step is $-\pi/4$ and its target value ϕ_{xt} is $\pi/4$, during the fourth step, ϕ_x first changes from $-\pi/4$ to 0 and then changes to $\pi/4$. When ϕ_x becomes 0, nuts C1 and C2 reach the same height and length l_s becomes its shortest value. At this time, nut C3 may hit at the end of its stroke. To avoid this problem, we use the methods described in Cases I and II to ensure that $\phi_x\phi_{xt} \ge 0$ before the fourth step. In the third step, if the paths are planned using the method described in Case III, length l_s is increased to l_{s2} ($l_{s2} < l_{s3}$). As long as l_{s3} is within the stroke of B3-C3, l_{s2} is also within the stroke.

V.   Design of Path Planner

Figure 2.13 shows the path generation process of the FSPP method. Based on this method, a path planner is developed. This planner has the following advantages:

   1) The paths are planned using the basic movements shown in **Fig. 2.3**. The carts move with a
      uniform velocity, except for the movements of A2 in the third step. This simplifies the
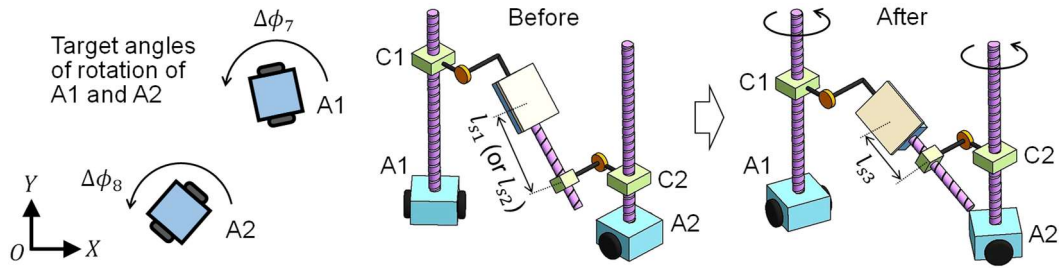
Fig. 2.12 Paths of carts and motions of platform in fourth step of path planning.
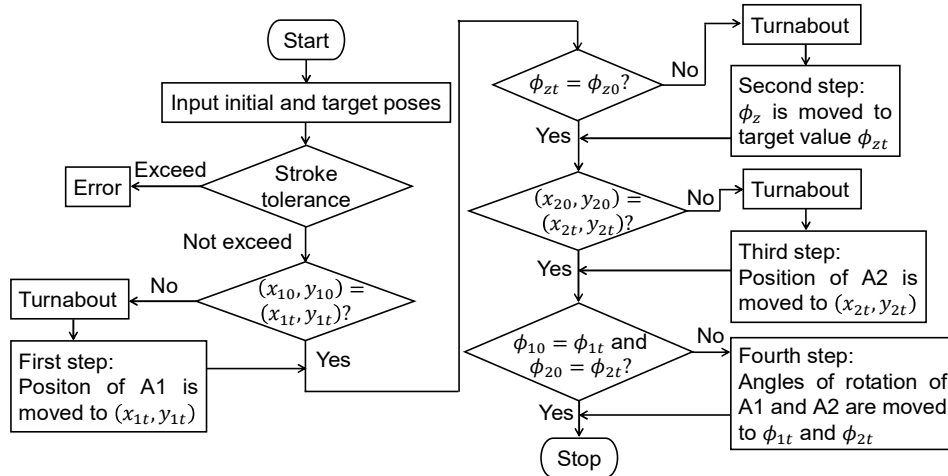

Fig. 2.13 Flow chart of FSPP method.

decentralized control system for the carts.

2) Only the initial and target poses of the platform need to be input into the planner. B3-C3 will never travel out of its stroke during the four steps as long as its initial and target screw displacements are within the stroke. Therefore, measurement devices for the movements of B3-C3, such as proximity sensors, are unnecessary.

3) B3 is rotated mainly in the fourth step. Thus, drastic changes in ϕ_y can be avoided in the first three steps.

In the next two sections, the performance of this planner is evaluated using simulations and experiments.

2.5 SIMULATION

The above kinematic analysis and path planning method were based on the rolling-without-slipping condition for carts A1 and A2 which is represented by Eq. (2.8). However, if the moving carts deviate from the specified paths due to small wheel slips, this deviation may accumulate during cart motion. Therefore, a feedback control strategy is needed for the carts to track the paths. Various feedback controller based on the dynamic models of mobile robots have been proposed. Jiang and Nijmeijer gave a simplified dynamic model for a mobile robot and applied backstepping control to realize both the local and global stabilization of this robot [72]. Fierro and Lewis also constructed a dynamic model for a nonholonomic vehicle and presented a controller using backstepping [73]; and then they presented a neural network controller for three navigation problems: trajectory tracking, path following, stabilization about a specified posture [74]. Uncertainties in a vehicle model, such as

errors in the sizes of vehicle body and wheels, may adversely affect the stability of feedback control. Fukao *et al.* discussed this problem and gave some adaptive control rules to eliminate the effect of unknown parameters in the vehicle's model on the control stability [75, 76]. On the other hand, many formation control methods [81–84] have also been presented for multi-mobile-robot systems to perform complicated tasks [77], such as transportation [78, 79] and environment exploration [80].

All the above studies focused on the control methods based on the dynamics of mobile robots. Such methods are particularly valid for high-velocity moving robots. However, with the low-velocity condition, kinematics-based tracking control methods are also effective and can be realized more easily. For example, Samson and Ait-Abderrahim gave several control principles for a kinematic cart model in a Cartesian space [70]. Normey-Rico *et al.* developed a simple PID controller, which was robust to any model errors, for a nonholonomic mobile robot [71]. In this research, for the developed kinematic model of VEMOPAM, a simpler and more realizable tracking control method proposed by Kanayama *et al.* is employed [69].

In this section, some simulations are performed to verify the validity of the FSPP method and the tracking control strategy. The changes in the pose of the platform and the carts in each step are investigated.

I. Tracking Control Strategy

Vectors $\boldsymbol{p}_i = \{x_i, y_i, \phi_i\}^T$ and $\boldsymbol{p}_{a,i} = \{x_{a,i}, y_{a,i}, \phi_{a,i}\}^T$ are utilized to represent the planned and actual positions and angles of rotation of A1 and A2, respectively. If the carts deviate from the planned paths, the difference between $\boldsymbol{p}_i$ and $\boldsymbol{p}_{a,i}$ with respect to $O_{c,i} - X_{c,i} Y_{c,i} Z_{c,i}$ can be given as follows:

$$\begin{Bmatrix} x_{e,i} \\ y_{e,i} \\ \phi_{e,i} \end{Bmatrix} = \begin{bmatrix} \cos\phi_{a,i} & \sin\phi_{a,i} & 0 \\ -\sin\phi_{a,i} & \cos\phi_{a,i} & 0 \\ 0 & 0 & 1 \end{bmatrix} (\boldsymbol{p}_i - \boldsymbol{p}_{a,i}), (i = 1, 2). \tag{2.27}$$

Following Kanayama *et al.* [69], the actual translational and rotational velocity commands for the carts, i.e., $v_{c,i}$ and $\omega_{c,i}$, are obtained using the planned translational velocity v_i and rotational velocity ω_i as follows:

$$\begin{aligned} v_{c,i} &= v_i \cos\phi_{e,i} + K_x x_{e,i}, \\ \omega_{c,i} &= \begin{cases} \omega_i + v_i \left(K_y y_{e,i} + K_\phi \sin\phi_{e,i} \right), (\text{if } v_i \geq 0), \\ \omega_i + v_i \left(K_y y_{e,i} - K_\phi \sin\phi_{e,i} \right), (\text{if } v_i < 0), \end{cases} (i = 1, 2), \end{aligned} \tag{2.28}$$

where K_x, K_y, and K_ϕ are positive constants. They are set to $K_x = 1$ s^{-1}, $K_y = 25$ m^{-2}, and $K_\phi = 5$ m^{-1}. This control rule has been proven to be stable using Lyapunov stability theory [69]. By substituting $v_{c,i}$ and $\omega_{c,i}$ into the following equation, the rotational speeds of the left and right drive wheels of each cart, i.e., $\omega_{l,i}$ and $\omega_{r,i}$, can be obtained:

$$\begin{Bmatrix} \omega_{l,i} \\ \omega_{r,i} \end{Bmatrix} = \frac{1}{r} \begin{bmatrix} 1 & -w \\ 1 & w \end{bmatrix} \begin{Bmatrix} v_{c,i} \\ \omega_{c,i} \end{Bmatrix}, (i = 1, 2), \tag{2.29}$$

where r is the radius of the drive wheel, and w is the distance between the CP of the cart and the touchdown point of the drive wheel (see **Fig. 2.2**). To make the carts smoothly track the paths, a limiter is applied to limit the maximum rotational speed of the drive wheels to 1.91π rad/s.

Table 2.2 Initial and target poses of platform and carts.

	x [mm]	y [mm]	z [mm]	ϕ_x [rad]	ϕ_v [rad]	ϕ_z [rad]
Initial pose	0	0	542.5	0	0	0
First target pose	600	300	450	$\pi/4$	$-\pi/2$	$2\pi/3$
Second target pose	1200	600	500	$\pi/6$	$\pi/2$	$\pi/3$
	x_1 [mm]	y_1 [mm]	ϕ_1 [rad]	x_2 [mm]	y_2 [mm]	ϕ_2 [rad]
Initial pose	150	-113.5	0	-150	308	0
First target pose	605.2	476.2	15.0π	451.2	40.9	-11.7π
Second target pose	1365.0	677.9	8.2π	919.1	589.0	-6.7π
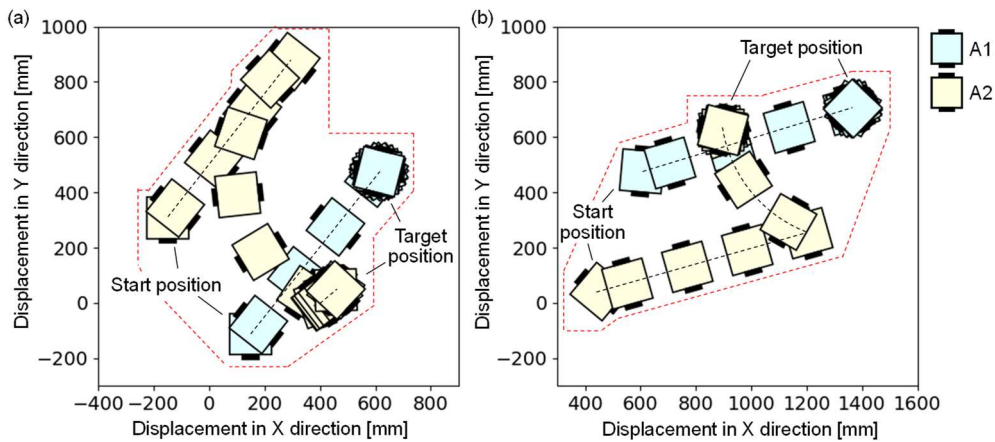
Fig. 2.14 Planned paths for simulations: (a) from initial pose to first target pose and (b) from first target pose to second target pose.

II. Simulation Conditions and Results

The parameters for VEMOPAM's model (see **Fig. 2.2**) used for the simulations are shown in **Table 2.1** in Section 2.3-III. The next section introduces an experimental prototype of VEMOPAM with the same parameters and explains the design of these parameters in detail. Two sets of simulations, in which the initial and target poses of the platform and the carts are set as shown in **Table 2.2**, are performed. First, the platform is moved from the initial pose to the first target pose (first set). Then, it is moved from the first target pose to the second target pose (second set)

Under the above simulation conditions, the motions of A1 and A2 were planned by the FSPP method as shown in **Fig. 2.14**. The red dotted lines show the space necessary for the carts to move. As long as no obstacles exist in this space, the carts can reach the target positions. The poses of the carts were then simulated; the results of the simulations are shown in **Fig. 2.15**. The results in the ideal situation are indicated by solid lines and the target poses shown in **Table 2.2** are indicated by black horizontal dotted lines. To demonstrate the effectiveness of the tracking control method, a situation in which the carts deviated due to disturbances was simulated. The disturbances acted on A1 at 35, 80, 101.8, and 115 s, and acted on A2 at 0, 18, 115, and 126 s. These disturbances all had the same magnitude. **Fig. 2.15** shows that the carts automatically tracked the planned paths even when they were disturbed, which verifies the validity of the tracking control strategy. And the screw pairs did not exceed their strokes during the motion. These results verify the three advantages of the FSPP method shown in Section 2.4-V.

Changes in the pose of the platform in the four steps were also simulated; **Fig. 2.16** shows the results. As shown in this figure, with the tracking control method, the platform can be accurately
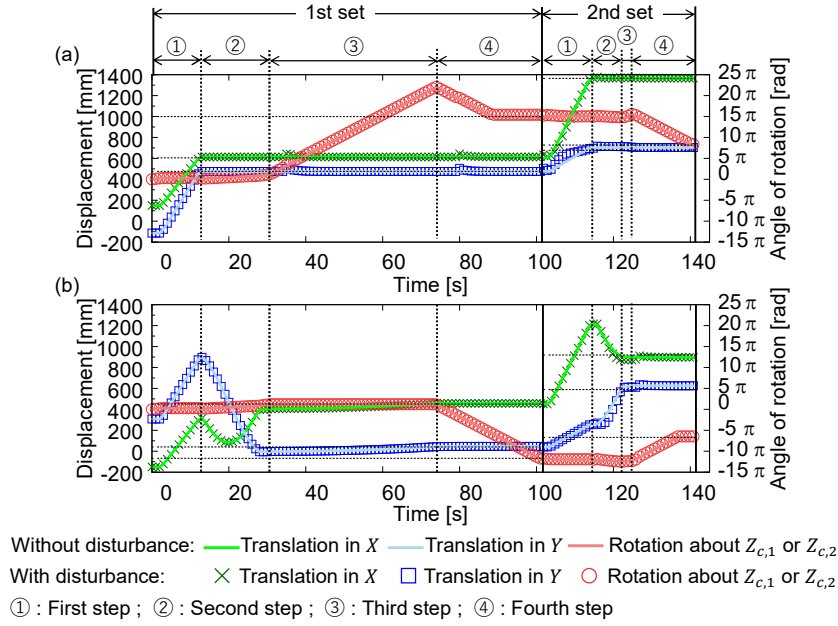
Fig. 2.15 Poses of (a) A1 and (b) A2 in four steps of path planning.
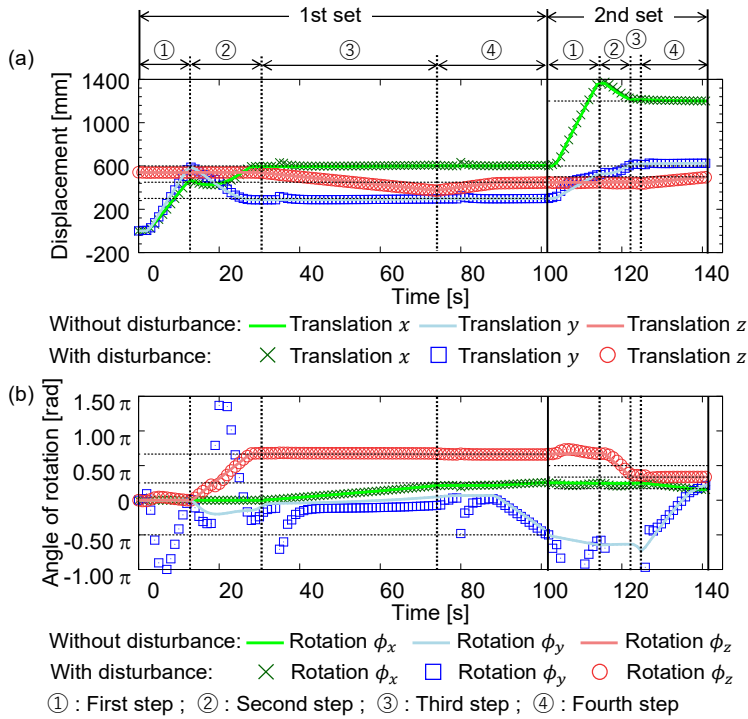
Fig. 2.16 Simulation results of (a) position and (b) orientation of platform in four steps of path planning.

moved to its first and second target poses. The changes in the position $\{x, y, z\}$, yaw ϕ_x, and roll ϕ_z of the platform caused by the disturbances were very small. However, the pitch ϕ_x drastically changed. This result indicates that the sensitivity of ϕ_y to external disturbances is significantly larger than those of the other five outputs, which agrees with the prediction in Section 2.2-III. The next section discusses how to reduce the sensitivity of ϕ_y using a speed reduction mechanism.

2.6   EXPERIMENT

This section introduces the constructed prototype of VEMOPAM and shows the experimental results.

I. Development of Prototype

A prototype of VEMOPAM was constructed (see **Fig. 2.17**). The specifications of this prototype are shown in **Table 2.1**. Regarding the design of these specifications, this study first considered the specifications of the screw pairs (the strokes, leads, etc.), then determined the workspace of the platform, and finally designed the sizes of the other structures to guarantee that the size of the whole mechanism is small and that the two carts could avoid with each other. This prototype had two 2WD carts A1 and A2 that were separately controlled. Each cart had a mini-computer and two motors. Appendix 2 shows the detailed design of the carts. In this experiment, the load on the platform is its own weight.
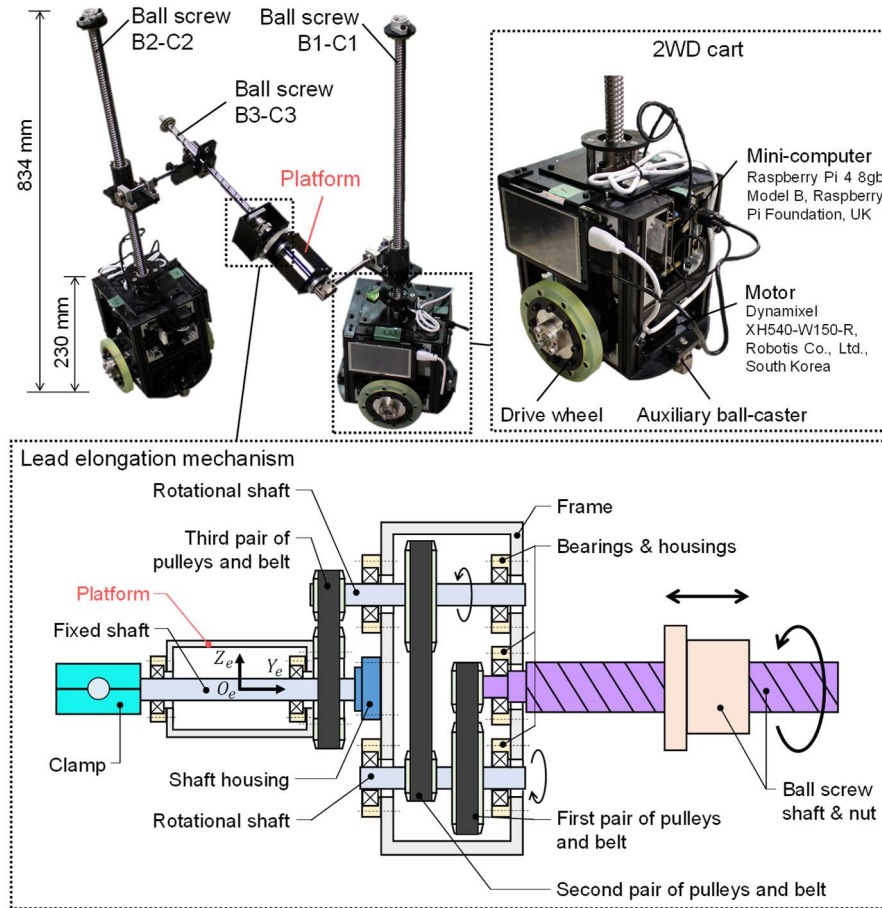

Fig. 2.17 Prototype of VEMOPAM, close-up view of 2WD cart, and structure of lead elongation mechanism.
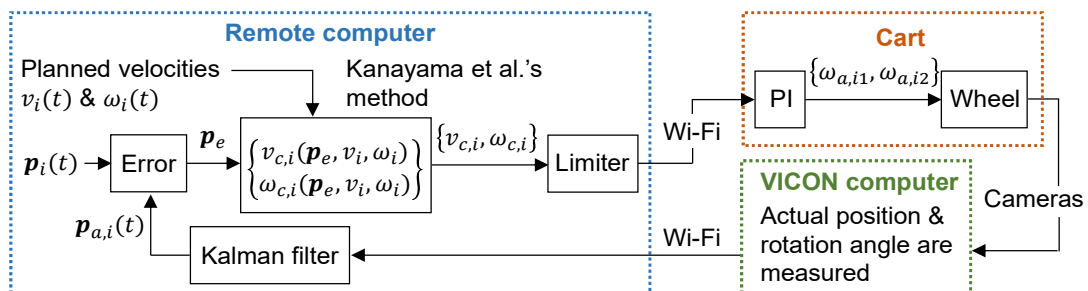

Fig. 2.18 Feedback tracking control system.

Three ball screws were used as screw pairs B1-C1, B2-C2, and B3-C3. As shown in **Table 2.1**, B1-C1 and B2-C2 had the same stroke (450 mm) and lead (20 mm/r), and B3-C3 had a shorter stroke (190 mm) and a larger lead (160 mm/r). These strokes and leads guaranteed that ϕ_x could change within the range of $-\pi/2$ to $\pi/2$, and ϕ_y and ϕ_z could change within the range of $-\pi$ to π. However, most large-lead ball screws on the market are large and heavy, which adversely affects the stability of the mechanism. Therefore, a ball screw with a lead of 20 mm/r was selected as B3-C3; and a speed reducer, named the lead elongation mechanism (LEM), to increase the equivalent lead of B3-C3 to 160 mm/r. As shown in **Fig. 2.17**, the LEM had three pairs of timing pulleys and belts; the transmission ratio of each pair was 1:2. Screw shaft B3 was connected to the LEM via a radial bearing with a proper allowable thrust load. With this configuration, for every eight rotations of B3, one rotation was transmitted to the platform. Hence, a 1-mm error in the screw motion of B3-C3 results in a 2.25° error of ϕ_y, which is considered to be tolerable.

II. Feedback Control System

Figure 2.18 shows the feedback control system for VEMOPAM. To measure the motions of the platform and the carts, six markers were fixed on the platform and three markers were fixed on the each of the carts. Six VICON motion capture cameras (VICON MX Bonita, Vicon Motion Systems Ltd., UK) surrounding VEMOPAM were used to measure the positions of the markers. **Table 2.3** gives the specifications for the cameras. A computer with a VICON motion tracking application (VICON Tracker) installed was used to record and send the position information of markers to a remote computer. A Kalman filter was used to eliminate inaccuracies and noise in the position information. Then, on the remote computer, the forward and rotation speed commands of the carts were determined using Kanayama's method [69], as described in the previous section. These commands were sent from the remote computer to the mini-computers on the carts every 0.1 s. The speed commands of the drive wheels were then calculated and sent to the motors. To accurately output these speed commands, a proportional-integral (PI) controller for each motor was used (the gains were $K_p = 100$ and $K_i = 1920$). The computers communicated with each other over Wi-Fi. The commands from the remote computer were sent to A1 and A2 in simultaneous multithreading mode, which ensured that they started moving at precisely the same moment. Before the experiment, we conducted preliminary experiments to decide the parameters for the control system (e.g., the gains) and to confirm its stability.
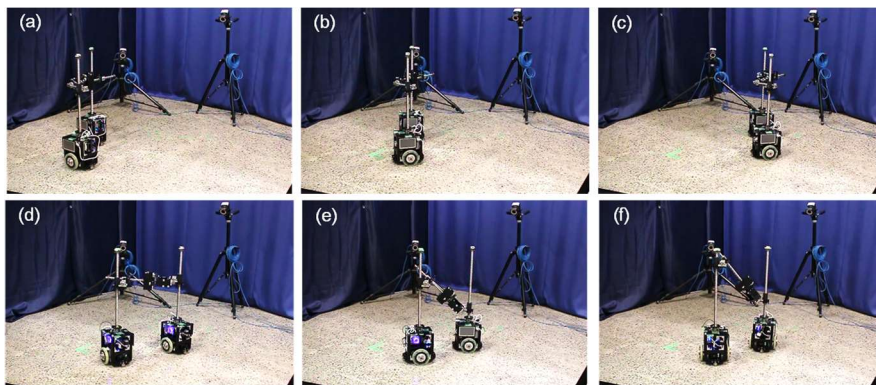

Fig. 2.19 Image sequence of carts during experiment. (a) Initial pose; (b) start of first step; (c) end of first step/start of second step; (d) end of second step/start of third step; (e) end of third step/start of fourth step; and (f) target pose.

Table 2.3 Specifications for VICON motion capture cameras.

Frame rate	Maximum shutter time	Resolution
240 Hz	0.5 ms	0.3 megapixel [640×480]
System latency	Operating range	Focal length of lens
2 ms	12 m	4−12 mm

III. Experimental Results and Discussions

By using the prototype, an experiment was conducted to assess the validity of the FSPP method. The initial and target poses of the platform were the same as those in the first set of simulations (i.e., the initial and the first target poses given in **Table 2.2**). **Fig. 2.19** shows photographs of the carts during the experiment. As shown, the prototype worked as expected.

Figure 2.20 shows the poses of A1 and A2 in the experiment. With the feedback control system, the carts approximately tracked the planned paths, verifying the validity of the FSPP method. However, a deviation of 429.9° occurred in the angle of rotation of A1 when the motion stopped. This might have occurred for the following reason. In the third step, due to the load from C1, A1 excessively rotated, which resulted in an error in the angles of rotation of the carts, i.e., $\phi_{e,i}$. The control rule represented by Eq. (2.28) indicates that when the carts were planned to be stopped in the fourth step (i.e., $v_i = \omega_i = 0$), $\phi_{e,i}$ could not be corrected in time because $\omega_{c,i} = 0$.

Figure 2.21 shows the pose of the platform in the experiment. The errors between the desired pose and the actual pose were measured every 0.1 s; and the average errors are shown in **Fig. 2.22**. The error bars show the confidence interval at a 5% significance level. As shown in these figures, displacements x and y approximately reached their target values, whereas z deviated by 13.5 mm. The result of Welch's t-test demonstrates that the average error in z for the fourth step was significantly larger than those for the other steps, which is considered to have been caused by the deviation in the rotation of A1. Orientation angles ϕ_x and ϕ_z approximately reached their target values, whereas ϕ_y deviated by about 57.9° from the target value. The result of Welch's t-test shows that the average errors in ϕ_y were significantly larger than those of ϕ_x and ϕ_z for all four steps. This agrees with the prediction that ϕ_y has a high sensitivity. Welch's t-test also shows that the average error in ϕ_y for the fourth step is significantly larger than those for the other steps, as shown in **Fig. 2.22(b)**. The reason for this is that ϕ_y was changed mainly in the fourth step, as planned.

Then, the possibility of improvement through the optimization of the design parameters is discussed. First of all, increasing the transmission ratio of the LEM can reduce the sensitivity of ϕ_y. For example, if the current transmission ratio is doubled to 1:16, the errors in ϕ_y can be theoretically reduced by 50%. However, in this case, with the current stroke of B3-C3 (190 mm), the movable range of ϕ_y becomes smaller ($-\pi/2$ to $\pi/2$). Conversely, to maintain the current movable range of ϕ_y, a stroke of the twice length is required. Thus, the parameters should be optimized by considering the error tolerance, movable range, and the size of the robot. Additionally, another approach to handle the error of ϕ_y can be considered. As described above, the errors in ϕ_y become significantly large in the fourth step. Thus, a robust control system for the rotations of the carts in this step would also effectively reduce the errors in ϕ_y.

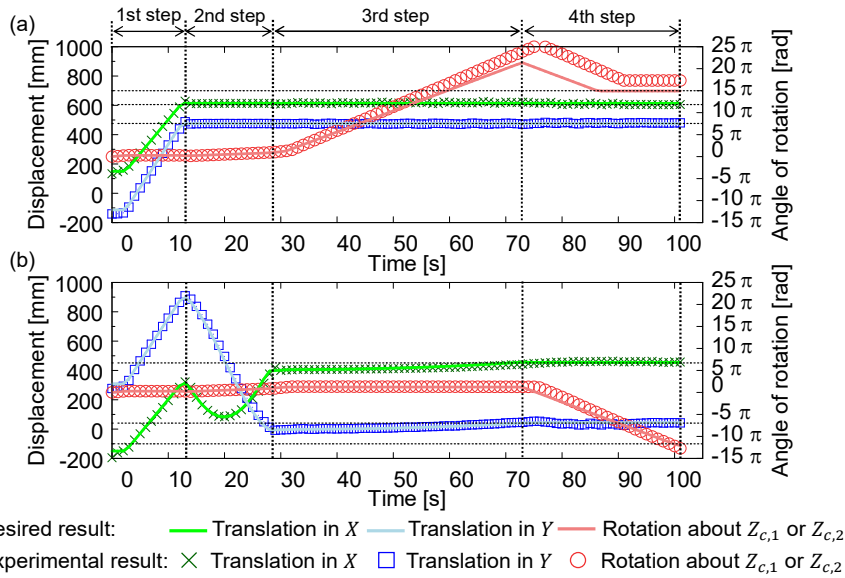**Fig. 2.20** Experimental results of poses of (a) A1 and (b) A2.
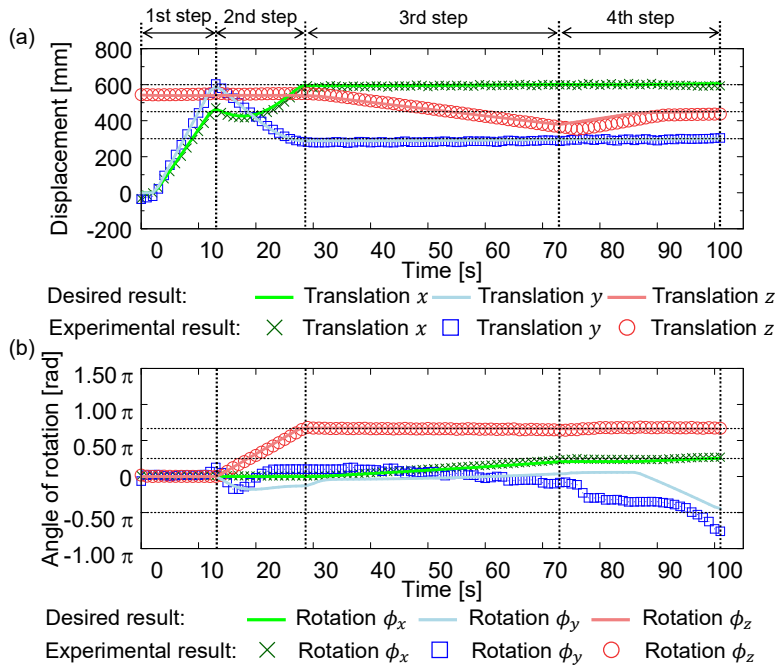

Fig. 2.21 Experimental results of (a) position and (b) orientation of platform.
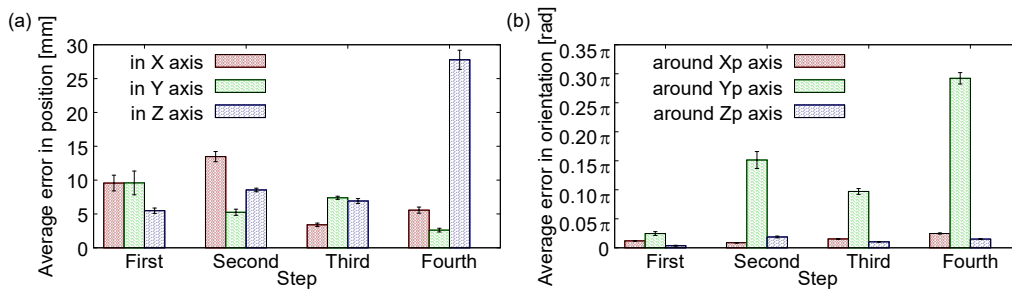
Fig. 2.22 Average errors in (a) position and (b) orientation of platform.

2.7 SUMMARY

This research proposed a novel MPM named VEMOPAM that consists of two 2WD carts and a parallel mechanism. The 6-DOF pose of the platform of VEMOPAM is controlled by the 2-DOF motions of the carts. Compared with conventional MPMs, VEMOPAM has fewer motors, which reduces the cost, weight, and size of the robots. A series of analyses and experiments were conducted in this study; the obtained analysis results are given below:

1) This chapter described the structure of VEMOPAM and analyzed the inverse kinematics.

2) This chapter proposed a path planning method for the two carts, and described the path generation in detail. This path planning method is also applicable for parallel mobile manipulators with other types of nonholonomic carts.

3) Simulations were conducted to investigate the motions of the platform. The simulation results confirmed that the platform reached the target pose as desired, and showed that its pitch ϕ_y is significantly sensitive to disturbances.

4) A prototype of VEMOPAM was developed for experiments. The experimental results showed that the pose, except for ϕ_y, of the platform approximately reached the target pose.

Two screw shafts B1 and B2 are unilaterally fixed on carts A1 and A2, respectively. However, in the future, all the movable parts of this prototype could be mounted on one frame to improve vibration resistance. The optimal design method for each part will be discussed. An obstacle avoidance method for the carts will also be considered in future research. In addition, the dynamics of VEMOPAM will be analyzed; and a robust controller will be developed to improve the control accuracy of ϕ_y.

CHAPTER 3

Effect of Viewpoint Change on Body Motion- and Button-Based Robot Operation

3.1 INTRODUCTION

The previous chapters introduced the use of mobile manipulators, including MSMs and MPMs, and proposed an MPM, namely VEMOPAM. A TP with multiple buttons can be used to operate such mobile manipulators. However, if a TP is used to carry out complicated robot operations, it is difficult for novice operators to quickly understand the role of each button and learn how to operate it. Thus, comparing with this button-based operation method, operating robots by human upper or lower limbs, i.e., the body motion-based operation method, is known to be much easier for novice operators.

Chapter 1 has showed some previous research on the body motion-based operation methods, and raised a problem of viewpoint change. As shown in **Fig. 1.9**, if a mobile manipulator is remotely operated by an operator who is sitting or standing in a fixed position, because of the horizontal motions of this mobile manipulator on the floor, the viewpoint of the operator relative to the manipulator frequently changes. When such viewpoint changes occur, depending on the operation method, the operator needs to imagine the manipulator's current orientation relative to the desired direction of movement, which makes it difficult to operate the manipulator as expected. Rotating a three-dimensional object in one's mind is commonly called "mental rotation" and defined as one of the main factors within human's spatial ability [109, 110]. It has been found that the reaction time of such a mental rotation generally becomes longer as the angle of rotation of the object increases [111, 112]. Most of the earlier research measured the reaction time using paper-and-pencil tests [113, 114], in which the observed objects were static. Hunt *et al.* added moving elements into the assessment of spatial ability for the first time [115]; the characteristics of dynamic spatial ability have been investigated by D'Oliveira [116].

It has been verified that mental rotation ability has a strong correlation with the teleoperation performance of robots [117], and therefore recent studies on the influence of mental rotation on robot teleoperation has been vigorous. Ito *et al.* evaluated the work efficiency of heavy machines in an unmanned construction environment in which image processing technology was used, and conducted a comparative experiment to investigate the effect of image conditions from multiple viewpoints on the operator's psychological workload [118]. Menchaca-Brandan *et al.* assessed the operator's spatial identification and perspective-taking abilities when operating a robotic arm remotely on a spacecraft [119]. DeJong *et al.* discussed the workload caused by the viewpoint change between the robot and cameras and between the operator and monitors, and surveyed the influence of this viewpoint change in single-camera-display and multi-camera-display devices [120]. Long *et al.* investigated the influence of visual spatial ability on the completion time and safety of the teleoperation of an uninhabited ground vehicle [121, 122]. Pan *et al.* evaluated the effects of spatial ability and cognitive style on the performance of cross-aiming teleoperation based on the cognitive fit theory [123, 124]. Besides, Nakagomi *et al.* showed how to improve the operability by displaying several VR vectors on the screen of the operation monitor to show the direction of movement [125].

Notably, the above-mentioned research examined the influence of viewpoint change for only one specific operation method. Nevertheless, it is quite possible that viewpoint change has a different influence on different operation methods. To date, a method for evaluating viewpoint changes that can be applied uniformly to different operation methods has been unavailable, making it impossible to effectively compare the effect of viewpoint change on different operation methods, measure differences in working time, or determine the cause of any detected differences. This makes the selection of an operation method based on a quantitative evaluation of the relative effects of viewpoint change extremely difficult. In response, an evaluation method is proposed to evaluate the influence of viewpoint change on the operability of various operation methods. To demonstrate its potential, this method is applied to quantify the effect of viewpoint change on the button- and body motion-based methods.

3.2   EVALUATION SYSTEM

Under the assumption that a mobile manipulator will be operated with either a TP or an operator's upper limb gestures, an evaluation system was constructed to evaluate the effect of viewpoint change on the operability of the two teaching methods. Below is an outline of the proposed system, which is based on the evaluation system developed in the earlier study [100].

I. Outline of Evaluation System

In the current study, the focus is on robot operation by novice operators. There are two reasons for this: first, the operation methods cannot be assessed fairly if the operator is proficient in one of the two methods; second, as the use of robots becomes more widespread, it will become increasingly necessary to hire individuals who are relatively unfamiliar with robots to work as operators.

For such novices to operate easily and safely, rather than operating a real robot in real space, the operators in this study were asked to manipulate an imaginary robotic hand (IRH) of a mobile manipulator in a virtual operation space (VOS). As shown in **Fig. 3.1**, the VOS was represented by a cube with five green frames and one red frame, so that the orientation of the VOS could be easily
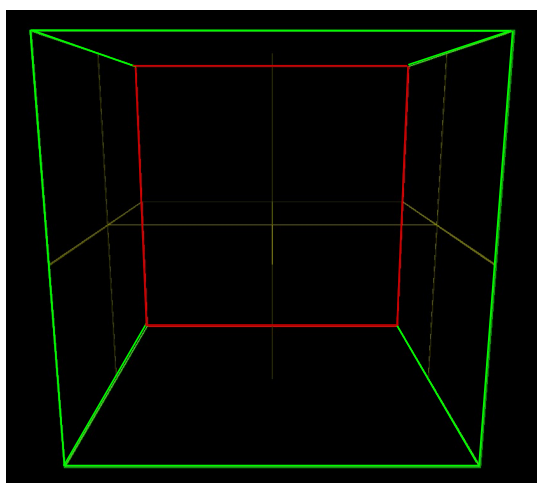

Fig. 3.1 Virtual operation space (VOS) on the screen with five green faces and one red face.
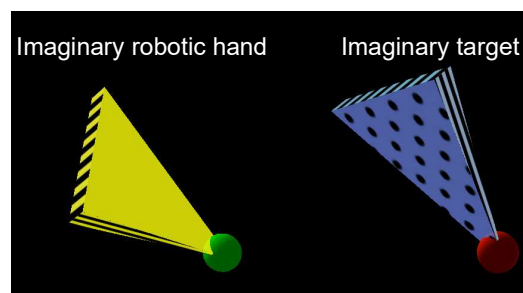
Fig. 3.2 Imaginary robotic hand (IRH, yellow, on left) and target (blue, on right) displayed as two triangular objects with a ball on vertex, a polka dot pattern on back side, and some stripes on lateral and bottom sides.

confirmed when the viewpoint was changed. Furthermore, as shown in **Fig. 3.2**, the IRH manipulated by the operator was represented by a yellow triangle, while its target status was represented by a blue triangle. The spheres fixed to the tips of the triangles denote the positions of the IRH and target, and the orientations of these triangles denote their postures. Polka dot patterns were attached to the back sides of these triangles to distinguish their front and back sides. In addition, stripes with different directions were attached to the lateral and bottom sides. The two triangles had the same shape, size, and pattern on their surfaces, and were only different in color.

Figure 3.3 is a schematic diagram showing the configuration of the evaluation system. The VOS and IRH created in the PC were displayed to the operator on a screen using a dedicated projector. The operator was able to watch the image on the screen stereoscopically by wearing 3D glasses; he/she sat on a chair in front of the screen to perform the operation. The viewpoint was changed by

Fig. 3.3 Schematic diagram of evaluation system.

Fig. 3.4 Two reference frames used to depict position and posture of operator's hand: (a) operator frame fixed to body; and (b) hand frame fixed to tip of right hand.

Fig. 3.5 Two reference frames used to depict position and posture of IRH: (a) VOS frame fixed to center of VOS; and (b) IRH frame fixed to its sphere.

altering the orientation of the VOS displayed to the operator, as described below.

II.   Reference Frames and Viewpoint Change

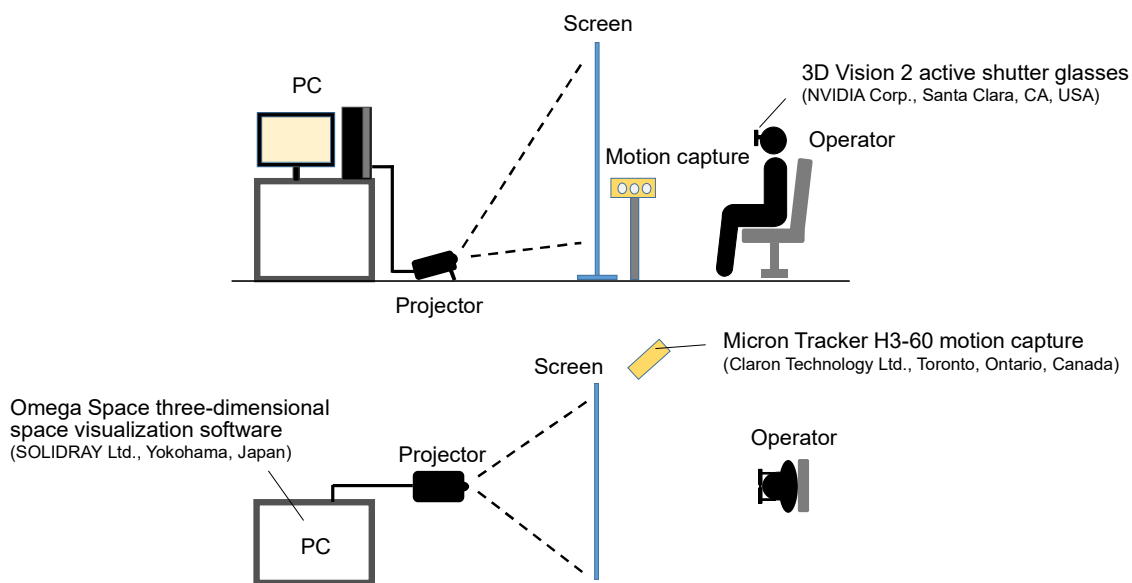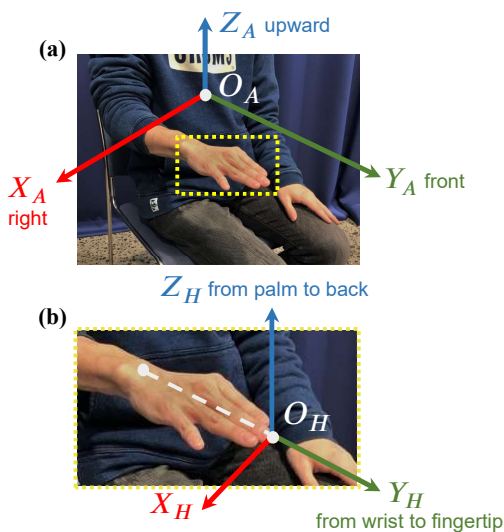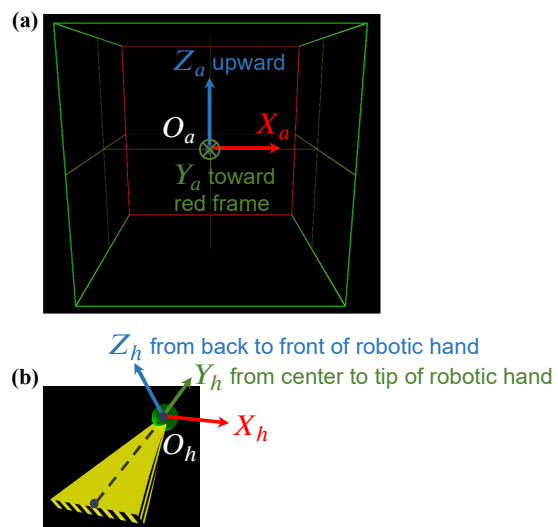To depict the position and posture of the operator's hand, two right-hand reference frames, i.e., the operator frame $O_A-X_AY_AZ_A$ and hand frame $O_H-X_HY_HZ_H$ shown in **Fig. 3.4**, were defined. And, the IRH's position and posture were depicted using the VOS frame $O_a-X_aY_aZ_a$ and IRH frame $O_h-X_hY_hZ_h$ shown in **Fig. 3.5**. This VOS frame $O_a-X_aY_aZ_a$ is equivalent to a robot frame fixed to the robot base, which is used in actual robot operation.

Figure 3.6 illustrates the concept of viewpoint change used in this thesis. **Fig. 3.6(a)** shows that an operator faces a fixed robot while walking around this robot along the perimeter of a circle whose center is the robot. At any point, the operator's position is described by the central angle α, which is defined as the viewpoint angle. **Fig. 3.6(b)** shows that an operator stands in a fixed position and faces a mobile robot. This robot is rotating around its own center. At any point, the angle of rotation of the robot is also described by the viewpoint angle $-\alpha$. Importantly, the viewpoint angle can be used to describe two situations. In this study, the viewpoint change is realized by rotating the VOS displayed on the screen around Z_a rather than having the operator move. With this method, it is unnecessary for the operator to move, and all experimental conditions other than viewpoint change can be fixed, which guarantees the validity of the evaluation of the influence of viewpoint change on operability. When the directions of the three axes X_A, Y_A, and Z_A are the same with those of X_a, Y_a, and Z_a, respectively, the viewpoint angle is $\alpha = 0°$.

III.   Body Motion-Based Operation Method

As an illustrative body motion-based operation method, this study adopted a leader-follower type of method to operate the six DOFs of the robotic hand's position and posture. The IRH was moved so that the changes in the position and posture of the operator's hand and the IRH observed from the operator's viewpoint were the same in the operation. However, since the range of motion (ROM) of a human hand is restricted, the IRH's ROM was also limited in a simple one-to-one correspondence of leader-follower type of operation. Moreover, if the operator manipulates the IRH in an unreasonable posture for an extended period of time, the operator tends to tire, and the operation efficiency may decrease. Therefore, in this research, it was possible to switch between a state in which the operation is active (the operation-on state) and a state in which the operation is inactive (the operation-off state). In the operation-on state, the position and posture of the operator's hand at
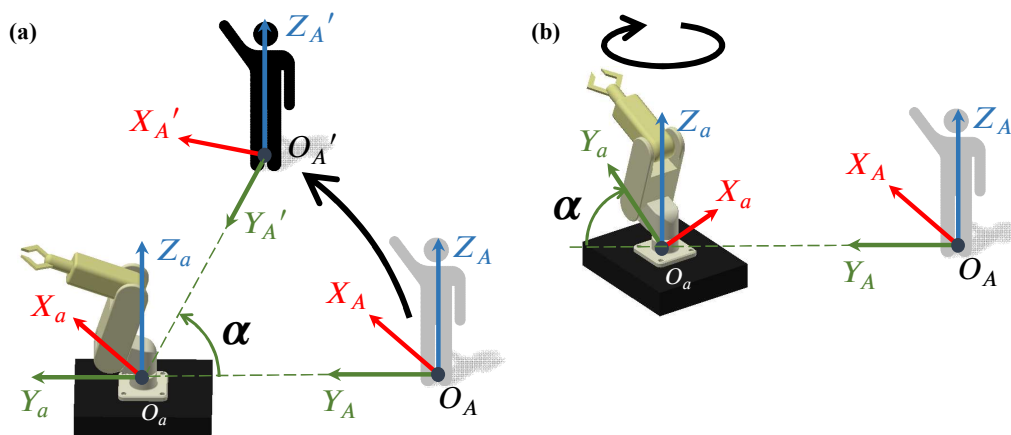

Fig. 3.6 Two definitions of viewpoint angle with (a) revolution of operator frame, and (b) rotation of robot frame (i.e., VOS frame).

the moment the operation was turned on were set as a reference, and displacements from this reference were measured and calculated. The calculated values were then used as the real-time operation commands and sent to the IRH. In the operation-off state, no operation commands were issued regardless of the hand movement, so that the IRH's position and posture at the moment the operation was turned off were preserved. In this way, when the upper limb approached the ROM limit during the operation-on state, the operation was switched to the operation-off state and the hand could be returned to a comfortable position and posture. The operation could then be switched back to the operation-on state, which makes it possible to continue the operation without difficulty.

For the type of viewpoint changes shown in **Fig. 3.6(b)**, since the operator frame $O_A{-}X_AY_AZ_A$ and the VOS frame $O_a{-}X_aY_aZ_a$ differed in their directions, there was a transformation of these reference frames when the command values from the movement of the operator's upper limb to the IRH were generated. This transformation is as follows:

$$
\begin{aligned}
{}^aq &= cT_q{}^Aq, \\
{}^ar_h &= T_r{}^Ar_H,
\end{aligned}
\tag{3.1}
$$

where

$$
T_q = T_r = \begin{bmatrix} \cos\alpha & \sin\alpha & 0 \\ -\sin\alpha & \cos\alpha & 0 \\ 0 & 0 & 1 \end{bmatrix}.
\tag{3.2}
$$

Here, ${}^aq$ and ${}^ar_h$ are respectively the position vector and posture matrix of the IRH with respect to $O_a{-}X_aY_aZ_a$, ${}^Aq$ and ${}^Ar_H$ are respectively the position vector and posture matrix of the operator's hand with respect to $O_A{-}X_AY_AZ_A$, and c is a constant that represents the ratio of the motion scale of the operator's hand to the IRH.

As illustrated in **Fig. 3.7**, to measure the movement of the operator's hand, markers were attached to the operator's right hand via a brace, and their positions and postures were measured by a 3D real-time motion capture shown in **Fig. 3.3**. A switch-type device was used to switch between the operation-on and operation-off states. The experiment was in the operation-on state whenever the operator held down the device's button and in the operation-off state whenever the operator released the button. This device was operated by the operator's left hand.

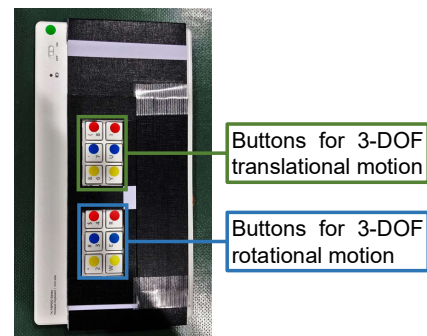**Fig. 3.7** Main and assistant markers for hand movement measurement.

Fig. 3.8 Simplified teaching pendant with 12 buttons for translation and rotation.

IV. Button-Based Operation Method

A simplified button-based operation method was used in the research. An actual TP has many buttons, including buttons for switching the operation axes and recording teaching points, which makes it difficult for novices to operate. Hence, a simplified TP with minimum number of functions to manipulate the IRH to an arbitrary position and posture was used. The simplified TP is shown in **Fig. 3.8**. It has 12 buttons, each of which corresponds to a positive or negative control command of 6-DOF position and posture. The IRH translated along the axis X_a, Y_a, or Z_a while pressing a position operation button and rotated around the axis X_h, Y_h, or Z_h while pressing a posture operation button. When multiple buttons were pressed at the same time, the combined movement was communicated to the IRH.

3.3 EXPERIMENT

In order to evaluate the influence of viewpoint change on the body motion- and button-based methods, this study applied the above-described evaluation system in a series of experiments.

I. Evaluation Game

Figure 3.9 illustrates the flow of the evaluation games used in the experiments. Before a game begins, the viewpoint angle α is set to 0°, and the IRH frame $O_h-X_hY_hZ_h$ is set parallel to the VOS frame $O_a-X_aY_aZ_a$. The VOS is then smoothly rotated to a specific viewpoint angle. (If the specific viewpoint angle is $\alpha = 0°$, the rotation of the VOS is omitted.) After the viewpoint changes, a target appears with a random position and posture. Some targets whose front and back sides might not be easily distinguished were excluded, since in such cases it would be difficult for the operator to correctly recognize the posture. The length of the side of the VOS was set at 30 (a dimensionless quantity), which is equivalent to 600 mm in the real space. The IRH's position vector is denoted by $^aq = \{^ax, {}^ay, {}^az\}^T$, and the target's position vector is denoted by $^aq_t = \{^ax_t, {}^ay_t, {}^az_t\}^T$. If the condition $(|^ax - {}^ax_t|, |^ay - {}^ay_t|, |^az - {}^az_t|) \leq 1$ was satisfied, it was considered that the positions of the IRH and target matched. In this status, the green sphere at the tip of the IRH turned red. The

I. Initial state of virtual space and hand

II. Viewpoint changes and a target appears

III. Matching state of position and posture
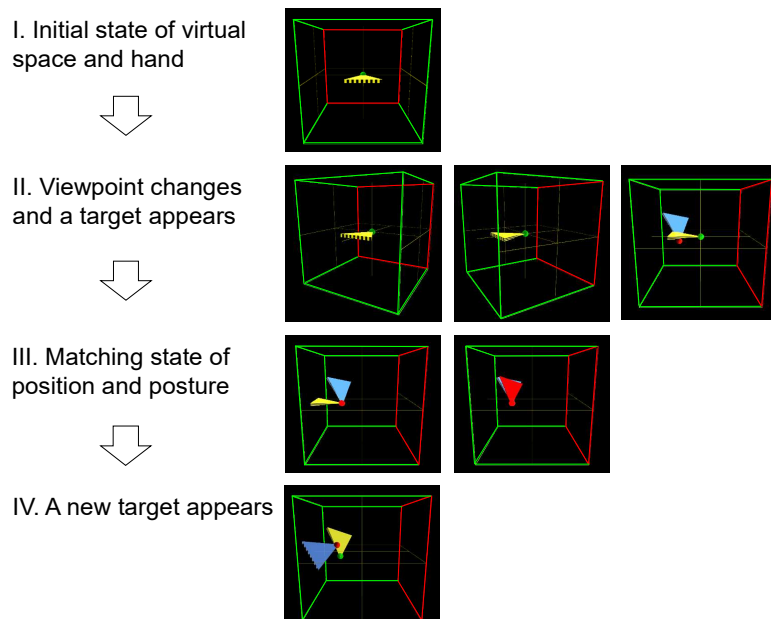
IV. A new target appears

Fig. 3.9 Process of evaluation game when viewpoint angle is set to 90°. (For easy understanding, frame line is shown thick.)

IRH's posture matrix is denoted by ${}^a\boldsymbol{r}_h = \left\{ {}^a\boldsymbol{r}_x, {}^a\boldsymbol{r}_y, {}^a\boldsymbol{r}_z \right\}^T$ and the target's posture matrix is denoted by ${}^a\boldsymbol{r}_{ht} = \left\{ {}^a\boldsymbol{r}_{xt}, {}^a\boldsymbol{r}_{yt}, {}^a\boldsymbol{r}_{zt} \right\}^T$. If the angle between the vectors ${}^a\boldsymbol{r}_{xt}$ and ${}^a\boldsymbol{r}_x$ and the angle between the vectors ${}^a\boldsymbol{r}_{yt}$ and ${}^a\boldsymbol{r}_y$ were within 10°, i.e., $\min\left(\langle {}^a\boldsymbol{r}_{xt}, {}^a\boldsymbol{r}_x \rangle, \langle {}^a\boldsymbol{r}_{yt}, {}^a\boldsymbol{r}_y \rangle \right) \geq 0.985$, it was considered that the postures of the IRH and target matched. When both the position and posture of the IRH agreed with those of the target, the entire IRH turned red. Once this status had lasted for 1 s (holding time), the current target was cleared and disappeared from the screen, and the next target appeared at another random position and posture. These operations were repeated until ten targets were cleared, which was regarded as one game set.

II. Evaluation Outline

The effects of age and gender differences in spatial ability have been surveyed in the previous studies [126–128]. In order to eliminate the effects of age and gender and conduct the experiments fairly, ten examinees in our experiments were all young healthy adult males with no physical injuries or disabilities (average age ± standard deviation was 22.5 ± 0.5 years). All experiments were approved by the Kyoto University Graduate School of Engineering Ethics Committee.

A chair for the examinees was placed opposite the center of the screen. The examinees were instructed to think of the IRH as a real robotic hand and to move it to match the target's position and posture as quickly as possible. After the VOS and IRH were projected, it was confirmed that the examinees could see them three-dimensionally by wearing 3D glasses.

A brief introduction to the body motion- and button-based methods was given to the examinees. Prior to the experiments involving the body motion-based operation, the ROM of the hand was shown to the examinees by using a cubic frame with 300 mm sides; they were asked to move their hands within this range. The examinees were verbally instructed to change their hand posture within a range in which they felt comfortable. An explanation of how to match the position and posture of the IRH with the target was then given. The examinees were also told that if their hands were about to deviate from the above ROM or if they felt uncomfortable, they could turn off the operation, move their hands into a comfortable posture around the center of the ROM, and then turn the operation back on. Prior to the experiments involving the button-based operation, the function of each button was explained. The examinees performed two training game sets before the actual games began, which ensured that the operation methods were fully understood.

In the actual games, five of the ten examinees were required to perform the body motion-based operation experiments first; the other five examinees performed the button-based operation experiments first. Eight versions of the evaluation game sets were used. Each version had a different viewpoint angle: 0°, 45°, 90°, 135°, 180°, 225°, 270°, or 315°. Each examinee played each game set one time, for a total of eight game sets, in random order. The experiment ended for the examinee after he cleared all 160 targets (ten targets in each of the eight game sets for the two operation methods). The examinees were given a one-minute break between game sets.

After the experiments, a questionnaire survey was administered in which the examinees were asked to indicate how they felt about the two operation methods. The survey was conducted once for each operation method. In the questionnaire, the Visual Analogue Scale (VAS) evaluation method [129–131] was used and the evaluation item was set as "whether it was easy to operate or not." A horizontal line was shown on the questionnaire sheet, the left and right ends of which were labeled "difficult to operate" and "easy to operate", respectively. The examinee marked the most applicable position along the line. The evaluation was quantified by converting the distance from the left end of

the line to the marked position into a score from 0 to 100. In comparison with other questionnaire methods, such as the five-point scale method, the VAS method is considered to be particularly effective for an ambiguous and subjective evaluation since it can detect slight differences in the evaluation. In addition to the VAS questionnaire, the comments from the examinees regarding what they felt about the operation were also recorded.

Although the research in this study focuses on the body motion- and button-based methods, the proposed evaluation system can be applied to other operating methods. This makes it possible to discuss differences in the effect of viewpoint change on various operation methods in a standardized manner by using differences in working time as a basis for comparison.

3.4   EXPERIMENTAL RESULTS

The results of the evaluation experiments were analyzed to provide insights into the influence of viewpoint change on the operability of the two operation methods.

I.   Comparison between Body Motion- and Button-Based Methods

First, the experimental results of the body motion- and button-based methods were compared.

The total clearing time required for clearing the ten targets, i.e., for completing one game set, for each viewpoint angle and each examinee was measured. Note that the holding time (1 s × 10 targets = 10 s) has been removed from the clearing times. Grubbs' method was used to reject outliers in the examinee clearing times for each viewpoint angle. The results are shown in **Fig. 3.10**. From this figure, it is clear that the clearing times for the body motion-based method were shorter than those for the button-based method for all eight viewpoint angles. Applying Welch's t-test to the average clearing times confirmed that there was a significant difference between the clearing times for the two operation methods for every viewpoint angle. Thus, the body motion-based method was shown to be superior to the button-based method in terms of working time, regardless of whether viewpoint was changed or not, and regardless of what the viewpoint angle was.

Figure 3.11 shows the distribution of the examinees' subjective evaluation scores from the VAS questionnaire survey. As indicated, the operability scores for the button-based method are in the range of 0−60, centering on 20−40, while the scores for the body motion-based method are mostly in the higher range of 40−100. **Fig. 3.12** shows the average operability scores for the two operation methods.
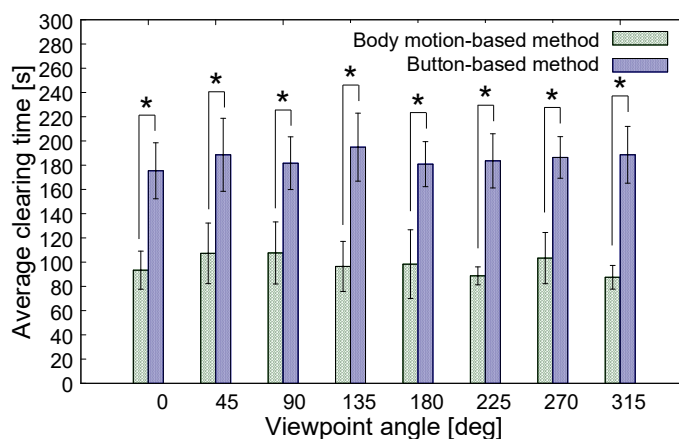

Fig. 3.10 Average clearing time of all examinees for each viewpoint angle with confidence intervals at 5% significance level (*: $p \leq 0.05$).
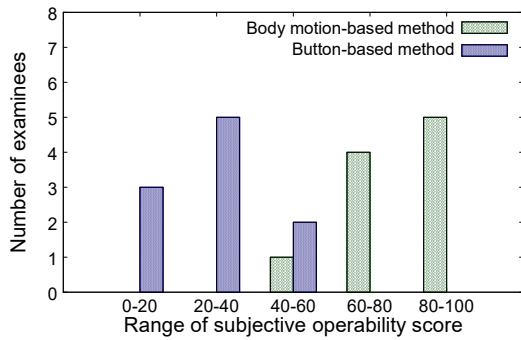
Fig. 3.11 Distribution of subjective operability scores in VAS questionnaire survey.
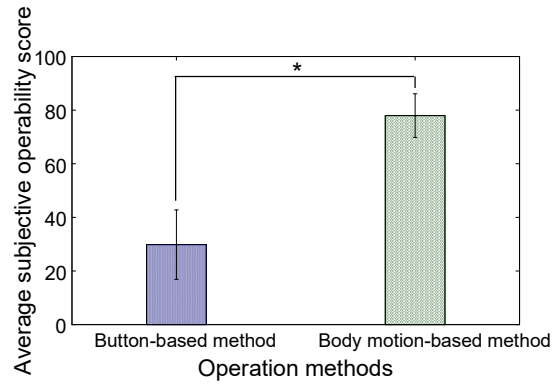
Fig. 3.12 Average subjective operability scores of body motion- and button-based methods in VAS questionnaire survey with confidence intervals at 5% significance level (*: $p \leq 0.05$).
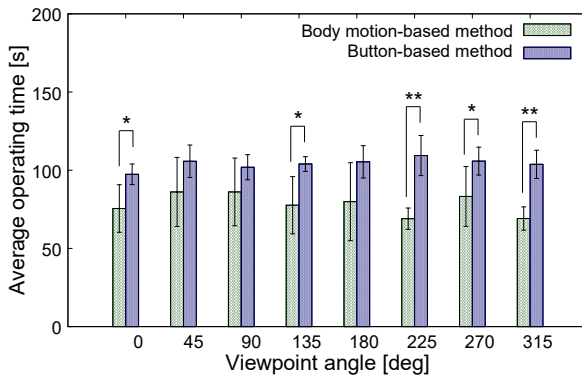
Fig. 3.13 Average operating times of body motion- and button-based methods for each viewpoint angle with confidence intervals at 5% significance level (*: $p \leq 0.05$; **: $p \leq 0.01$).
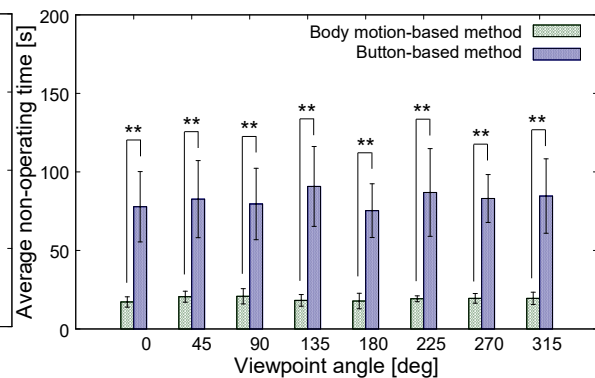
Fig. 3.14 Average non-operating times of body motion- and button-based methods for each viewpoint angle with confidence intervals at 5% significance level (*: $p \leq 0.05$; **: $p \leq 0.01$).

The average evaluation score for the button-based method was 29.8, while the average for the body motion-based method was 78.0. The ratio of the two scores is approximately 1:2.6. These results suggest that the body motion-based method is superior to the button-based method in terms of the user's subjective impression of operability, even when the viewpoint angle is changed.

Next, the operating and non-operating times were compared between the two operation methods. Operating time refers to the time during which the IRH is actually being operated. For the button-based method, operating time corresponds to the time when one or more buttons are being pressed. For the body motion-based method, operating time corresponds to the time when the system is in the operation-on state. Non-operating time refers to the time during which no operation command is being given to the IRH. For the button-based method, the non-operating time corresponds to the time when no button is being pressed. For the body motion-based method, the non-operating time corresponds to the time when the system is in the operation-off state. All the operating and non-operating times for the two operation methods for each viewpoint angle were monitored. By applying Grubbs' method to the data, the averages for each of the two methods were obtained and shown in **Figs. 3.13** and **3.14**. The p-values produced by Welch's t-test are also shown.

As can be seen in **Fig. 3.13**, the average operating time for the button-based method is longer than that for the body motion-based method for all viewpoint angles; in particular, there are significant differences when the viewpoint angle α is 0°, 135°, 225°, 270°, or 315°. The difference is most pronounced when α is 225° or 315°. These results suggest that the button-based method tends to be more difficult when the viewpoint angle α is "slanted" (i.e., not a multiple of 90°). The likely reason for this is that, in the operation of the simplified TP, when the viewpoint is changed, the correspondence between the function of each button and the moving direction of the IRH also changes, making it necessary for the operator to re-think the relation between the buttons and motions. To illustrate, with $\alpha = 0°$ as the reference, if α changes to 90°, when the operator presses the button corresponding to the "move forward" command, he/she will observe that the IRH displayed on the screen actually moves to the right. Therefore, the operator needs to "re-recognize" the function of this button as the command to "move to the right." On the other hand, if α changes to 45°, when the operator presses the button corresponding to the "move forward" command, he/she will observe that the IRH displayed on the screen actually moves in the front-right direction. To move the IRH forward, the operator would need to press the "move forward" and "move to the left" buttons at the same time. In such a situation, i.e., where the viewpoint is slanted, re-recognizing the buttons' functions can become quite difficult, as the intended operation and the button to be pressed are no longer in a one-to-one relationship. Given this increased complexity, the operating time for the button-based method is likely to be extended. On the other hand, in the case of body motion-based operation, there is no need for such re-recognition since the direction of movement of the operator's hand and that of the IRH are always the same for any viewpoint angle.

Figure 3.14 shows a comparison of the non-operating times between the two methods. As can be seen in the figure, the non-operating time for the button-based method was significantly longer than that for the body motion-based method for all viewpoint angles. One plausible explanation for this is that the non-operating time for the button-based operation includes the time it takes for the operator to decide in which direction the IRH should be moved next, the time it takes to move his/her line of sight from the screen to the simplified TP, the time it takes to check the button position by looking directly at it, and the time it takes to select the button for the intended operation. In contrast, the non-operating time for the body motion-based method includes only the time it takes to move the hand from a limited position to a comfortable position. With the body motion-based method, there is no need for the operator to look directly at his/her hand since it can be perceived sensibly; moreover, the time for the selection of the next movement direction is shorter since the movement of the IRH corresponds to that of the operator's hand. Thus, the operator is able to intuitively operate the IRH while maintaining his/her line of sight toward the screen, making the time during which the operation is paused shorter than in the case of the button-based operation.

Figures 3.15 and **3.16** show the operating and non-operating times as a percentage of the clearing times for the two operation methods. The operating times for the button-based method are divided according to the number of buttons being simultaneously pressed. As can be seen in the figures, the percentages are nearly constant across all viewpoint angles for both the body motion- and button-based methods. In the case of the button-based method, the time during which the operator was operating two buttons simultaneously was significantly shorter than the time operating only one button. The time during which three or more buttons were being operated simultaneously was close to 0. Reflecting this difference, the operating time percentages for one-button operation were in the range of 51.4−54.5%, whereas for two-button operation, the range was 2.8−5.2%, indicating that the one-button percentage was more than ten times the two-button percentage. This result suggests that
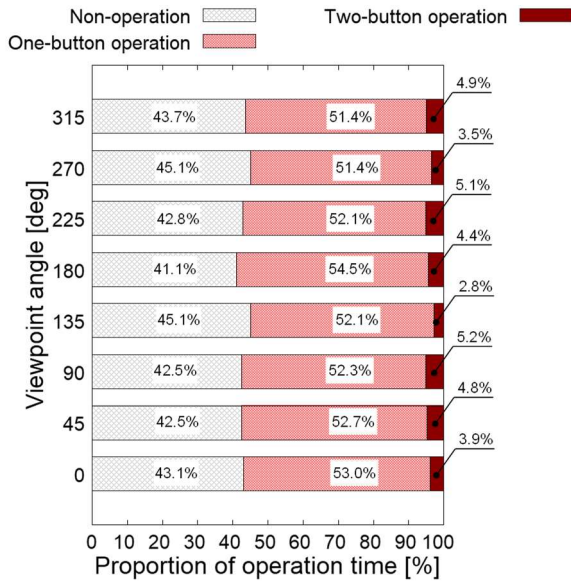
Fig. 3.15 Proportions of operating and non-operating times in clearing times for body motion-based method.
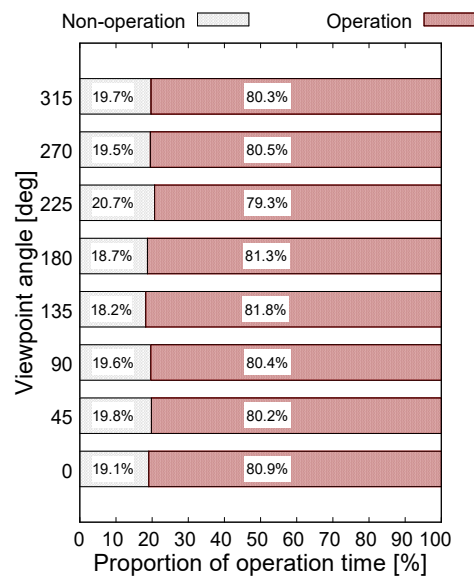
Fig. 3.16 Proportions of operating and non-operating times in clearing times for button-based method.

for the button-based operation, the operator mainly manipulates only one DOF at a time, while with the body motion-based operation, it is relatively easy for the operator to operate six DOFs simultaneously. This is considered as one of the primary reasons that the clearing times of the body motion-based method were shorter than those of the button-based method.

Based on the above analysis, it can be reasonably concluded that (i) the differences in clearing times between the body motion- and button-based methods are mainly caused by differences in their non-operating times and that the influence of viewpoint change on this result is small, and (ii) viewpoint change mainly influences operating times for the button-based method.

II. Trial-and-Error in Button-Based Operation

The relationship between the operator's behavior and the viewpoint angle in the button-based operation was also examined. One of the effects of viewpoint change was an increase in the number of button operations. In the previous study [100], a number of examinees commented that "it was difficult to immediately recall the relation between each button of the simplified TP and the moving directions of the IRH, so I tried many buttons to find the correct one." Based on this, in the current study, the possibility that efforts by the examinees to try multiple buttons in order to find the correct one using "trial-and-error" would be even greater was recognized, since the relation between the buttons and the moving directions was made more complicated by the changes in viewpoint. Hence, the current research considered instances in which the IRH moved far from the target position and posture while a button was being pressed as indicating that the operator was employing trial-and-error. The number of such trial-and-error cases was tracked and compared.

Figures 3.17 and 3.18 show the number of trial-and-error instances for the position and posture operations, respectively. For the position operation (Fig. 3.17), the number of times that trials-and-errors were used by the operator was smallest when the viewpoint angle α was 0°, second smallest when α was 90°, and largest when α was 225°. There were significant differences between the cases when α were 0° and 225° and the cases when α were 90° and 225°. This result agrees with the conclusion in Section 3.4-I that the button-based operation becomes more difficult when the

Fig. 3.17 Number of trial-and-error instances for each viewpoint angle for position operation using button-based operation method with confidence intervals at 5% significance level (*: $p \leq 0.05$; **: $p \leq 0.01$).

Fig. 3.18 Number of trial-and-error instances for each viewpoint angle for posture operation using button-based operation method with confidence intervals at 5% significance level (*: $p \leq 0.05$; **: $p \leq 0.01$).
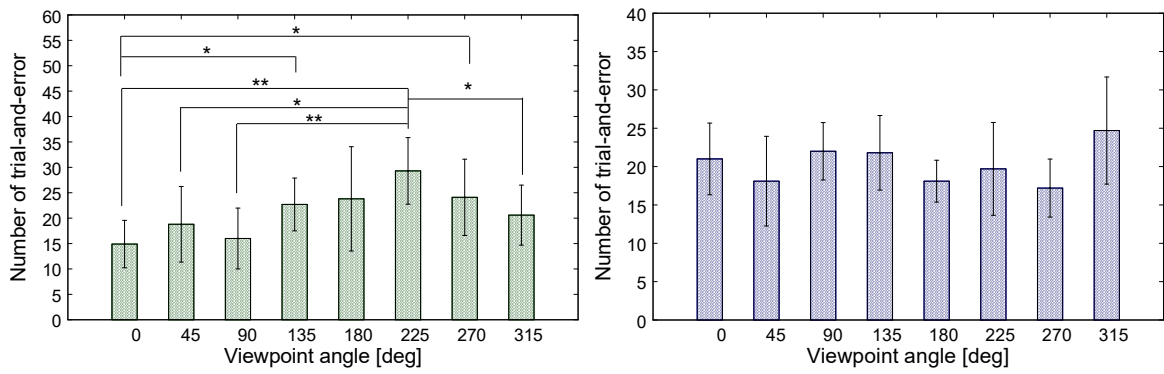
viewpoint angle is slanted. However, since the operating time for one-button operation is not constant, a large number of trial-and-error instances does not necessarily mean that the clearing time is long. On the other hand, as shown in **Fig. 3.18**, there were no significant differences between the results for the different viewpoint angles in the posture operations. There would appear to be two reasons for this. One is that trial-and-error operation was unnecessary in the posture operation since the IRH could be operated in either the positive or the negative direction to approach the target posture angle. The other reason is that recognition of the posture is likely to remain unchanged even when the viewpoint is changed since the posture change is based on the reference frame fixed on the IRH. In sum, it is suggested that a change in viewpoint makes the position operations for the button-based method more difficult, whereas its effect on the posture operations is relatively small.

III. Ideality of Body Motion-Based Method

As a part of the analysis, this section seeks to develop a measure of ideality for the body motion-based method could be used to assess the effect of viewpoint change. More specifically, an ideality index was produced in order to indicate how close the IRH was to the target position and posture after one operation; the premise being that the higher the index value, the less trials-and-errors were used. Since, in the body motion-based method, six DOFs of position and posture are operated simultaneously, the DOFs of some movements may affect the DOFs of others. In such cases, it is difficult to clearly determine the number of trial-and-error instances. Such fuzziness and vagueness in human-machine systems can be eliminated using fuzzy set theory [132]. Therefore, this research applied the fuzzy inference method proposed in the previous study [133] to define ideality and used the result as an evaluation index.

The method for calculating ideality can be explained by first considering the case of the position operation as an example. As shown in **Fig. 3.19**, in one operation, the positional relationship between the position before the operation, the position after the operation, and the target position is expressed by L_0, L_1, and θ_e. At this point, the following fuzzy sets A and B are used [134, 135].

A: The difference between the ideal moving direction and the actual moving direction of the IRH is small (i.e., θ_e is small).

B: The distance between the IRH and the target position becomes shorter (i.e., $L_1 < L_0$).
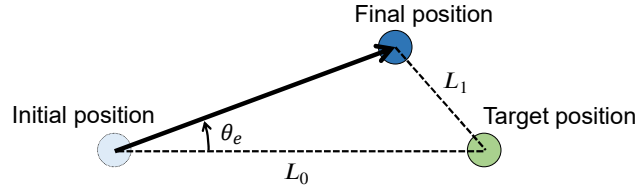
Fig. 3.19 Ideality model of IRH's movement during single operation-on state.

Four rules are considered with respect to the fuzzy sets A and B; the ideality I_j $(j = 1, 2, 3, 4)$ for each rule is given as follows:

Rule 1: if A and B, then the ideality is $I_1 = 3$;

Rule 2: if $\overline{A}$ and B, then the ideality is $I_2 = 2$;

Rule 3: if A and $\overline{B}$, then the ideality is $I_3 = 1$;

Rule 4: if $\overline{A}$ and $\overline{B}$, then the ideality is $I_4 = 0$.

Next, in order to quantitatively evaluate the degree to which A and B are satisfied, membership functions μ_A, $\mu_{\overline{A}}$, μ_B, and $\mu_{\overline{B}}$ are introduced. All of these membership functions are designed so that their maximum value is 1 and minimum value is 0 [136]. As shown in **Fig. 3.19**, μ_A is assumed to decrease in proportion to θ_e, since the smaller θ_e is, the closer the IRH's moving direction is to the target direction. In addition, μ_B is assumed to decrease in proportion to L_1/L_0, since the smaller L_1/L_0 is, the closer the IRH's position is to the target position after the operation.

$$\mu_A(\theta_e) = 1 - \frac{\theta_e}{\pi} \quad (0 \le \theta_e \le \pi),$$

$$\mu_{\overline{A}}(\theta_e) = 1 - \mu_A(\theta_e) = \frac{\theta_e}{\pi} \quad (0 \le \theta_e \le \pi),$$

$$\mu_B\left(\frac{L_1}{L_0}\right) = \begin{cases} 1 - \dfrac{L_1}{L_0} & \left(0 \le \dfrac{L_1}{L_0} < 1\right), \\ 0 & \left(1 \le \dfrac{L_1}{L_0}\right), \end{cases} \tag{3.3}$$

$$\mu_{\overline{B}}\left(\frac{L_1}{L_0}\right) = 1 - \mu_B\left(\frac{L_1}{L_0}\right) = \begin{cases} \dfrac{L_1}{L_0} & \left(0 \le \dfrac{L_1}{L_0} < 1\right), \\ 1 & \left(1 \le \dfrac{L_1}{L_0}\right). \end{cases}$$

Rules 1−4 are then defuzzificated using Takagi and Sugeno's method [137, 138]. Here, C_j $(j = 1, 2, 3, 4)$ is defined as the goodness of fit for Rules 1−4 by the following equations:

$$\begin{aligned} C_1 &= \min(\mu_A, \mu_B), \\ C_2 &= \min(\mu_{\overline{A}}, \mu_B), \\ C_3 &= \min(\mu_A, \mu_{\overline{B}}), \\ C_4 &= \min(\mu_{\overline{A}}, \mu_{\overline{B}}). \end{aligned} \tag{3.4}$$

The gained C_j $(j = 1, 2, 3, 4)$ is used to calculate the ideality of one positional operation I_{total} according to the following equation:
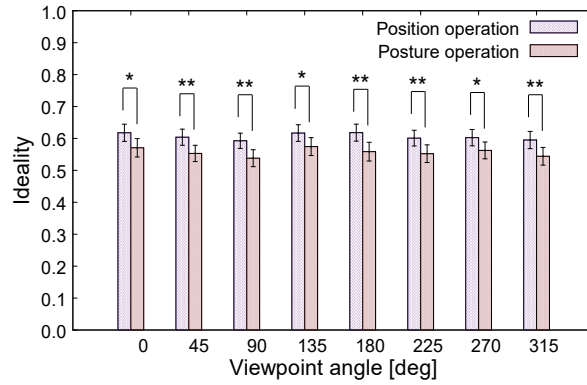
Fig. 3.20 Ideality of position and posture operation of body motion-based method for each viewpoint angle with confidence intervals at 5% significance level (*: $p \leq 0.05$; **: $p \leq 0.01$).

$$I_{\text{total}} = \left(\sum_{j=1}^{4} C_j I_j \right) \Big/ \left(I_{\max} \sum_{j=1}^{4} C_j \right), \tag{3.5}$$

where $I_{\max} = \max(I_1, I_2, I_3, I_4) = 3$ is used for the normalization of the ideality's value. By converting from the positional space shown in **Fig. 3.19** to the postural space, the ideality of the posture operation can be derived in the same way.

Figure 3.20 shows the average idealities of the position and posture operations produced in the experiments for each viewpoint angle. No significant differences between viewpoint angles for either the position or posture operations were found, indicating that the body motion-based method is robust to viewpoint change. It is also noted that the idealities for the positional operations were higher than those for the postural operations for any viewpoint angle. These are the same tendencies as in the previous study [133], whereby the robustness of the body motion-based method to viewpoint change is considered to be supported.

3.5 SUMMARY

The use of body gestures to give operation commands to mobile manipulators has been proposed and explored in a number of studies. However, no studies dealing with situations in which there are changes in the positional relation between the operator and the mobile manipulator have been reported. This study constructed an evaluation system based on a virtual space in which the viewpoint angle between the operator and the operated robot could be changed, and conducted a series of experiments to evaluate and compare the effect of viewpoint change on the operability of a body motion-based operation method that uses the movements of the operator's upper limbs and the operability of a simplified version of the more conventional button-based operation method. The main features and findings of this study are summarized below:

1) To evaluate the operability of robot operation that involves viewpoint change, in this study, an evaluation system was constructed for manipulating an imaginary robotic hand in a virtual operation space. And a method was proposed to simulate the operator's viewpoint change by rotating the virtual space.

2) Several experiments were conducted using the proposed evaluation system. In terms of both clearing time and subjective assessments of operability, the body motion-based method was

shown to be superior to the button-based method for all viewpoint angles.

3) Clearing time was divided into the operating time and non-operating time. It was found that the differences in the clearing times of the two operating methods were mainly due to differences in the non-operating times. Viewpoint change was shown to mainly influence the operating time of button-based method, the degree of this influence was especially notable when the viewpoint angle was slanted.

4) The assessment of the button-based operation is focused on the number of times the operator used trial-and-error to determine the function of the various buttons. This analysis revealed that viewpoint change made the positional operation much more difficult, but had a relatively smaller influence on the postural operation.

5) The ideality of body motion-based operations was analyzed. It was found that the ideality did not depend on the viewpoint angle, indicating that the body motion-based method may be robust to viewpoint changes.

To focus on the effect of viewpoint change on the button- and body motion-based operation methods, the evaluation conditions were simplified in this research. In the next phase, to simulate the actual conditions, such as collisions or interferences between a robot and a manipulated object, an actual or digital-twin operation environment will be constructed. Additionally, to show the versatility of the proposed evaluation system, it is also expected to be applied for the other interfaces or operation methods (e.g., a joy-stick-based method, a direct teaching method, a VR-based method) in future research.

CHAPTER 4
Experimental Evaluation for Robot Operation Using Toe Movements

4.1 INTRODUCTION

Human upper limbs are used on a daily basis to finish complicated tasks by flexion and extension movements of fingers, thus they have been the subject of numerous studies, including research on the features of finger motions in the medical field [147, 148] and motion analyses of finger joints in the engineering field [149, 150]. And many operation devices using upper limbs, such as TPs and leader-follower operation devices which have been discussed in the previous chapter, have been presented. In contrast, very few studies focused on the operation approaches using the movements of lower limbs, including legs, feet, and toes. Actually, toe movements, especially flexion and extension movements, are also considered to be applicable for robot operations. Toes are certainly not as dexterous as fingers; different toes have different musculoskeletal structures, thus some movement may be easy for some toes but difficult for the other toes. Additionally, when two toes are operated at the same time, the movement of one toe can affect that of the other. Such movement characteristics of toes have not been clarified. To realize high toe operability, it is important to gain a better understanding of the features of toe movements for consideration in terms of operation methods.

Some research focusing on toes has shown that toes play an important role in maintaining balance and preventing falls during walking [151, 152]. Medical studies on toes include investigations about joint ROM flexor muscle force during full extension [153, 154], the motions and contact surfaces of the joints in the great toe [155], and some other studies based on electroencephalograms [156, 157]. Moreover, research in the nursing field have compared the grip strength of toes in dominant and non-dominant feet [158], and revealed how toe training affected gait speed and step length [159, 160]. Sun *et al.* also found that different walking speeds had different effects on foot inter-segment kinematics, ground reaction forces, and lower limb joint moments [161]. Utilizing the pressing motions of toes, a computer mouse operated by toes has been reported [162]. However, since a device appropriate for measuring toe movements has yet to be developed, the characteristics of toe motions have not been sufficiently evaluated, which makes the developments of robot operation devices using toes difficult.

To solve the above problems, in this chapter, a new measuring device that can assess flexion and extension motions in small-sized toes with a small ROM is proposed. This newly developed device allows the features of toe movements in position operation tasks to be evaluated. This research uses the proposed device to experimentally investigate the movement characteristics of the great (first) and long (second) toes. In addition, the differences between flexion and extension movements, great and long toes, and one- and two-toe operations are clarified. Finally, toes and fingers movements are experimentally compared and discussed.

4.2 MUSCULOSKELETAL STRUCTURE AND FLEXION/EXTENSION OF TOES

Before discussing the investigation of movement characteristics, a brief description of the

anatomical structure of toes is presented in this section. Kai *et al.* compared the maximum gripping force and the time required to reach this maximum force between dominant and non-dominant feet and observed no significant difference [158], which suggested that toes in dominant and non-dominant feet have the same operability. Then, this section focuses on the right human foot, and carries out a comparison with the right hand. The investigation targets the great and long toes (first and second toes from the left when the sole is facing downward) and the index and middle fingers (second and third fingers from the left when the palm is facing downward). In this chapter, flexion is defined as when the toe or finger is bending downward; and extension is defined as when the toe or finger is stretching upward. The configuration of the bones and joints of each finger and toe considered in this section are shown in **Figs. 4.1** and **4.2**. The great toe has three phalanges: the distal phalange, proximal phalange, and metatarsal bone (in order from the tip of great toe). The joint between the distal and proximal phalanges and that between the proximal phalanges and metatarsal bone are known as the proximal interphalangeal (PIP) and metacarpophalangeal (MP) joints, respectively. The long toe has four phalanges, including an additional phalange between the distal and proximal phalanges known as the middle phalange. The joint between the distal and middle phalanges, and that between the middle and proximal phalanges are known as the distal interphalangeal (DIP) and PIP joints, respectively. The index and middle fingers also have four phalanges and three joints with the same names as those in the long toe.

Next, a brief introduction of the extensor and flexor muscles affecting extension and flexion movements is given. **Fig. 4.3** shows the three main muscles from the back of foot that affect toe extension movements [163]. The extensor halluces longus (EHL) muscle extends from the fibula to the tip of the great toe, four extensor digitorum longus (EDL) muscles, which belong to the same muscle group, extend from the tibia to the tips of the toes, excluding the great toe, and extensor digitorum brevis (EDB) and extensor hallucis brevis (EHB) muscles, which belong to the same muscle group, extend from the ankle to the tips of the toes, excluding the little toe. The MP and PIP joints in the great toe are stretched by the EHB and EHL muscles, respectively, while the DIP, PIP, and MP joints in the long toe are all stretched by the EDL and EDB muscles.

The five main muscles acting on the bending movements of the toes, which are distributed in three layers (the shallow, middle, and deep layers), are shown from the sole of the foot in **Fig. 4.4**. Four flexor digitorum brevis (FDB) muscles, which belong to the same muscle group, extend from the calcaneus to the PIP joints of the toes, excluding the great toe, and act on the flexion movement of the PIP and MIP joints in the long toe. In the middle layer, the flexor hallucis longus (FHL) muscle extends from the fibula to the tip of the great toe and acts on the flexion movement of the PIP joint in the great toe. Four flexor digitorum longus (FDL) muscles, which belong to the same muscle group,
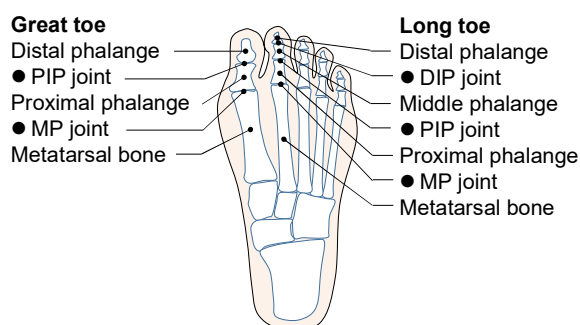
Fig. 4.1 Bones and joints in feet.
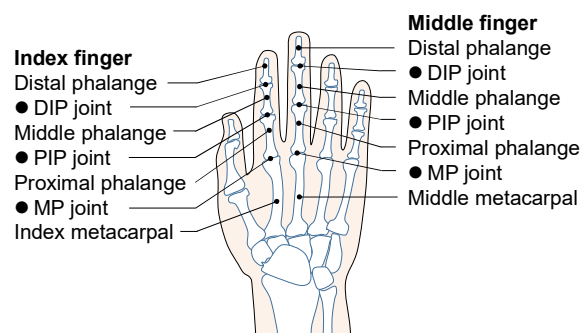
Fig. 4.2 Bones and joints in hands.

extend from the fibula to the toes, excluding the great toe, and act on the flexion movement of the DIP, PIP, and MP joints. The flexor hallucis brevis (FHB) muscle extends from the lower surface of the cuboid bone to the MP joint in the great toe and acts on its bending movement. Moreover, four lumbrical muscles in the deep layer, which belong to the same muscle group, extend from the inside of the FDL muscle and adhere to the tips of the toes, excluding the great toe, and act on the flexion movement of the MP joint in the long toe. The quadratus plantae and interossei muscles also assist the flexion movement of the toes.

As shown above, the great toe is considered to be able to bend or stretch relatively easily since it has its own extensor and flexor muscles. Conversely, it is considered difficult for the long toe to move separately from the other toes since their extensor and flexor muscles belong to the same muscle group. It is also known that the long toe has fewer muscles for extension than for flexion, and that the flexor muscle has a larger physiological cross-sectional area than the extensor muscle in the great toe [163]. In addition, toes are frequently bent to maintain stability during walking, whereas stretching movements are rarely used in daily life [164]. From this, it is expected that flexion

Extensor digitorum brevis muscle (EDB) & Extensor hallucis brevis muscle (EHB)

Extensor digitorum longus muscle (EDL)

Extensor hallucis longus muscle (EHL)

Fig. 4.3 Extensor muscles in feet.

Deep layer

Middle layer

Shallow layer

(a) Three layers of a foot with flexor muscles.

Flexor digitorum brevis muscle (FDB)

Flexor hallucis brevis muscle (FHB)

Flexor digitorum longus muscle (FDL)

Flexor hallucis longus muscle (FHL)

Lumbrical muscle

(b) Shallow layer.   **(c)** Middle layer.   **(d)** Deep layer.

Fig. 4.4 Flexor muscles in feet.

movements are easier and more accurate than extension movements in the toes. Based on this expectation, with a focus on the flexion and extension movements of the great and long toes, some experiments were conducted to examine and compare the differences between flexion and extension movements, the great and long toes, and fingers and toes. The purpose of these experiments was to illustrate quantitatively how quickly toes and fingers operate, as well as differences in their operability.

4.3   MEASUREMENT DEVICE AND EVALUATION EXPERIMENTS FOR SINGLE TOE MOVEMENTS

In this section, a description of the evaluation for the accuracy and speed of movement of a single toe or finger when bent or stretched at a specific angle is given. To conduct this evaluation, a new system that involved a device to measure and compare differences in the flexion and extension movements of a single toe or finger was developed. 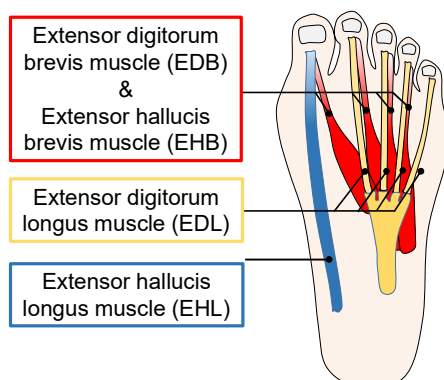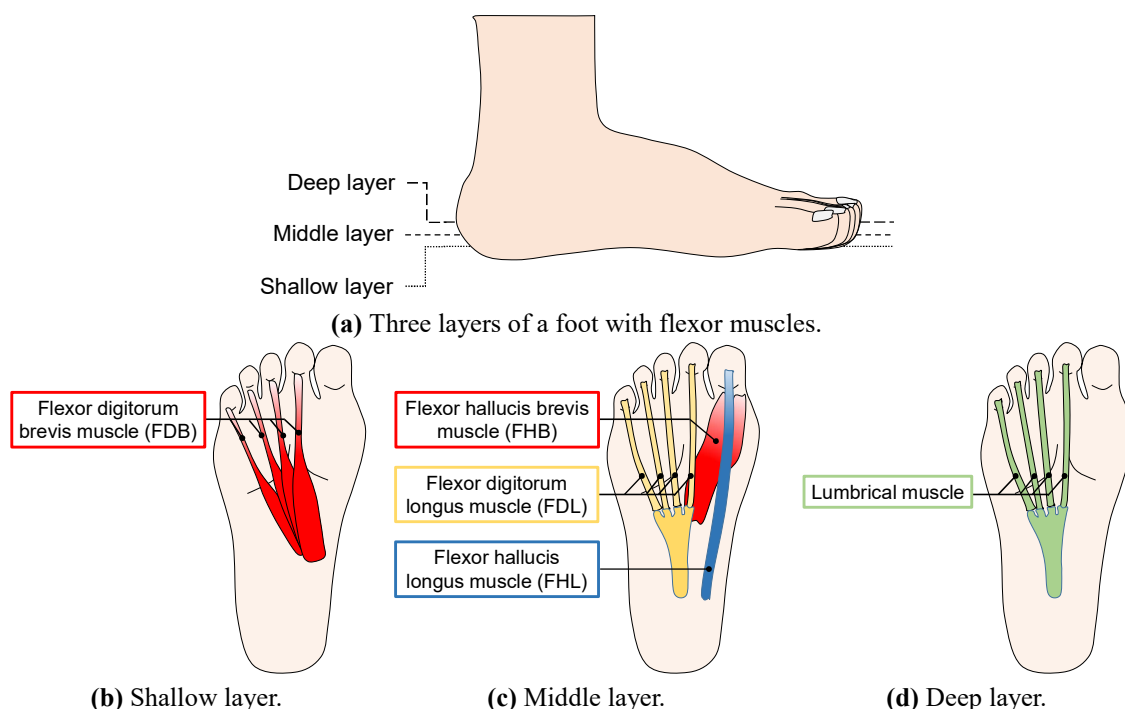For the purpose of the present study, the flexion and extension movements of the MP joints of the right foot and hand were specifically measured.

I. Development of a Measurement Device for Toe and Finger Movements

A new device for measuring flexion and extension movements of toes and fingers was developed. It is more difficult to measure toe than finger movements because toes are smaller than fingers. To our knowledge, few studies have involved devices for measuring toe movements, so the development of such a device was a focus of this study. Furthermore, this device has the potential to be used as the assistant operation device for leader-follower teleoperation systems.

Some studies in the medical field have used dynamometers or strain gauges to measure toe movements or toe gripping, force during flexion [165, 166]. However, few studies have been conducted on the development of a measurement device for toe flexion and extension. Mita *et al.* investigated changes in the angle of the MP joint in the great toe during walking using a potentiometer-type rotation angle sensor [167]. However, it is difficult to measure flexion and extension angles in the other toes with this device because it cannot be fixed on toes other than the great toe.

On the other hand, many studies have been conducted on measurement methods for finger movements. In particular, measurement devices using optical systems have frequently been used, such as extracting the outlines of fingers from imaging information on finger movements [168], as have detection methods for markers on the hands using cameras [169, 170, 171]. Using these optical methods makes it possible to measure the movements of multiple fingers. However, finger movements sometimes cannot be measured using these methods because of interference involving
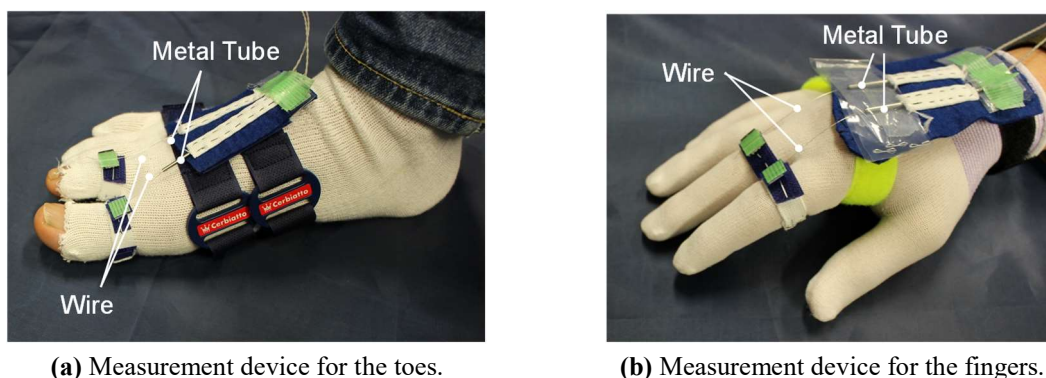

(a) Measurement device for the toes.   (b) Measurement device for the fingers.
Fig. 4.5 Placement of the wire displacement sensor on the foot and hand.

the markers fixed on the fingers, and this is considered to be even more problematic when measuring toes owing to their smaller size.

To solve these problems, contact-type sensors were used instead of optical methods to measure toe movements. The developed measurement device is shown in **Fig. 4.5(a)**. A wire-type magnetic displacement sensor (Wire-In Pulse Coder, LEVEX Corp., Kyoto, Japan) that consists of a wire fixed on the toe and a metal tube fixed on the back of the foot was used. This sensor outputs a voltage according to the amount of wire ejected from and inserted into the metal tube when the toe is bent and stretched, respectively. Variations in the measured voltage indicate changes in the angle of the toe. The linearity of this sensor ±2%/F.S, so the repeat accuracy is within this range. This method has the following merits: i) it is easy to fix the sensor on small toes since the wire is thin (ϕ0.2 mm); ii) the flexion movements of the toe can be tracked by this wire because of its softness; iii) the sensor is so light that the burden on the body is small; and iv) the same measurement device can also be applied to fingers, as shown in **Fig. 4.5(b)**.

The measured flexion amount of toes Y_{toe} is calculated as follows:

$$Y_{toe} = 100 \times \frac{2V_{toe} - V_{toe,max} - V_{toe,min}}{V_{toe,max} - V_{toe,min}}, \tag{4.1}$$

where V_{toe} is the voltage of the sensor, $V_{toe,min}$ is the voltage of the sensor when the toe is fully bent, and $V_{toe,max}$ is the voltage of the sensor when the toe is fully stretched. When V_{toe} is $V_{toe,min} \leq V_{toe} \leq V_{toe,max}$, the value of Y_{toe} is $-100 \leq Y_{toe} \leq 100$. Thus, the closer Y_{toe} is to 100, the larger the toe stretching angle, whereas the closer Y_{toe} is to -100, the larger the toe bending angle. In addition, when the toe flexion is about $Y_{toe} = 0$, i.e., $V_{toe} = (V_{toe,max} + V_{toe,min})/2$, it is considered to indicate a relaxed position for the flexor and extensor muscles [172]. Although the range of toe flexion and extension varies with each individual, these values can be expressed relatively based on the value Y_{toe} of as defined by Eq. (4.1), which makes it possible to provide participants with roughly equivalent operation conditions.

II. Construction of the Evaluation System and Game

Figure 4.6(a) shows the constructed evaluation system. The operator wears one sock or glove on the right foot or hand, onto which the developed measurement device is attached. The operator then sits on a chair facing a PC monitor. The foot is placed on a platform on the floor so that the toes can move freely, as shown in **Fig. 4.6(b)**. The inclination angle of the platform is 20°. The right hand is placed on the armrest of the chair with the palm facing downward so that the fingers can also move freely.

The PC monitor displays a blue circular marker, a green circular target, and a rectangular frame surrounding these circles, as shown in **Fig. 4.7**. The vertical positions of the marker and target within the rectangular frame vary. As shown in **Fig. 4.8**, the coordinate value of the top, center, and bottom positions of the rectangular frame are +100, 0, and −100, respectively. The coordinate value of the marker corresponds to the value of Y_{toe}, which makes it possible to move the marker vertically using toe flexion and extension. The operator is expected to move the marker to the target position. In these experiments, the operator moves his or her toes to clear the target appearing in various positions, and the toe movements are measured and evaluated.

The evaluation game is implemented using the evaluation system described above. In this game,

(a) Operator and experimental setup.   **(b)** Platform for the foot.
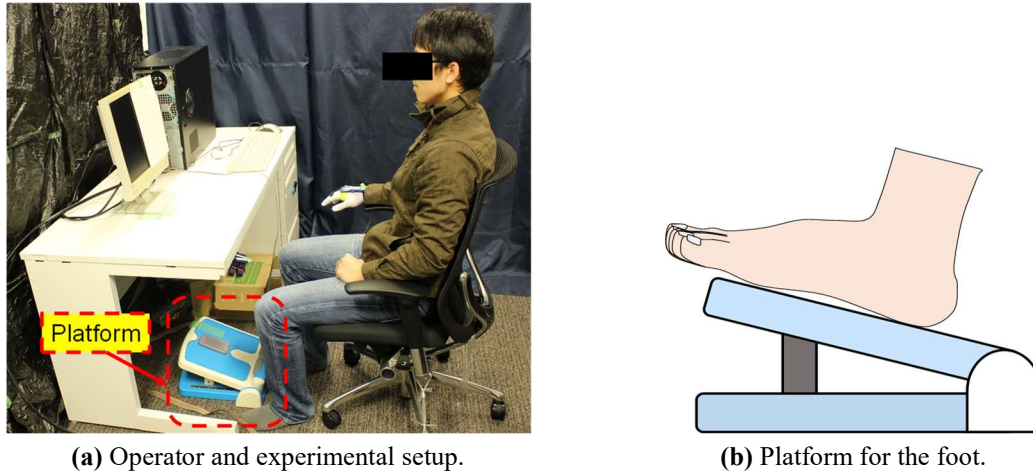
Fig. 4.6 Experimental setup.
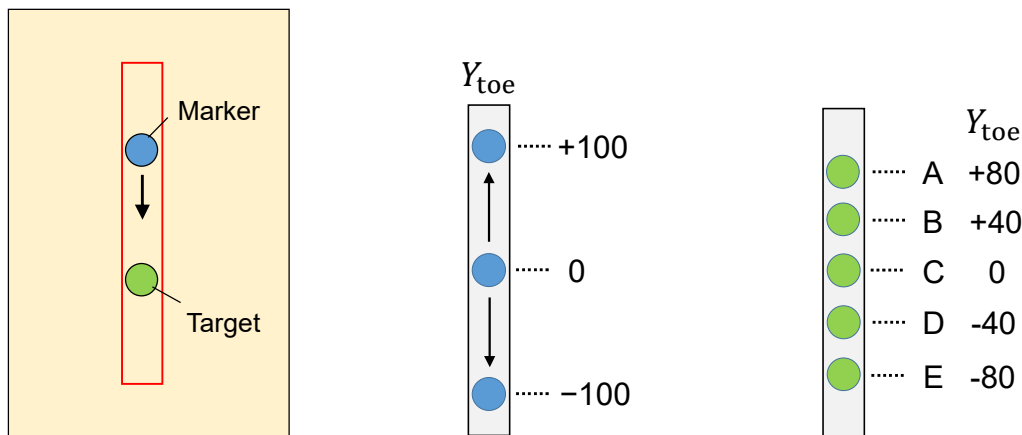
Fig. 4.7 Evaluation game as displayed **Fig. 4.8** Range of marker move- **Fig. 4.9** Appearance positions of
on the monitor.   ment.   the target.

participants are required to operate the marker using a specified toe or finger from among the great
and long toes and index and middle fingers. When the position of the marker matches the position of
the target, the target is cleared and the next one is displayed at a different position. The game ends
when this operation is repeated and a certain number of targets are cleared.

Regarding the setting of the target position, first, within the range from −100 to 100 shown in
Fig. 4.8, the positions where targets may appear are set to as A (+80), B (+40), C (0), D (−40), or E
(−80), as shown in **Fig. 4.9**. The position of the first target in the game is C, and that of the second is
selected from one of the other four positions (A, B, D, or E). Next, the position of the third target is
selected from the remaining positions, and that of the fourth is selected from the remaining two.
These four targets comprise one target set, and the game consists of $_4P_3 = 24$ sorts of target sets in
total. In this evaluation game, all 24 target sets are displayed in random order for each participant.
However, participants may become aware that the fourth target in one target set always appears at
position C, which can adversely affect the fairness of the experiments. Therefore, cases in which the
marker moves from other positions to C were not considered and the experimental data for these
cases were excluded. Therefore, 16 types of operation patterns were considered in this evaluation
game (**Fig. 4.10**). These patterns are named based on the starting and finishing marker positions; for
example, the pattern in which the marker is moved from C to A is named pattern CA. The movement
distance of the marker (flexion amount of the toe) for each operation pattern is shown in **Table 4.1**.

Regarding the conditions for determining the match between the marker and the target in this evaluation game, participants move the marker up and down to approach the target using toe movements. The range of the marker's movement is −100 to 100, as shown in **Fig. 4.8**, and match status is achieved when the position of the marker is within ±2.5 of the position of the target. If this match status lasts for 1 s, which is called the holding time, the target is cleared and disappears from the monitor. Then, the next target appears at a new position. In this experiment, the repeat accuracy of the measurement device described in the Section 4.3-I was not considered to directly affect the experimental results. The participants always moved their toes or fingers just to make the marker match the target according to the visual feedback, which implies that the participants compensated the repeat errors without the intension even if such errors occurred in the evaluation game.

III. Experimental Outline

Experiments using the developed evaluation system were conducted on 10 male adult participants (mean age ± standard deviation, 22.4 ± 0.92 years) without disability or toe or finger injury. In these experiments, the time intervals from the moment when one target was cleared to the moment when the next target was cleared were measured and referred to as the clearing time; this was used as the main evaluation index. The holding time of 1 s required to clear a target was subtracted from the clearing time. The participants were required to clear all target as soon as possible. It was considered that the shorter the clearing time, the higher the operability. All participants conducted in this study were approved by the Kyoto University Graduate School of Engineering Ethics Committee.

Table 4.1 Displacement of the marker for each operation pattern.

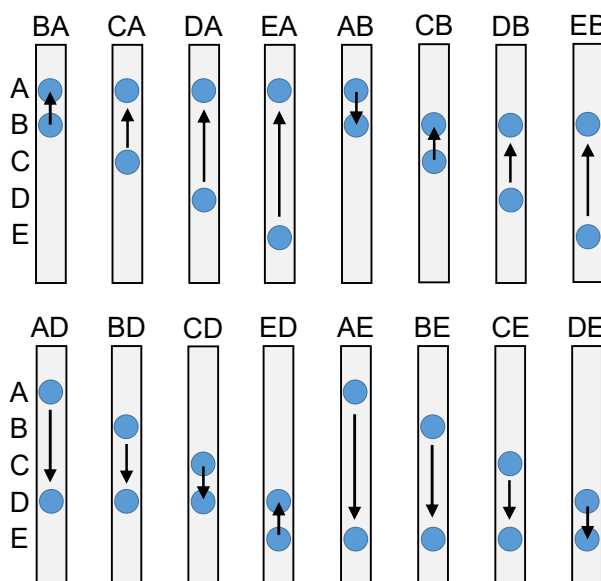| Operation pattern	Marker displacement Y_{toe}
CB, CD, AB, BA, DE, ED	40
CA, CE, BD, DB	80
AD, BE, DA, EB	120
AE, EA	160

Fig. 4.10 The 16 operation patterns used in the evaluation game.

Before the evaluation games, a training game was conducted so that each participant could become familiar how to operate the marker. In total, 25 targets, which consisted of six target sets with 24 targets and a single target appearing at position C at the end of the game, comprised a game set. In the training game, one game set was performed. After the training game, a test game with four game sets, which consisted of 100 targets for each toe or finger, was started, with a 1-min break between each game set. Additionally to the 1-min break, the participants were asked to take a break if they felt fatigued or uncomfortable, even just a little. Therefore, the fatigue of toes was considered to be so limited that it had no significant effect on the experimental results.

IV. Experimental Results and Discussion

Figure 4.11 shows the experimental results of the average clearing times for the great and long toes and the index and middle fingers. In this figure, the error bars indicate the CI at a 5% significance level. Grubbs' method was used to reject the outliers observed in the experimental data for the same toe/finger and the same operation pattern in all participants. As shown in the figure, the average clearing time increased in the order of the index finger, middle finger, great toe, and long toe. The average clearing time of the middle finger was about 1.03 times longer than that of the index finger, the average clearing time of the great toe was about 1.43 times longer than that of the index finger, and the average clearing time of the long toe was about 1.55 times longer than that of the index finger. **Fig. 4.11** also shows the test results of the differences in average values using Welch's t-test at a 5% significance level. Although no significant differences were observed between the average clearing time of the index and middle fingers, significant differences were observed for all other cases.

The results from this experiment are discussed here. First, regarding a comparison between the fingers and toes, the toes showed lower operability, which was predicted before the experiment began. The average clearing time of the toes was 1.45 times longer than that for the fingers, which suggests that the operation speed of the toes is about 69% that of the fingers. A comparison of the results for the two toes indicated that the great toe had a better operability than the long toe. This result agrees with the discussion of the musculoskeletal structure presented in Section 4.2. The average clearing time for the great toe was 0.92 times shorter than that of the long toe, which suggests than the operation speed of the great toe is about 109% that of the long toe. The great toe was considered to have substantially better operability than the long toe because unlike the long toe, the great toe has
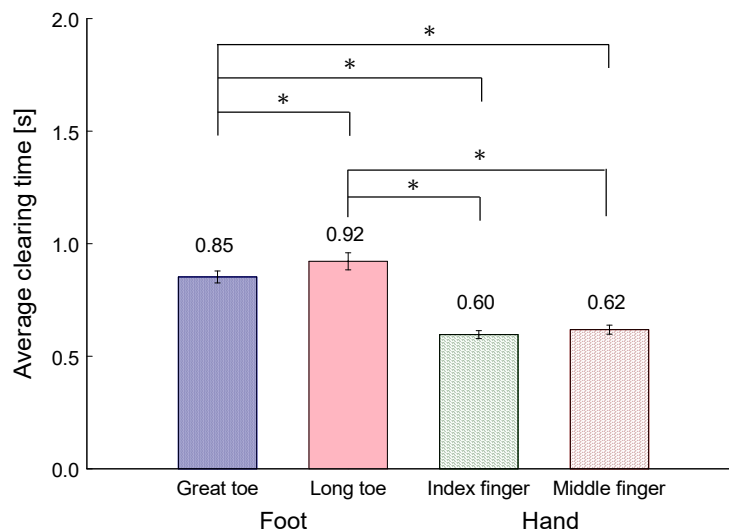
Fig. 4.11 Average clearing time of each toe and finger in the operation experiments (*: $p \leq 0.05$).

its own individual flexor and extensor muscles. However, the difference in operation speed between these two toes was small, at only 9%. The result also indicated that the operability of the index and middle fingers was equivalent since no difference was observed. To our knowledge, such quantitative results have not been reported in previous studies.

The 16 operation patterns shown in **Fig. 4.10** were considered. The average clearing time and Cis at a 5% significance level for the toes and fingers for each operation pattern are shown in **Fig. 4.12**. The differences of these mean values were tested using Welch's t-test at a significance level of 5%. The test results are shown in **Table 4.2**. Among the 16 patterns, significant differences between toes and fingers were observed in 12: CA, AB, CB, DB, EB, AD, BD, CD, ED, AE, BE, and CE. These results indicated that the operability of the toes was significantly lower than that of the fingers

Table 4.2 Result of Welch's t-test for the toes or fingers for all operation patterns (*: Significantly different; No: Not significantly different).

| Operation pattern		Long toe	Index finger	Middle finger	Operation pattern		Long toe	Index finger	Middle finger
CA, AB, DB, EB, CD, BE, CE	Great toe	No	*	*	DA	Great toe	No	No	No
	Long toe		*	*		Long toe		*	*
	Index finger			No		Index finger			No
CB, AD, ED, AE	Great toe	*	*	*	EA	Great toe	*	*	No
	Long toe		*	*		Long toe		No	No
	Index finger			No		Index finger			No
BD	Great toe	*	*	*	DE	Great toe	*	*	*
	Long toe		*	*		Long toe		No	*
	Index finger			*		Index finger			No
BA	Great toe	No	*	No					
	Long toe		*	No					
	Index finger			*					
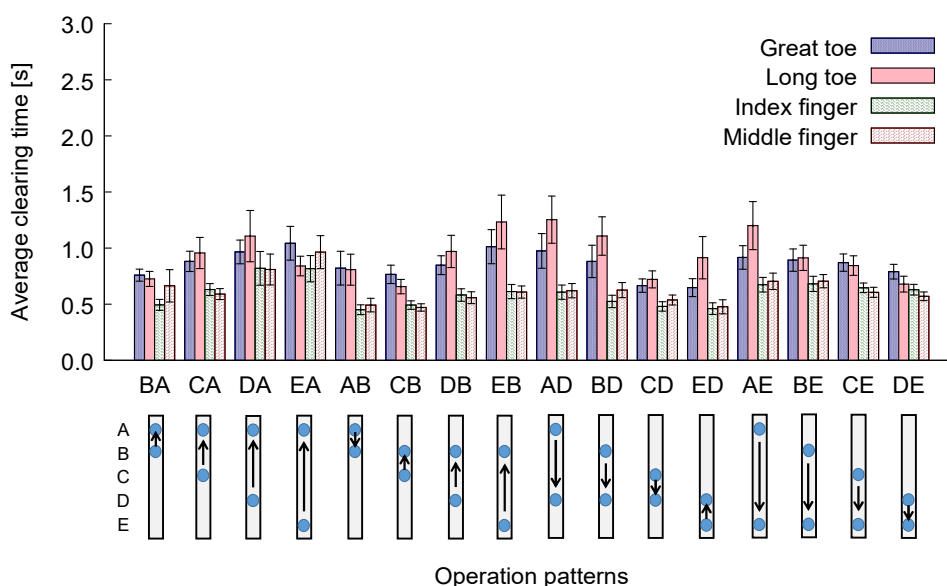
Fig. 4.12 Average clearing time of each toe and finger in the operation experiments (*: $p \leq 0.05$).

for these patterns. Although no significant differences between toes and fingers were observed for some comparisons of the other four patterns (BA, DA, EA, and DE), it was confirmed that average clearing time of the toes was longer than that of the fingers for almost all patterns. Among these four patterns, the marker was moved from lower positions to the A position in patterns BA, DA, and EA. This suggests that differences in operability between the toes and fingers are unlikely to occur when substantial extension is required. Moreover, according to the result of a comparison between the two toes, no significant differences in the average clearing time were observed for operation patterns BA, CA, DA, AB, DB, EB, CD, BE, or CE, whereas significant differences were observed for patterns EA, CB, AD, BD, ED, AE, and DE. The operability of great toe was significantly better than that of the long toe for patterns AD, BD, ED, and AE, whereas the operability of the long toe was significantly better for patterns EA, CB, and DE. Regarding the comparison between the two fingers, significant differences in the average clearing time were observed for patterns BA and BD, whereas no significant differences were seen in the other most patterns. This indicates that there were no differences in operability between the index and middle fingers.

Next, the flexion and extension of the toes were considered. We focus on the following operation pattern pairs in which the marker has the same movement distance and opposite movement directions: AB and BA, AD and DA, AE and EA, BD and DB, BE and EB, and DE and ED. Because of having the same movement distance, only the influence of the movement direction, that is, flexion and extension, could be analyzed. The results of the comparison of average clearing times based on Welch's t-test are shown in **Fig. 4.13**. Patterns AB, AD, AE, BD, BE, and DE are flexion movements, in which the extensor muscles of the toes relax and the flexor muscles become tense, whereas patterns BA, DA, EA, DB, EB, and ED are extension movements, in which the extensor muscles become tense and the flexor muscles relax. In patterns AB, AD, BD, DB, EB, and ED, which are marked with a ● in **Fig. 4.13**, the toe or finger must be bent or stretched toward the center position C since the target appears at position B or D. By contrast, in patterns BA, DA, AE, EA, BE, and DE, without a ●, the toe or finger is required to be bent or stretched toward the end of the operating range since the target appears at position A or E. To compare the results between these movements, first, the average clearing times of the great toe were tested for all patterns. A significant difference was observed for patterns DE and ED, and the average clearing time for DE was longer than that for ED. On the other hand, no significant difference in average clearing time was observed for any other pattern pairs. Therefore, the operability in terms of the flexion and extension of the great toe was considered to be equivalent. As discussed in Section 4.2, toe flexion was predicted to have better operability than extension. However, the experimental results contrasted with this prediction. In addition, the average clearing time for the long toe when the target appeared at position A or E (patterns BA, DA, BE, and DE in **Fig. 4.13**) was shorter than that when the target appeared at position B or D (AB, AD, EB, and ED). Especially significant differences were observed for pattern pairs BE and EB, and DE and ED. In other words, the results suggested that the operability of the long toe was higher when it was moved toward the end of the operating range compared with the center position in both flexion and extension. When the target appeared at position A or E, the flexor or extensor muscles became tense, since the long toe had be moved around the boundary of the ROM, whereas it was not necessary to exert the flexor or extensor muscles strongly when the target appeared at position B or D. Therefore, it was predicted that the long toe could be operated with ease if the target appeared at position B or D. However, the experimental results gave the opposite conclusion. When the target appeared at position B or D, it was necessary to stop the movement of the long toe at a specific position near the center of the ROM. However, such delicate movement is difficult for the long toe. As described above, no significant characteristics were seen in the operation patterns of the great toe, while some
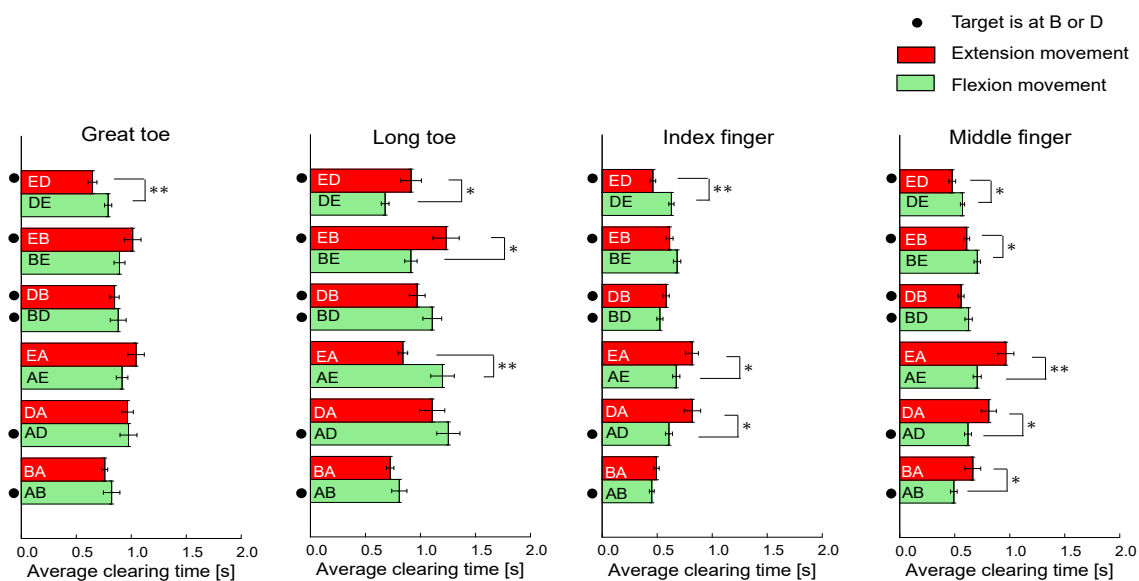
Fig. 4.13 Comparisons of clearing times of operation patterns with the same movement distance and opposite movement direction for one-toe and -finger operation (*: $p \leq 0.05$; **: $p \leq 0.01$).

significant characteristics were seen in those of the long toe.

Next, the experimental results for the fingers were analyzed. As shown in **Fig. 4.13**, the average clearing times for the patterns with target position A or E (BA, DA, BE, and DE) was significantly longer than those with target position B or D (AB, AD, EB, or ED) for the index finger. The same results were also seen for the middle finger. These findings suggest that the operability of the fingers was lower when bent or stretched toward the end of the ROM compared with the center position, which is the opposite of the results of the long toe. One reason for this difference may be that fingers are frequently used around the center position of the ROM in daily life, so they are considered to be accustomed to subtle movements in this range. In addition, the average clearing time of the fingers was significantly longer for pattern EA than for pattern AE, which suggests that the operability of the fingers when bent at a large angle is substantially better than when stretched at a large angle. One reason for this may be that humans always grasp objects using flexion, so flexion movements are easier than extension movements. On the other hand, no significant differences were seen between patterns BD and DB. Therefore, when bending or stretching angles of the fingers are small, no differences in the operability of flexion and extension movements are apparent.

4.4 EVALUATION EXPERIMENTS FOR THE MOVEMENT OF TWO TOES

In the evaluation experiments described in the previous section, when a specific toe was in operation, the adjacent toe could be moved freely. The conclusion in the previous section are valid if only one toe is used for operation; whether the conclusions are also valid when two toes are used at the same time remains unclear. It is therefore necessary to gain an understanding of the influence of the interaction of two adjacent toes during two-toe operation. In particular, since some of the flexor and extensor muscles of the great and long toes belong to the same muscle group, the movements of one toe may affect those of the other. Hence, in this section, the investigation of the operation of two adjacent toes is described.

Frame for the great toe or index finger
(moved toe or finger in this case)

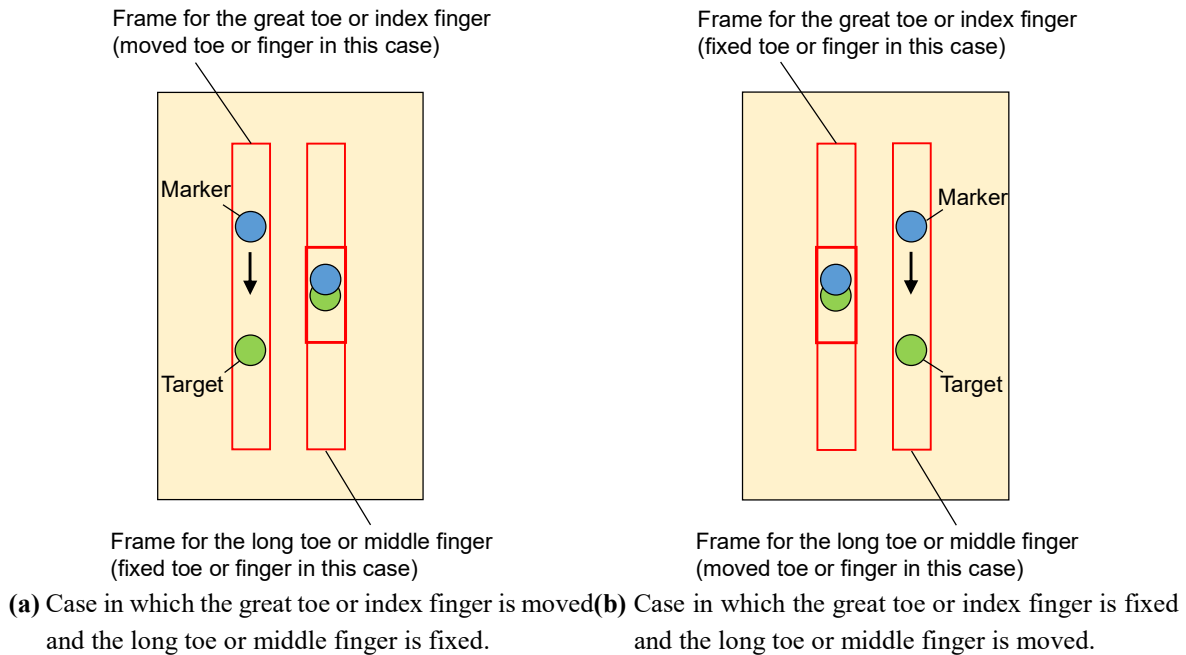Frame for the great toe or index finger
(fixed toe or finger in this case)

Marker

Marker

Target

Target

Frame for the long toe or middle finger
(fixed toe or finger in this case)

Frame for the long toe or middle finger
(moved toe or finger in this case)

(a) Case in which the great toe or index finger is moved **(b)** Case in which the great toe or index finger is fixed
and the long toe or middle finger is fixed.   and the long toe or middle finger is moved.

Fig. 4.14 Evaluation game displayed on the monitor to evaluate the motion of two toes or fingers.

I. Evaluation System for the Movement of Two Toes

A description of the evaluation system for the movements of two toes is shown in **Fig. 4.14(a)**. The basic construction of this system is the same as that for one toe, except that two sets of markers, targets, and rectangular frames are displayed on the monitor. The left marker is operated by the movements of the great toe or index finger, whereas the right marker is operated by the movements of the long toe or middle finger. The experimental participants can see and operate these markers at the same time.

Next, the target position settings are explained. **Fig. 4.14(a)** shows the monitor when the long toe or middle finger is maintained at the center position and the great toe or index finger is moved. The target in the left frame is arranged in the same way as that in the experiments described in the previous section. The target in the right frame is always placed at position C within the frame. The participants are required to move the left marker up and down while simultaneously maintaining the right marker at the center position C. A small rectangular frame with red lines that instructs the participants to maintain the marker's position is displayed near the center position of the right rectangular frame. When the right marker deviates from the center position and touches the red lines (i.e., the value of Y_{toe} exceeds ± 20), the game set is redone. **Fig. 4.14(b)** shows the monitor when the great toe or index finger is maintained at the center position and the long toe or middle finger is moved, with the frames for the movable and fixed toes/fingers placed on the right and left sides, respectively.

II. Experimental Outline

The participants in this experiment were the same 10 adult men as those in the previous experiment. In this experiment, the following four situations were considered: operating the long toe while fixing the great toe, operating the great toe while fixing the long toe, operating the middle finger while fixing the index finger, and operating the index finger while fixing the middle finger. Four game sets were carried out for each situation.

III. Experimental Results and Discussion

Figure 4.15 shows the average clearing times and CIs for each toe and finger at a 5% significance level based on the experimental data, where the outliers were excluded using Grubbs' method. According to the results of Welch's t-test, no significant difference was found between the great and long toes or between the index and middle fingers. However, significant differences were observed between the toes and fingers. The average clearing time of each toe or finger in ascending order was the index finger, middle finger, great toe, and long toe. The average clearing time of the middle finger was 1.04 times longer than that of the index finger, that of the great toe was 3.57 times longer than that of the index finger, and that of the middle finger was 3.64 times longer than that of the index finger. The mean value of the two toes' average clearing time was about 3.51 times as long as that of the fingers, which illustrates quantitatively that the operation speed of the toes is about 28.5% that of the fingers. No significant difference was observed when comparing the great and long toes; therefore, the operability of the two toes was considered to be the same. We predicted that the great toe would have higher operability because of its individual flexor and extensor muscles. However, the experimental results did not agree with this prediction. The experimental results also indicated that the two fingers have equivalent operability.

A comparison between the experimental results for one toe shown in **Fig. 4.11** and two toes is shown in **Table 4.3**. Although the average clearing time of movements using fingers increased slightly, it was still about 0.6 s, which means that the status of one finger did not significantly influence the movements of the other. Nevertheless, the average clearing time of two-toe movements

Table 4.3 Comparison between the experimental results using one toe or finger and two toes or fingers.

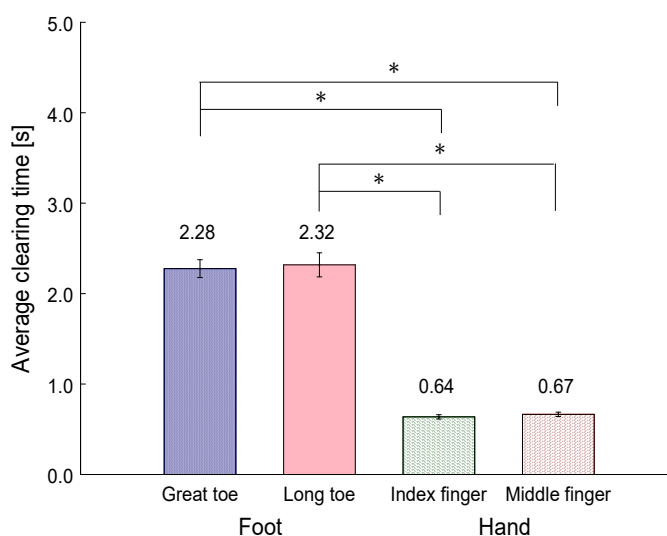| Toe/Finger	Average clearing time using one toe/finger [s]	Average clearing time using two toes/fingers [s]	Increase rate of average clearing time
Great toe	0.85	2.28	+167.1%
Long toe	0.92	2.32	+151.5%
Index finger	0.60	0.64	+6.9%
Middle finger	0.62	0.67	+7.6%

Fig. 4.15 Average clearing time for each toe and finger in the experiment using two-toe or two-finger operation (*: $p \leq 0.05$).

increased significantly compared with that of a single toe (167.1% for the great toe and 151.5% for the long toe). This result confirmed quantitatively that when one toe is bent or stretched while the posture of the other is maintained, the operability of the toes is greatly deteriorated compared with simply bending or stretching one toe. The reason for this is considered to be the mutual interference between toes in flexion and extension movements. As mentioned in Section 4.2, many muscles that belong to the same muscle group are attached to each toe. For this reason, interaction between toes occurs, and when one toe is moved, the other is dragged. Regarding the comparison between the great and long toes, **Fig. 4.11** shows that the great toe had a slightly but significantly shorter clearing time than the long toe. Conversely, the difference between two toes became small and not significant, as shown in **Fig. 4.15**. This finding indicates that the great toe has higher operability than the long toe when only a single toe is used, whereas the difference in operability for these two toes becomes smaller if the two toes are used for operation.

Figure 4.16 shows the average clearing time for each operation pattern, and **Table 4.4** shows the results of Welch's t-test. Regarding the comparison between the toes and fingers, significant differences in the average clearing time were observed for all patterns. These findings suggest that fingers are more operable than toes for all patterns. Regarding the comparison of the great and long toes, the average clearing time of the great toe was shorter in the case that the toe was stretched at a

Table 4.4 Result of Welch's t-test for the toes or fingers for all operation patterns (*: Significantly different; No: Not significantly different).

Operation pattern		Long toe	Index finger	Middle finger	Operation pattern		Long toe	Index finger	Middle finger
BA	Great toe	*	*	*	CB	Great toe	No	*	*
	Long toe		*	*		Long toe		*	*
	Index finger			*		Index finger			*
CA, DA, EB, CD, ED, CE, DE	Great toe	*	*	*	EA, AB, DB, AD, BD, AE, BE	Great toe	No	*	*
	Long toe		*	*		Long toe		*	*
	Index finger			No		Index finger			No
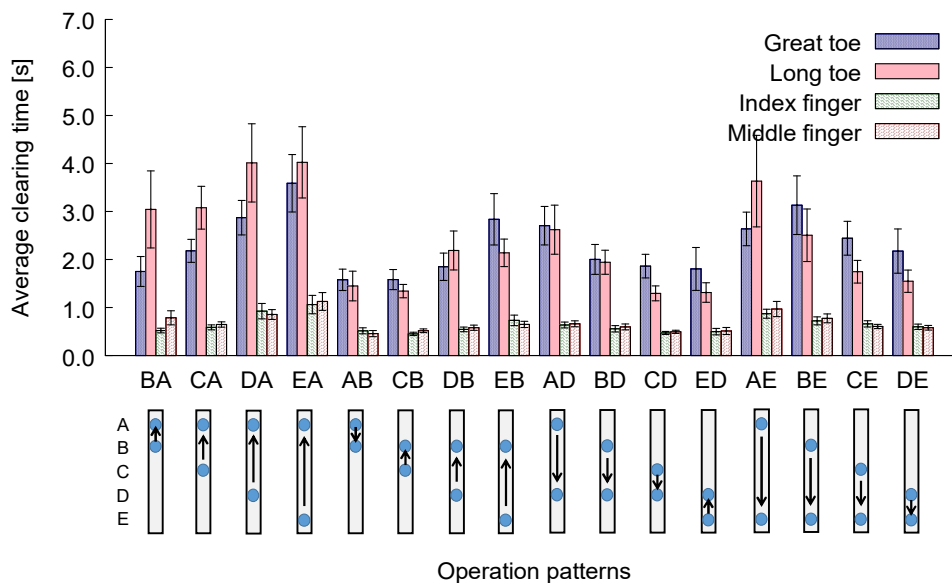
Fig. 4.16 Average clearing time of each toe and finger in the operation experiments (*: $p \leq 0.05$).

large angle, such as patterns BA, CA, DA, and EA. In particular, significant differences were observed for patterns BA, CA, and DA. On the other hand, for patterns in which the target appears at position D or E (patterns AD, BD, CD, ED, AE, BE, CE, and DE), the average clearing time of the long toe was shorter than that of the great toe, except for pattern AE. Highly significant differences were observed for the patterns that only involved positions C, D, and E, such as patterns CD, CE, DE, and ED. This finding suggests that the long toe is easier to operate than the great toe when the toe is moved on the bending side from the center position.

Similarly, **Fig. 4.17** focuses on the pairs of operation patterns in which the marker had the same movement distance and opposite movement directions (AB and BA, AD and DA, AE and EA, BD and DB, BE and EB, and DE and ED) and shows the results of a comparison of average clearing times for these pattern pairs. The average clearing time when the target for the great toe appeared at position A or E (DE, BE, DA, and BA) was longer than that when it appeared at position B or D (ED,

Fig. 4.17 Comparisons of clearing times of operation patterns with the same movement distance and opposite movement direction for two-toe and -finger operation (*: $p \le 0.05$; **: $p \le 0.01$).

Fig. 4.18 Ratios of average clearing time of the evaluation experiments using one and two toes or fingers.

EB, AD, and AB). Similarly, based on the experimental results for the long toe, highly significant differences were observed when comparing DA and DA and BA and AB. In other words, when a toe was moved to clear a target that appeared close to the boundary 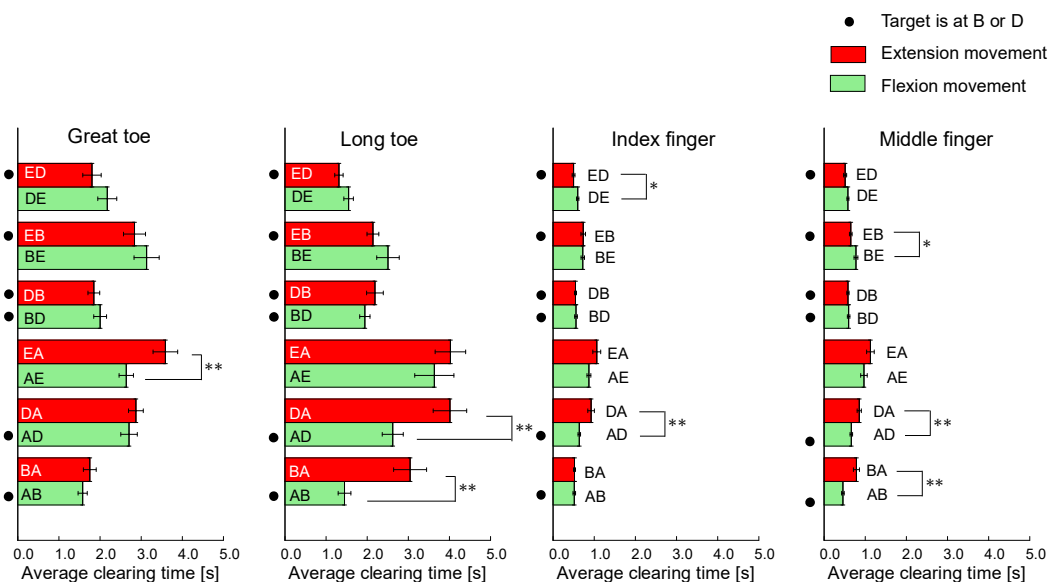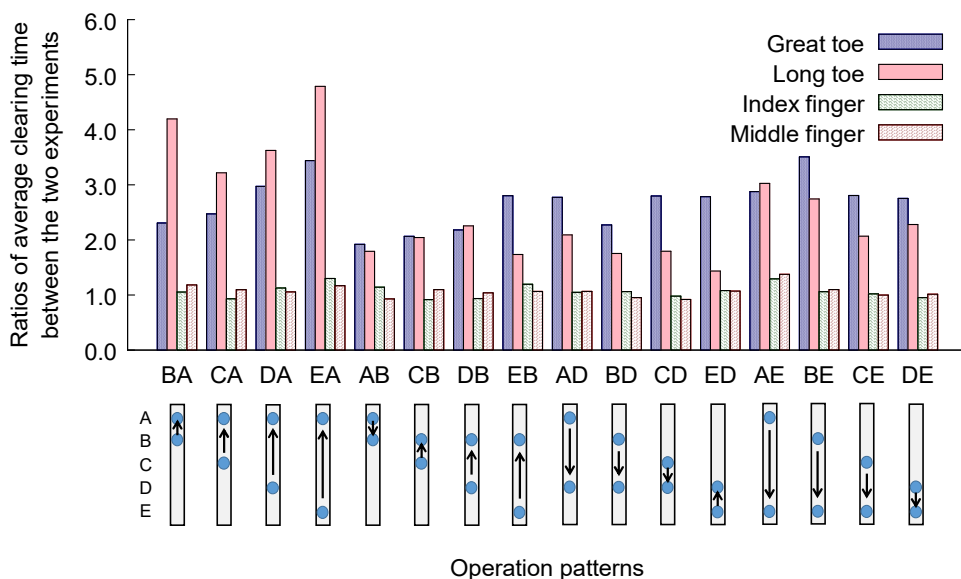of that toe's ROM, such as position A or E, the adjacent toe tended to drag. As a result, this movement became difficult. In the experiment for one-toe operation described in the previous section, no such tendency was observed for the great toe. As for the long toe, in one-toe operation, the average clearing time was shorter when the target was at A or E compared with at B or D. This means the tendency was opposite between the one- and two-toe experiments, and indicates that attention should be paid to this characteristic when toes are used for operation. In other words, whether movements are easy or difficult differs when one or two toes are used for operation. It is easy for operators to bend or stretch the toe at a large angle when only one toe is used, whereas it is easy to bend or stretch one toe at a small angle when two adjacent toes are used. It is thus desirable to understand this characteristic before constructing a toe-operating system. **Fig. 4.18** shows the ratio of the average clearing times gained in the one- and two-toe experiments, and clarifies how much worse the two-toe operations were in comparison with the one-toe operations. As shown in **Fig. 4.18**, the ratio for the long toe was larger in the patterns in which the target appeared at position A and the toe was greatly extended (BA, CA, DA, and EA), while that of the great toe was larger in the patterns in which the toe was bent (AD, BD, CD, BE, CE, and DE). This result suggests that if two toes are used for operation, extension of the long toe becomes more difficult than the great toe, whereas flexion of the great toe becomes more difficult than the long toe.

4.5 SUMMARY

In this chapter, which focused on operation by toe movements, a measurement device for toe flexion and extension characteristics was developed, and a new evaluation system using this device was constructed. Several experiments using this evaluation system were conducted to clarify the motion characteristics and operability of the great and long toes and index and middle fingers when used for operation. The following results were obtained:

1) A device for measuring toe flexion and extension was developed using wire displacement sensors. This device can also be applied to fingers.

2) An evaluation system was constructed to evaluate the flexion and extension movements of toes when used to operate a marker displayed on a PC monitor.

3) The results of evaluation experiments involving operation with a single toe or finger were as follows: i) a difference in the operability of the toes and fingers was confirmed quantitatively, in that the average clearing time of the toes was 1.45 times longer than that of the fingers; ii) the great toe showed higher operability than the long toe, and the difference in clearing time with two toes was approximately 9%; and iii) no significant difference was observed in the clearing time between the index and middle fingers.

4) The results of comparisons of each operation pattern in the experiments with the single toe were as follows: i) the operability of the long toe was higher when it was bent or stretched toward the boundary of its ROM than when it was moved toward the center position of this ROM; ii) no such characteristic was found in the experiments with the great toe, meaning that the great and long toes showed different characteristics; and iii) the operability of the fingers when moved toward the boundary of their ROM was lower than that when they were moved toward the center position, which disagreed with the experimental results for the long toe.

5) The results of the evaluation experiments regarding operation with two toes or fingers were

as follows: i) the toes required a clearing time 3.51 times longer than that of the fingers; and ii) no significant difference was found when comparing the great and long toes or the index and middle fingers.

6) A comparison of operation using one or two toes indicated that: i) the clearing time of the great and long toes increased by 167.1% and 151.5%, respectively, which confirmed quantitatively that the operability of two toes was greatly deteriorated compared with a single toe; and ii) the operability of the fingers showed no apparent difference between one- and two-finger operations.

7) Similarly, the experimental results for each pattern analyzed for operation with two toes were as follows: i) when toes were moved on the bending side from the center position, the long toe showed higher operability than the great toe; and ii) it was easier to operate toes around the center than around the boundary position of the ROM. In one-toe operation, the great toe showed no such tendency and the long toe showed the opposite tendency. This finding indicated that whether the movements of the toes were easy or difficult differed when operating with one or two toes.

In the future, these research results are expected to be used for the development of a toe operation device. By using the results, the operability of the operation device can be improved.

CHAPTER 5
Conclusions and Future Works

Modularizing an automated production line can reduce the cost, enhance the utilization rate, and improve the flexibility. Mobile manipulators, including MSMs and MPMs, are expected to be applied for the modular designs of production lines. MSMs have a dexterous open-loop manipulator and can thus perform complicated operations, whereas MPMs have a closed-loop mechanism with higher stiffness and positioning accuracy and can thus finish transporting and positioning tasks of objects. Regarding these two kinds of mobile manipulators, three topics were discussed in this thesis.

Chapter 2 proposed a novel MPM, named VEMOPAM, which is composed of two 2WD carts, a parallel mechanism (SLPTM), and a platform. With the nonholonomic structure of VEMOPAM, only four motors mounted on the carts are used to control the 6-DOF spatial movements of the platform. In comparison with the conventional MPMs, VEMOPAM has fewer motors and only one loop in its parallel structure, and therefore it has a lower development cost and a relatively smaller occupied area, which are the foremost advantages of this proposed mechanism. Based on the kinematics, this study gave a Jacobian matrix for VEMOPAM, and revealed its singular and failure configurations. Using these kinematic analysis results, this study proposed a path planning method (FSPP method) for the two carts, and constructed a feedback tracking control system for the carts to track the planned paths. A path planner based on the proposed FSPP method can generate non-optimal paths excluding the influence of the complex structural condition of VEMOPAM on the movements of the carts. Therefore, only the initial and target poses of VEMOPAM need to be input into this planner, which simplifies the path generation process and reduce the computational cost. Two sets of simulations were conducted to verify the effectiveness and advantages of the FSPP method. Furthermore, an experimental prototype of VEMOPAM was developed for the validations of the proposed mechanism and methods.

The developed prototype of VEMOPAM has a simple structure similar to its conceptual diagram (see **Figs. 2.2** and **2.17**). Such a prototype can be used to clarify the basic kinematic characteristics of VEMOPAM under a low-velocity condition. However, the current version of the prototype cannot transport a heavy object nor move with a high velocity. It is also problematic in terms of stiffness and vibration resistance, since screw shafts B1 and B2 are respectively unilaterally fixed on carts A1 and A2. During the motions of the two carts, because of the internal friction, one of the drive wheels of a cart may leave from the floor, which makes this cart unable to move as desired. Appendix 3 gives a detailed description of these problems, and proposes a practical design of VEMOPAM that can solve them. The future research will focus on this new mechanism of VEMOPAM, analyze its kinematics and dynamics, propose a new robust controller for the control of the pose of the platform, and discuss how to optimize the paths of the carts. On the other hand, since other kinds of vehicles and parallel mechanisms can also be used in VEMOPAM, the future research will compare and analyze the characteristics of these new mechanisms and the current mechanism.

In Chapter 3, an evaluation system was proposed for quantitatively evaluating the effects of viewpoint changes on the two operation methods, i.e., the button- and body motion-based methods. A three-dimensional virtual operation space which had an imaginary robotic hand and a target was constructed. Operators wore 3D glasses and were instructed to move the position and posture of the

imaginary robotic hand to the target as soon as possible. In the button-based operation experiments, the examinees operated a simplified teaching pendant; in the body motion-based operation experiments, they operated a bracket with multiple markers that was fixed to their hands. The viewpoint changes were simulated by rotating the virtual operation space. For eight kinds of viewpoint angles, the clearing times for the two operation methods were measured. The experimental results quantitatively confirmed that the average clearing times for the body motion-based method were significantly shorter than those for the button-based method for all the viewpoint angles, and that the differences in the clearing times of the two operating methods were mainly due to differences in the non-operating times. For the button-based operation method, the numbers of times the operator used trial-and-error were also measured and analyzed; from the analysis results, it was illustrated that viewpoint change made the positional operation much more difficult, but had a relatively smaller influence on the postural operation. For the body motion-based method, the ideality for each of the viewpoint angles was defined; the analysis results of the idealities showed that the body motion-based method may be robust to viewpoint changes.

In the future, a real robotic arm with more details will be used, and more environmental elements (e.g., some obstacles around the robotic arm) will be added into the virtual operation space, which makes it possible to simulate more real situations. With viewpoint changes, the effects of these environmental elements on the operability will be quantitatively assessed. In addition, an operation system with an actual operation environment will also be constructed. This operation system is expected to be used as a training system for novice operators to get used to viewpoint changes quickly.

Chapter 4 proposed a new operation device that could measure the flexions and extensions of operators' toes. An operation system with this device that allowed operators to perform various position operations by stretching and bending toes was developed. Such a system was used to conduct experiments to evaluate the operability and movement characteristics of the great and long toes. The experimental results quantitatively clarified the differences between the operability of great and long toes, between the operability of one-toe and two-toe operations, and between the operability of toes and fingers. These experimental results showed that human toes had the potential for simple position operations.

In the future research, a further investigation on the operability of toes is needed for practical applications. For example, it is necessary to assess the influence of fatigue if the toes are used for operations for a long time.

Appendixes

APPENDIX 1
Geometrical Relations in VEMOPAM

Here, the geometric relations among the modules of VEMOPAM are shown. First, **Fig. A** shows the reference pose of VEMOPAM. As have been described in chapter 2, the reference position of the platform with respect to $O-XYZ$ is defined as $\{x, y, z\} = \{0, 0, z_{con}\}$, and the reference orientation of that is defined as the orientation when axes X_p, Y_p, and Z_p have the same directions with X, Y, and Z, respectively. The current orientation angles ϕ_x, ϕ_y, and ϕ_z of the platform are obtained by rotating the platform from the reference orientation to the current orientation about the three axes in the order of Z_p, X_p, and Y_p.

Then, based on the above definitions of the reference pose, the relations between the poses of the carts and the platform can be obtained. **Fig. B** shows the projection of VEMOPAM on plane $O-XY$. From this figure, the relations between the positions of the carts and the platform with respect to $O-XY$ can be derived as follows:

$$
\begin{aligned}
x_1 &= x + l_1 \sin \phi_z + l_2 \cos \phi_z + l_3 \cos \phi_x \sin \phi_z, \\
y_1 &= y - l_1 \cos \phi_z + l_2 \sin \phi_z - l_3 \cos \phi_x \cos \phi_z, \\
x_2 &= x - l_1 \sin \phi_z - l_2 \cos \phi_z - l_s \cos \phi_x \sin \phi_z, \\
y_2 &= y + l_1 \cos \phi_z - l_2 \sin \phi_z + l_s \cos \phi_x \cos \phi_z.
\end{aligned}
\tag{A.1}
$$

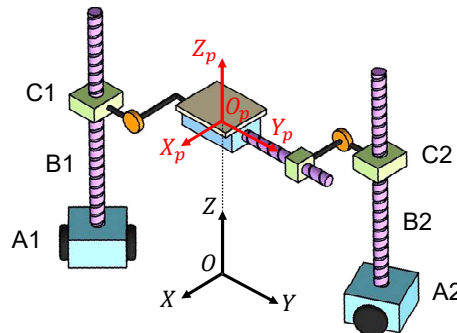Next, **Fig. C** shows the relations between the vertical displacements of the platform and nuts C1 and
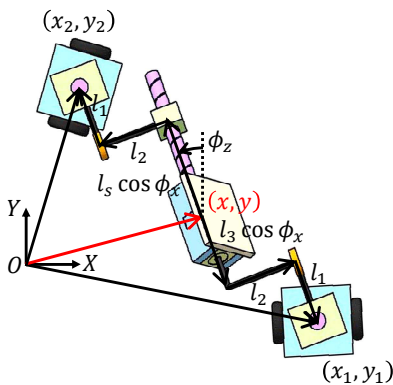

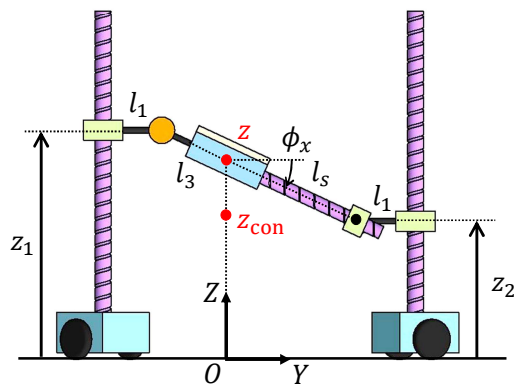**Fig. A** Reference pose of VEMOPAM.

Fig. B Top-view of VEMOPAM.

Fig. C Side-view of VEMOPAM.

C2. The vertical displacements of C1 and C2, i.e., z_1 and z_2, are represented by the following equations,

$$z_1 = z - z_{\text{con}} - l_3 \sin \phi_x ,$$
$$z_2 = z - z_{\text{con}} + l_s \sin \phi_x . \tag{A.2}$$

The values of z_1 and z_2 are determined by the screw motions of B1-C1 and B2-C2. The rotations of screw shafts B1 and B2 can be represented using the angles of rotation of carts A1 and A2, respectively. And, as shown in **Fig. B**, the rotations of nuts C1 and C2 can be also be represented using the roll angle ϕ_z of the platform. It is assumed that all the screw shafts in VEMOPAM have right-handed threads. Therefore,

$$z_1 = p_1(\phi_z - \phi_1)/2\pi ,$$
$$z_2 = p_1(\phi_z - \phi_2)/2\pi . \tag{A.3}$$

Equations (A.1), (A.2), and (A.3) show the geometric relations between the carts and the platform.

APPENDIX 2
Design of Carts of VEMOPAM Prototype

This appendix gives the detailed design of the carts in the developed prototype of VEMOPAM, which is shown in **Fig. D**. All the programs in the feedback tracking control system for the carts were developed using Python. The built-in PI controller for the motors with the default gains $K_p = 100$ and $K_i = 1920$ (given in Section 2.6-II) was used to accurately output the driving speeds of drive wheels of the carts. The effectiveness of these default gains was confirmed by preliminary experiments. Additionally, as described in Section 2.6-II, a Kalman filter (OpenCV library 4.5.3, Python version) was used to eliminate inaccuracies and noise in the pose information of the carts measured by the VICON cameras. According to the results of preliminary experiments, the estimated

Drive wheel   Auxiliary ball-caster

1: Motor (Dynamixel XH540-W150-R, Robotis Co., Ltd., South Korea);
2: Communication I/F (DXHUB, Best Technology Co., Ltd., Japan);
3: Mini-computer (Raspberry Pi 4 8gb Model B, Raspberry Pi Foundation, UK);
4: 5V power supply module with two batteries (18650) for the mini-computer;
5: 12V Battery for the motors (FML1220, The Furukawa Battery Co., Ltd., Japan);
6: Monitor (5inch HDMI, Seeed Studio, China).

Fig. D Design of carts of VEMOPAM.

Specifications of DC Motors

Stall torque: 7.3 Nm (at 12.0 V, 4.4 A);
No-load speed: 53 rpm (at 12.0 V);
Allowable axial load: 20 N;
Weight: 165 g;
Links: RS-485 Multi Drop;
Communication speed: 57.6k.
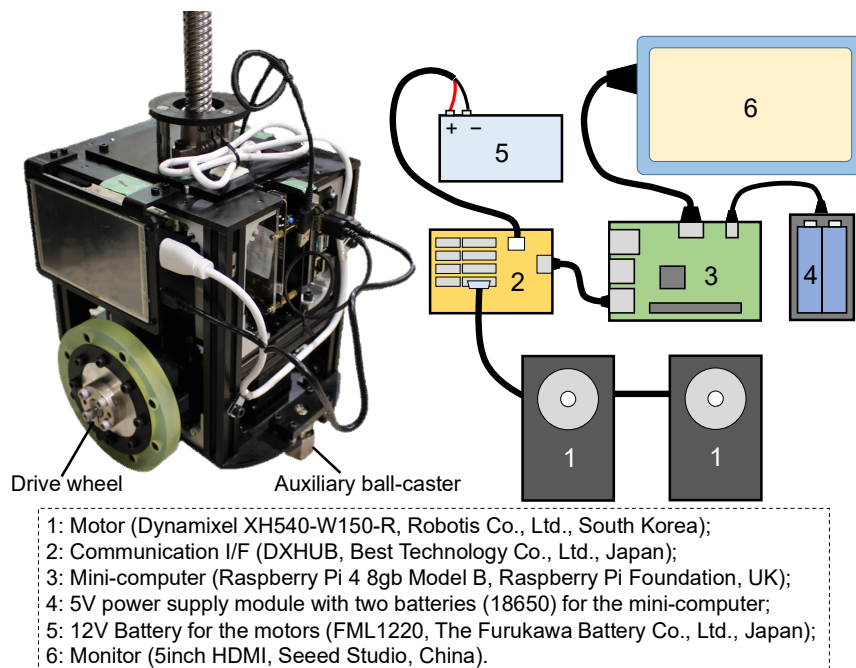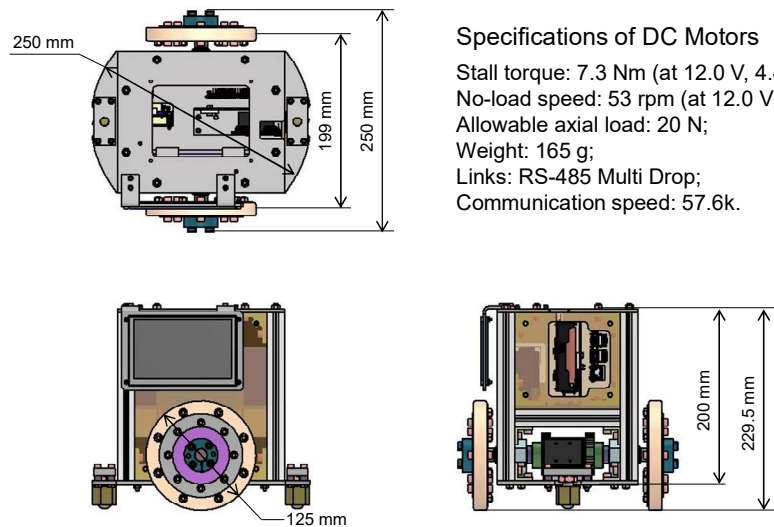
Fig. E Size of carts and specifications of driving motors.

error for the VICON cameras was measured to be about 0.01 mm, and the effect of the Kalman filter on the stability of this control system was sufficiently small.

Figure E shows the size of the carts. Each of the carts weighs about 7 kg. Such a design realizes the miniaturization of the cart and ensures that the two carts never collide with each other due to the internal constraints of VEMOPAM. **Fig. E** also gives the specifications of the used motors. These motors provide sufficient driving forces and guarantee that the carts move as desired.

APPENDIX 3
Practical Design of VEMOPAM

Chapter 2 shows an experimental prototype of VEMOPAM (see **Fig. 2.17**, Section 2.6-I). To clearly show the structure and movements of VEMOPAM, this prototype has a simple structure as shown in **Fig. 2.2** and is only used to verify the kinematic characteristics. However, some problems in this structure may adversely affect its practical applications. Some of the problems are shown in **Fig. F**. For example, as shown in **Fig. F(b)**, during the motions of the carts of VEMOPAM, because of the internal friction in screw shaft B3 and nut C3, it is possible that one of the drive wheels of the carts becomes unable to grip the floor, which makes the carts unable to move as planned. And, as shown in **Fig. F(c)**, if VEMOPAM is used to transport heavy objects, this heavy object fixed on the platform may cause collapse of the whole mechanism.

Various mechanical designs for the practical application of VEMOPAM have been considered to solve the above-described problems. In this appendix, a kind of practical design for VEMOPAM, whose conceptual diagram is shown in **Fig. G**, is proposed. This mechanism has a frame; both the ends of screw shafts B1 and B2 are connected to this frame through crossed roller bearings, linear rails and sliders, etc. The platform is also connected to the frame through shaft-sliding bushings so that it can move vertically over the frame. Comparing with the current mechanism, such a practical mechanical design has four advantages: i) since the carts are both connected to frame, the collapse of the carts shown in **Fig. F** can be avoided by the internal constraints; ii) since both the ends of B1 and B2 are connected to the frame, the stiffness of this mechanism can be improved, and vibrations in shafts B1 and B2 during the motion can be reduced; iii) if there is an object on the platform, interference between this object and B1 and B2 can be avoided; iv) compared with the current
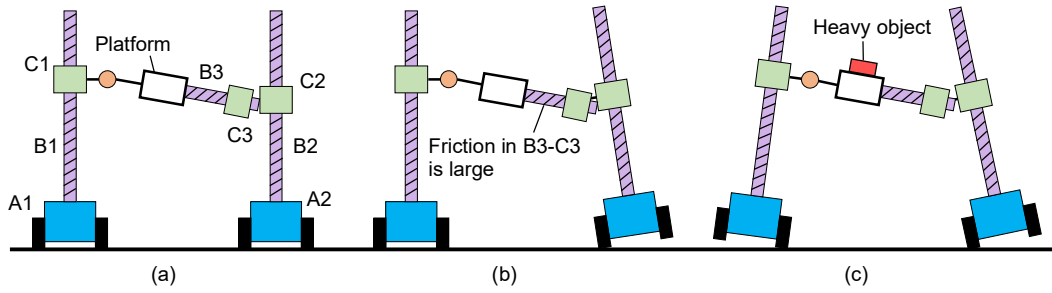
Fig. F Some problems in current structure of VEMOPAM: (a) normal status; (a) low gripping ability due to friction in B3-C3; (b) falling down due to heavy object.

① Frame; ② Linear rail and slider; ③ Crossed roller bearing; ④ Bearing and housing; ⑤ Shaft-sliding bushing; ⑥ Connecting plate

Fig. G Practical design of VEMOPAM.
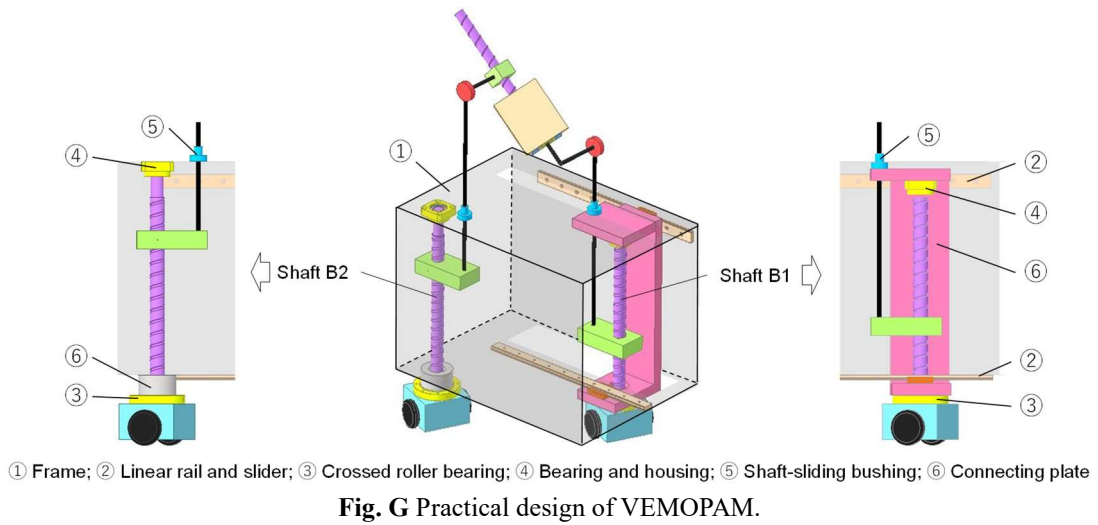
mechanism in which two mini-computers are used to control the two carts, this mechanism has the carts controlled by only one mini-computer fixed on the frame, which improves the control accuracy and cooperativity of the carts.

References

[1]   YA series, Yamaha Motor Co., Ltd.,
      <https://www.yamaha-motor.co.jp/robot/download/catalog/pdf/2021-2022_CATALOG_YA.pdf>

[2]   YK-XE series, Yamaha Motor Co., Ltd., <https://www.yamaha-motor.co.jp/robot/lineup/ykxg/yk-xe>

[3]   TT series, IAI Robot Co., Ltd., <https://iai-robot.co.th/product/table/tt.php>

[4]   VBL, Okura Yusoki Co., Ltd.,
      <https://www.okurayusoki.co.jp/product/conveyor/case/unicon5/vbl.html>

[5]   Shneier, M.O., Bostelman, R.V., "Literature review of mobile robots for manufacturing," *NISTIR–8022*, 2015.

[6]   Arai, T., "What is robot with integrated locomotion and manipulator, and its future (in Japanese)?" *Journal of the Robotics Society of Japan*, Vol.13, No.7, Oct. 1995, pp.896−899.
      <DOI: 10.7210/jrsj.13.896>

[7]   Hamner, B., Koterba, S., Shi, J., Simmons, R., and Singh, S., "An autonomous mobile manipulator for assembly tasks," *Autonomous Robots*, Vol.28, Sep. 2009, pp.131−149.
      <DOI: 10.1007/s10514-009-9142-y>

[8]   Bischoff, R., Huggenberger, U., and Prassler, E., "KUKA youBot – a mobile manipulator for research and education," in: *2011 IEEE International Conference on Robotics and Automation*, Shanghai, China, May 2011. <DOI: 10.1109/ICRA.2011.5980575>

[9]   Jain, A., and Kemp, C.C., "EI-E: an assistive mobile manipulator that autonomously fetches objects from flat surfaces," *Autonomous Robots*, Vol.28, No.1, Sep. 2010, pp.45−64.

[10] Yamamoto, Y., and Yun, X., "Coordinating locomotion and manipulation of a mobile manipulator," in: *Proceedings of the 31st IEEE Conference on Decision and Control*, Tucson, AZ, USA, Dec. 1992, pp. 2643−2648. <DOI: 10.1109/CDC.1992.371337>

[11] Minami, M., Fujiwara, N., and Tsuge, H., "Position and orientation control of manipulator mounted on autonomous mobile robot (in Japanese)," *Journal of the Robotics Society of Japan*, Vol.11, No.1, Jan. 1993, pp.156−164. <DOI: 10.7210/jrsj.11.156>

[12] Carius, J., Wermelinger, M., Rajasekaran, B., Holtmann, K., and Hutter, M., "Deployment of an autonomous mobile manipulator at MBZIRC," *Journal of Field Robotics*, Vol.35, Oct. 2018, pp.1−19.
      <DOI: 10.1002/rob.21825>

[13] Stewart, D., "A platform with six degrees of freedom," in: *Proceedings of the Institution of Mechanical Engineers*, Vol.180, No.1, Jun. 1965, pp.371−386. <DOI: 10.1243/PIME_PROC_1965_180_029_02>

[14] Arai, T., "Analysis and synthesis of a parallel link manipulator based on its statics (in Japanese)," *Journal of the Robotics Society of Japan*, Vol.10, No.4, Aug. 1992, pp.526−533. <DOI: 10.7210/jrsj.10.526>

[15] Kosuge, K., Okuda, M., Kawamata, H., Fukuda, T., Kozuka, T., and Mizuno, T., "Input/output force analysis of parallel link manipulator (in Japanese)," *Transactions of the Japan Society of Mechanical Engineers, Series C*, Vol.60, No.575, Jul. 1994, pp.2338−2344. <DOI: 10.1299/KIKAIC.60.2338>

[16] Lebret, G., Liu, K., and Lewis, F.L., "Dynamic analysis and control of a Stewart platform manipulator," *Journal of Robotic Systems*, Vol.10, No.5, Jul. 1993, pp.629−655. <DOI: 10.1002/rob.4620100506>

[17] Dasgupta, B., and Mruthyunjaya, T.S., "Closed-form dynamic equations of the general Stewart platform through the Newton-Euler approach," *Mechanism and Machine Theory*, Vol.33, No.7, Oct. 1998, pp.993−1012. <DOI: 10.1016/S0094-114X(97)00087-6>

[18] Dasgupta, B., and Mruthyunjaya, T.S., "A Newton-Euler formulation for the inverse dynamics of the Stewart platform manipulator," *Mechanism and Machine Theory*, Vol.33, No.8, Nov. 1998, pp.1135−1152. <DOI: 10.1016/S0094-114X(97)00118-3>

[19] Liu, M.J., Li, C.X., and Li, C.N., "Dynamics analysis of the Gough-Stewart platform manipulator," *IEEE*

Transactions on Robotics and Automation, Vol.16, No.1, Feb. 2000, pp.94−98. <DOI: 10.1109/70.833196>

[20] Fujita, T., and Sugawara, H., "Development of a parallel link arm for object handling by wheeled mobile robot," in: *2014 11th International Conference on Informatics in Control, Automation and Robotics (ICINCO)*, Vienna, Austria, Sep. 2014. <DOI: 10.5220/0005116905920598>

[21] Graf, R., and Dillmann, R., "Acceleration compensation using a Stewart platform on a mobile robot," in: *1999 Third European Workshop on Advanced Mobile Robots. Proceedings*, Zurich, Switzerland, Sep. 1999. <DOI: 10.1109/EURBOT.1999.827617>

[22] Dang, A.X.H., and Ebert-Uphoff, I., "Active acceleration compensation for transport vehicles carrying delicate objects," *IEEE Transactions on Robotics*, Vol.20, No.5, Nov. 2004, pp.830−839. <DOI: 10.1109/TRO.2004.832791>

[23] Yamawaki, T., Mori, O., and Omata, T., "4R and 5R parallel mechanism mobile robots (in Japanese)," *Journal of the Robotics Society of Japan*, Vol.23, No.2, Mar. 2005, pp.213−219. <DOI: 10.7210/jrsj.23.213>

[24] Li, Y., Xu, Q., and Liu, Y., "Novel design and modeling of a mobile parallel manipulator," in: *Proceedings 2006 IEEE International Conference on Robotics and Automation*, Orlando, FL, USA, May 2006. <DOI: 10.1109/ROBOT.2006.1641862>

[25] Elwin, M.L., "Human-multirobot collaborative mobile manipulation: the Omnid mocobots," *IEEE Robotics and Automation Letters*, Vol.8, No.1, Jan. 2023, pp.376−383.

[26] Tsai, L.W., and Tahmasebi, F., "Synthesis and analysis of a new class of six-degree-of-freedom parallel minimanipulators," *Journal of Robotics Systems*, Vol.10, No.5, Jul. 1993, pp.561−580. <DOI: 10.1002/rob.4620100503>

[27] Tsai, L.W., "The Jacobian analysis of parallel manipulator using reciprocal screws," *Advances in Robot Kinematics: Analysis and Control*, 1998, pp.327−336.

[28] Takamasu, K., Yoshida, K., Senoo, T., Chen, X., Kotani, K., and Takahashi, S., "Calibration of 6 DOF parallel mechanism driven by planar motors," in: *9th International Symposium on Measurement and Quality Control*, IIT Madras, Nov. 2007, pp.178−183.

[29] Ben-Horin, R., Shoham, M., and Djerassi, S., "Kinetics, dynamics and construction of a planarly actuated parallel robot," *Robotics and Computer-Integrated Manufacturing*, Vol.14, No.2, Apr. 1998, pp.163−172. <DOI: 10.1016/S0736-5845(97)00035-5>

[30] Shoval, S., Shoham, M., "Sensory redundant parallel mobile mechanism," in: *Proceedings 2001 ICRA. IEEE International Conference on Robotics and Automation*, Seoul, South Korea, May 2001. <DOI: 10.1109/ROBOT.2001.932961>

[31] Ben-Horin, P., Djerassi, S., Shoham, M., and Ben-Horin, R., "Dynamics of a six degree-of-freedom parallel robot actuated by three two-wheel carts," *Multibody System Dynamics*, Vol.16, No.2, Sep. 2006, pp.105−121. <DOI: 10.1007/s11044-006-9016-4>

[32] Long, S., Terakawa, T., and Komori, M., "Type synthesis of 6-DOF mobile parallel link mechanisms based on screw theory," *Journal of Advanced Mechanical Design, Systems, and Manufacturing*, Vol.16, No.1, Jan. 2022, JAMDSM0005. <DOI: 10.1299/jamdsm.2022jamdsm0005>

[33] Terakawa, T., Komori, M., Matsuda, K., and Mikami, S., "A novel omnidirectional mobile robot with wheels connected by passive sliding joints," *IEEE/ASME Transactions on Mechatronics*, Vol.23, No.4, Aug. 2018, pp.1716−1727. <DOI: 10.1109/TMECH.2018.2842259>

[34] Terakawa, T., Komori, M., and Fujimoto, K., "Control of an omnidirectional mobile robot with wheels connected by passive sliding joints," *Journal of Advanced Mechanical Design, Systems, and Manufacturing*, Vol.13, No.1, Jan. 2019, JAMDSM0006. <DOI: 10.1299/jamdsm.2019jamdsm0006>

[35] Hu, Y., Zhang, J., Wan, Z., and Lin, J., "Design and analysis of a 6-DOF mobile parallel robot with 3

limbs," *Journal of Mechanical Science and Technology*, Vol.25, No.12, Jan. 2012, pp.3215−3222. <DOI: 10.1007/s12206-011-0904-z>

[36] Tang, C.P., and Krovi, V.N., "Manipulability-based configuration evaluation of coorperative payload transport by mobile manipulator collectives," *Robotica*, Vol.25, No.1, Aug. 2006, pp.29−42. <DOI: 10.1017/S0263574706002979>

[37] Wada, M., and Mori, S., "Development of a holonomic and omnidirectional mobile robot (in Japanese)," *Journal of the Robotics Society of Japan*, Vol.15, No.8, Nov. 1997, pp.1139−1146. <DOI: 10.7210/jrsj.15.1139>

[38] Wada, M., "Design and analysis of a wheeled platform with a synchro caster-drive mechanism for holonomic and omnidirectional mobile robots (in Japanese)," *Journal of the Robotics Society of Japan*, Vol.19, No.6, Sep. 2001, pp.784−792. <DOI: 10.7210/jrsj.19.784>

[39] Chung, W., Moon, C., Jung, C., and Jin, J., "Design of the dual offset active caster wheel for holonomic omni-directional mobile robots," *International Journal of Advanced Robotic Systems*, Vol.7, No.4, Jan. 2010, pp.101−106. <DOI: 10.5772/10485>

[40] Komori, M., Matsuda, K., Terakawa, T., Takeoka, F., Nishihara, H., and Ohashi, H., "Active omni wheel capable of active motion in arbitrary direction and omnidirectional vehicle," *Journal of Advanced Mechanical Design, Systems, and Manufacturing*, Vol.10, No.6, Oct. 2016, JAMDSM0086. <DOI: 10.1299/jamdsm.2016jamdsm0086>

[41] Terakawa, T., Komori, M., Yamaguchi, Y., and Nishida, Y., "Active omni wheel possessing seamless periphery and omnidirectional vehicle using it," *Precision Engineering*, Vol.56, Mar. 2019, pp.466−475. <DOI: 10.1016/j.precisioneng.2019.02.003>

[42] Diegel, O., Badve, A., Bright, G., Potgieter, J., and Tlade, S., "Improved Mecanum wheel design for omni-directional robots," in: *Proceedings. 2002 Australasian Conference on Robotics and Automation*, Auckland, New Zealand, Nov. 2002, pp.117−121.

[43] Salih, J.E.M., Rizon, M., Yaacob, S., Adom, A.H., and Mamat, M.R., "Designing omni-directional mobile robot with Mecanum wheel," *American Journal of Applied Sciences*, Vol.3, No.5, May 2006, pp.1831−1835. <DOI: 10.3844/ajassp.2006.1831.1835>

[44] Tadakuma, K., and Tadakuma, R., "Mechanical design of 'omni-ball': spherical wheel for holonomic omnidirectional motion," in: *Proceedings of the 3rd Annual IEEE Conference on Automation Science and Engineering*, Scottsdale, AZ, USA, Sep. 2007, pp.788−794. <DOI: 10.1109/COASE.2007.4341852>

[45] Staicu, S., "Dynamics equations of a mobile robot provided with caster wheel," *Nonlinear Dynamics*, Vol.58, Feb. 2009, pp.237−248. <DOI: 10.1007/s11071-009-9474-3>

[46] Yun, X., and Yamamoto, Y., "Internal dynamics of a wheeled mobile robot," in: *Proceedings of 1993 IEEE/RSJ International Conference on Intelligent Robots and Systems*, Yokohama, Japan, Jul. 1993, pp.1288−1294. <DOI: 10.1109/IROS.1993.583753>

[47] Nandy, S., Shome, S.N., Chakraborty, G., and Kumar, C.S., "A modular approach to detailed dynamic formulation and control of wheeled mobile robot," in: *2011 IEEE International Conference on Mechatronics and Automation*, Beijing, China, Aug. 2011. <DOI: 10.1109/ICMA.2011.5985967>

[48] Li, Y., and Xu, Q., "Kinematics and inverse dynamics analysis for a general 3-PRS spatial parallel mechanism," *Robotica*, Vol.23, No.2, Mar. 2005, pp.219−229. <DOI: 10.1017/S0263574704000797>

[49] Tian, Y., Shirinzadeh, B., and Zhang, D., "Design and dynamics of a 3-DOF flexure-based parallel mechanism for micro/nano manipulation," *Microelectronic Engineering*, Vol.87, No.2, Feb. 2010, pp.230−241. <DOI: 10.1016/j.mee.2009.08.001>

[50] Kakino, Y., Matsubara, A., Li, Z., Ueda, D., Nakagawa, H., Takeshita, T., and Maruyama, H., "A study on the total tuning of feed drive systems in NC machine tools (1st report) – modeling of feed drive mechanism and identification of the parameters (in Japanese)," *Journal of the Japan Society for Precision*

Engineering, Vol.60, No.8, Aug. 1994, pp.1097−1101. <DOI: 10.2493/jjspe.60.1097>

[51] Holroyd, G., Pislaru, C., and Ford, D.G., "Modelling the dynamic behaviour of a ball-screw system taking into account the changing position of the ball-screw nut," *Transactions on Engineering Sciences*, Vol.44, 2003, pp.337−348.

[52] Zhang, J., Zhang, G., and Furusho, J., "A study on control of ball-screw driving system considering the characteristics of two-inertia-system (in Japanese)," *Journal of the Japan Society for Precision Engineering, Contributed Papers*, Vol.70, No.5, May 2004, pp.689−694. <DOI: 10.2493/jspe.70.689>

[53] Gosselin, C., and Angeles, J., "Singularity analysis of closed-loop kinematic chains," *IEEE Transactions on Robotics and Automation*, Vol.6, No.3, Jun. 1990, pp.281−290. <DOI: 10.1109/70.56660>

[54] Tsubouchi, T., Naniwa, T., and Arimoto, S., "Planning and navigation by a mobile robot in the presence of multiple moving obstacles and their velocities (in Japanese)," *Journal of the Robotics Society of Japan*, Vol.12, No.7, Oct. 1994, pp.1029−1037. <DOI: 10.7210/jrsj.12.1029>

[55] Stentz, A., "Optimal and efficient path planning for partially-known environments," in: *Proceedings of the 1994 IEEE International Conference on Robotics and Automation*, San Diego, CA, USA, May 1994, pp. 3310-3317. <DOI: 10.1109/ROBOT.1994.351061>

[56] Stentz, A., and Hebert, M., "A complete navigation system for goal acquisition in unknown environments," *Autonomous Robots*, Vol.2, Jun. 1995, pp.127−145. <DOI: 10.1007/BF00735431>

[57] Moon, I., Miura, J., and Shirai, Y., "Online viewpoint and motion planning method under uncertainty (in Japanese)," *Journal of the Robotics Society of Japan*, Vol.17, No.8, Nov. 1999, pp.1107−1113. <DOI: 10.7210/jrsj.17.1107>

[58] Koenig, S., and Likhachev, M., "D* Lite," *AAAI-02 Proceedings*, 2002, pp.476−483.

[59] Seki, H., Gao, Z., Kamiya, Y., Hikizu, M., and Zhang, Q., "Trajectory generation of wheeled mobile robot by repeatedly direct kinematics (in Japanese)," *Journal of the Japan Society for Precision Engineering, Contributed Papers*, Vol.71, No.4, 2005, pp.506−511. <DOI: 10.2493/jspe.71.506>

[60] AL-Taharwa, I., Sheta, A., and Al-Weshah, M., "A mobile robot path planning using genetic algorithm in static environment," *Journal of Computer Science*, Vol.4, No.4, 2008, pp.341−344. <DOI: 10.3844/jcssp.2008.341.344>

[61] Lamini, C., Benhlima, S., and Elbekri, A., "Genetic algorithm based approach for autonomous mobile robot path planning," *Procedia Computer Science*, Vol.127, Mar. 2018, pp.180−189. <DOI: 10.1016/j.procs.2018.01.113>

[62] Shibata, T., Fukuda, T., Kosuge, K., and Arai, F., "Path planning using Genetic Algorithm (in Japanese)," *Transactions of the Japan Society of Mechanical Engineers Series C*, Vol.58, No.553, Sep. 1992, pp.120−126. <DOI: 10.1299/kikaic.58.2714>

[63] Shibata, T., and Fukuda, T., "Path planning using Genetic Algorithm (2nd report, selfish planning and coordinative planning for multiple-mobile-robot systems) (in Japanese)," *Transactions of the Japan Society of Mechanical Engineers Series C*, Vol.59, No.560, Apr. 1993, pp. 1134−1141. <DOI: 10.1299/kikaic.59.1134>

[64] Kosuge, K., Oosumi, T., and Chiba, K., "Load sharing of decentralized-controlled multiple mobile robots handling a single object," in: *Proceedings of International Conference on Robotics and Automation*, Albuquerque, NM, USA, Apr. 1997, pp. 3373−3378. <DOI: 10.1109/ROBOT.1997.606803>

[65] Kosuge, K., Oosumi, T., and Chiba, K., "Decentralized control of multiple mobile robots handling a single object in coordination (in Japanese)," *Journal of the Robotics Society of Japan*, Vol.16, No.1, Jan. 1998, pp.87−95. <DOI: 10.7210/jrsj.16.87>

[66] Kosuge, K., Oosumi, T., Chiba, K., and Satou, M., "Coordinated transportation by two nonholonomic mobile robots based on decentralized control (in Japanese)," *Transactions of the Japan Society of Mechanical Engineers Series C*, Vol.65, No.634, Jun. 1999, pp.2379−2385.

<DOI: 10.1299/kikaic.65.2379>

[67] Laumond, J.P., Jacobs, P.E., Taix, M., and Murray, R.M., "A motion planner for nonholonomic mobile robots," *IEEE Transactions on Robotics and Automation*, Vol.10, No.5, Oct. 1994, pp.577−593. <DOI: 10.1109/70.326564>

[68] Hashimoto, M., Oba, F., and Eguchi, T., "Dynamic object-transportation control method by multiple mobile robots (in Japanese)," *Journal of the Robotics Society of Japan*, Vol.13, No.6, Sep. 1995, pp.886−893. <DOI: 10.7210/jrsj.13.886>

[69] Kanayama, Y., Kimura, Y., Miyazaki, F., and Noguchi, T., "A stable tracking control method for an autonomous mobile robot," in: *Proceedings., IEEE International Conference on Robotics and Automation*, Cincinnati, OH, USA, May 1990. <DOI: 10.1109/ROBOT.1990.126006>

[70] Samson, C., and Ait-Abderrahim, K., "Feedback control of a nonholonomic wheeled cart in cartesian space," in: *Proceedings., 1991 IEEE International Conference on Robotics and Automation*, Sacramento, CA, USA, Apr. 1991. <DOI: 10.1109/ROBOT.1991.131748>

[71] Normey-Rico, J.E., Alcala, I., Gomez-Ortega, J., and Camacho, E.F., "Mobile robot path tracking using a robust PID controller," *Control Engineering Practice*, Vol.9, No.11, Nov. 2001, pp.1209−1214. <DOI: 10.1016/S0967-0661(01)00066-1>

[72] Jiang, Z.P., and Nijmeijer, H., "Tracking control of mobile robots: a case study in backstepping," *Automatica*, Vol.33, No.7, Jul. 1997, pp.1393−1399. <DOI: 10.1016/S0005-1098(97)00055-1>

[73] Fierro, R., and Lewis, F.L., "Control of a nonholonomic mobile robot: backstepping kinematics into dynamics," in: *Proceedings of 1995 34th IEEE Conference on Decision and Control*, New Orleans, LA, USA, Dec. 1995, pp.3805−3810. <DOI: 10.1109/CDC.1995.479190>

[74] Fierro, R., and Lewis, F.L., "Control of a nonholonomic mobile robot using neural networks," *IEEE Transactions on Neural Networks*, Vol.9, No.4, Jul. 1998, pp.589−600. <DOI: 10.1109/72.701173>

[75] Fukao, T., Nakagawa, H., and Adachi, N., "Adaptive tracking control of a nonholonomic mobile robots," *IEEE Transactions on Robotics and Automation*, Vol.16, No.5, Oct. 2000, pp.609−615. <DOI: 10.1109/70.880812>

[76] Wang, H., Fukao, T., and Adachi, N., "Adaptive tracking control of nonholonomic mobile robots: a backstepping approach (in Japanese)," *Journal of the Robotics Society of Japan*, Vol.19, No.2, Mar. 2001, pp.271−276. <DOI: 10.7210/jrsj.19.271>

[77] Murray, R.M., "Recent research in cooperative control of multivehicle systems," *Journal of Dynamic Systems, Measurement, and Control*, Vol.129, No.5, Sep. 2007, pp.571−583. <DOI: 10.1115/1.2766721>

[78] Hashimoto, M., Oba, F., and Eguchi, T., "Dynamic object-transportation control method by multiple mobile robots (in Japanese)," *Journal of the Robotics Society of Japan*, Vol.13, No.6, Sep. 1995, pp.886−893. <DOI: 10.7210/jrsj.13.886>

[79] Ota, J., Buei, Y., Arai, T., Osumi, H., and Suyama, K., "Transferring control by cooperative of two mobile robots (in Japanese)," *Journal of the Robotics Society of Japan*, Vol.14, No.2, Mar. 1996, pp.263−270. <DOI: doi.org/10.7210/jrsj.14.263>

[80] Burgard, W., Moors, M., Stachniss, C., and Schneider, F.E., "Coordinated multi-robot exploration," *IEEE Transactions on Robotics*, Vol.21, No.3, Jun. 2005, pp.376−386. <DOI: 10.1109/TRO.2004.839232>

[81] Lewis, M.A., and Tan, K.H., "High precision formation control of mobile robots using virtual structures," *Autonomous Robots*, Vol.4, Oct. 1997, pp.387−403. <DOI: 10.1023/A:1008814708459>

[82] Cruz, C.D.L., and Carelli, R., "Dynamic modeling and centralized formation control of mobile robots," in: *IECON 2006 - 32nd Annual Conference on IEEE Industrial Electronics*, Paris, France, Nov. 2006. <DOI: 10.1109/IECON.2006.347299>

[83] Consolini, L., Morbidi, F., Prattichizzo, D., and Tosques, M., "Leader-follower formation control of nonholonomic mobile robots with input constraints," *Automatica*, Vol.44, May 2008, pp.1343−1349.

<DOI: 10.1016/j.automatica.2007.09.019>

[84] Shinnoh, A., Chong, N.Y., and Lee, G., "Novel extrapolating methods using exponential function in formation control of swarm robots (in Japanese)," *Transactions of the Society of Instrument and Control Engineers*, Vol.52, No.1, Jan. 2016, pp.28−36. <DOI: 10.9746/sicetr.52.28>

[85] Mizukawa, M., and Koyama, T., "The present and future of teaching method in industrial robots (in Japanese)," *Journal of the Robotics Society of Japan*, Vol.17, No.2, Mar. 1999, pp.180−185. <DOI: 10.7210/jrsj.17.180>

[86] Horiguchi, Y., Kurono, K., Nakanishi, H., Sawaragi, T., Nagatani, T., Noda, A., and Tanaka, K., "Configural display to support position teaching to industrial robot (in Japanese)," *Transactions of the Society of Instrument and Control Engineers*, Vol.47, No.12, Jan. 2012, pp.656−665. <DOI: 10.9746/sicetr.47.656>

[87] Inoue, Y., and Takaoka, K., "Teaching method for industrial robot (in Japanese)," *Journal of the Robotics Society of Japan*, Vol.14, No.6, Sep. 1996, pp.780−783. <DOI: 10.7210/jrsj.14.780>

[88] McGinn, C., Sena, A., and Kelly, K., "Controlling robots in the home: factors that affect the performance of novice robot operators," *Applied Ergonomics*, Vol.65, Nov. 2017, pp.23−32. <DOI: 10.1016/j.apergo.2017.05.005>

[89] Gong, D., Zhao, J., Yu, J., and Zuo, G., "Motion mapping of the heterogeneous master-slave system for intuitive telemanipulation," *International Journal of Advanced Robotic Systems*, Vol.15, No.1, Jan. 2018, pp.1−9. <DOI: 10.1177/1729881417748134>

[90] Grzejszczak, T., Mikulski, M., Szkodny, T., and Jedrasiak, K., "Gesture based robot control," in: *International Conference on Computer Vision and Graphics 2012: Computer Vision and Graphics*, Vol.7594, Berlin, Heidelberg, 2012, pp.407−413. <DOI: 10.1007/978-3-642-33564-8_49>

[91] Jackowski, A., Gebhard, M., and Graser, A., "A novel head gesture based interface for hands-free control of a robot," in: *2016 IEEE International Symposium on Medical Measurements and Applications*, Benevento, Italy, May 2016. <DOI: 10.1109/MeMeA.2016.7533744>

[92] Katsuki, Y., Yamakawa, Y., Watanabe, Y., and Ishikawa, M., "Development of fast-response master-slave system using high-speed non-contact 3D sensing and high-speed robot hand," in: *2015 IEEE/RSJ International Conference on Intelligent Robots and Systems*, Hamburg, Germany, Sep. 2015, pp.1236−1241. <DOI: 10.1109/IROS.2015.7353527>

[93] Wang, Z., Reed, I., and Fey, A.M., "Toward intuitive teleoperation in surgery: human-centric evaluation of teleoperation algorithms for robotic needle steering," in: *2018 IEEE International Conference on Robotics and Automation*, Brisbane, QLD, Australia, May 2018, pp.5799−5806. <DOI: 10.1109/ICRA.2018.8460729>

[94] Komori, M., Kobayashi, K., and Tashiro, T., "Method of position command generation by index finger motion to mitigate influence of unintentional finger movements during operation," *Precision Engineering*, Vol.53, Jul. 2018, pp.96−106. <DOI: 10.1016/J.PRECISIONENG.2018.03.003>

[95] Komori, M., Uchida, T., Kobayashi, K., and Tashiro, T., "Operating method of three-dimensional positioning device using moving characteristics of human arm," *Journal of Advanced Mechanical Design, Systems, and Manufacturing*, Vol.12, No.1, Jan. 2018, JAMDSM0009. <DOI: 10.1299/jamdsm.2018jamdsm0009>

[96] Hu, C., Meng, M.Q., Liu, P.X., and Wang, X., "Visual gesture recognition for human-machine interface of robot teleoperation," in: *Proceedings 2003 IEEE/RSJ International Conference on Intelligent Robots and Systems*, Las Vegas, NV, USA, Oct. 2003, pp.1560−1565. <DOI: 10.1109/IROS.2003.1248866>

[97] Miadlicki, K., and Pajor, M., "Real-time gesture control of a CNC machine tool with the use Microsoft Kinect sensor," *International Journal of Scientific and Engineering Research*, Vol.6, No.9, Sep. 2015, pp.538−543. <DOI: 10.14299/ijser.2015.09.010>

[98] Hameed, S., Khan, M.A., Kumar, B., Arain, Z., and Hasan, M., "Gesture controlled robotic arm using Leap Motion," *Indian Journal of Science and Technology*, Vol.10, No.45, 2017, pp.1−7. <DOI: 10.17485/ijst/2017/v10i45/120630>

[99] Du, G., Zhang, P., Mai, J., and Li, Z., "Markerless Kinect-based hand tracking for robot teleoperation," *International Journal of Advanced Robotic Systems*, Vol.9, No.2, Jan. 2012, pp.1−10. <DOI: 10.5772/50093>

[100] Komori, M., Terakawa, T., and Yasuda, I., "Operability evaluation system and comparison experiment of gesture operation and button operation of robot manipulator," *IEEE Access*, Vol.8, Jan. 2020, pp.24966−24978.

[101] Yoshinada, H., Okamura, K., and Yokota, S., "Master-slave control method for hydraulic excavator," *Journal of Robotics and Mechatronics*, Vol.24, No.6, Dec. 2012, pp.977−984.

[102] Nagano, T., Yajima, R., Hamasaki, S., Nagatani, K., Moro, A., Okamoto, H., Yamauchi, G., Hashimoto, T., Yamashita, A., and Asama, H., "Arbitrary viewpoint visualization for teleoperated hydraulic excavators," *Journal of Robotics and Mechatronics*, Vol.32, No.6, Dec. 2020, pp.1233−1243.

[103] Yamada, H., Kawamura, T., and Ootsubo, K., "Development of a teleoperation system for a construction robot," *Journal of Robotics and Mechatronics*, Vol.26, No.1, Feb. 2014, pp.110−111.

[104] Kamezaki, M., Yang, J., Iwata, H., and Sugano, S., "A basic framework of virtual reality simulator for advancing disaster response work using teleoperated work machines," *Journal of Robotics and Mechatronics*, Vol.26, No.4, Aug. 2014, pp.486−495.

[105] Kondo, D., "Projection screen with wide-FOV and motion parallax display for teleoperation of construction machinery," *Journal of Robotics and Mechatronics*, Vol.33, No.3, Jun. 2021, pp.604−609.

[106] Ikeda, T., Bando, N., and Yamada, H., "Semi-automatic visual support system with drone for teleoperated construction robot," *Journal of Robotics and Mechatronics*, Vol.33, No.2, Apr. 2021, pp.313−321.

[107] Bilberg, A., and Malik, A.A., "Digital twin driven human-robot collaborative assembly," *CIRP Annals*, Vol.68, No.1, 2019, pp.499−502. <DOI: 10.1016/j.cirp.2019.04.011>

[108] Whitney, D., Rosen, E., Ullman, D., Phillips, E., and Tellex, S., "ROS reality: a virtual reality framework using consumer-grade hardware for ROS-enabled robots," in: *2018 IEEE/RSJ International Conference on Intelligent Robots and Systems*, Madrid, Spain, Oct. 2018, pp.5018−5025. <DOI: 10.1109/IROS.2018.8593513>

[109] Linn, M.C., and Peterson, A.C., "Emergence and characterization of sex differences in spatial ability: a meta-analysis," *Child Development*, Vol.56, No.6, Dec. 1985, pp.1479−1498. <DOI: 10.2307/1130467>

[110] Mohler, J.L., "A review of spatial ability research," *Engineering Design Graphics Journal*, Vol.72, No.2, Mar. 2008, pp.19−30.

[111] Shepard, R.N., and Metzler, J., "Mental rotation of three-dimensional objects," *Science*, Vol.171, No.3972, Feb. 1971, pp.701−703.

[112] Pylyshyn, Z.W., "The rate of 'mental rotation' of images: a test of a holistic analogue hypothesis," *Memory & Cognition*, Vol.7, No.1, Jan. 1979, pp.19−28. <DOI: 10.3758/BF03196930>

[113] Ekstrom, R.B., French, J.W., and Harman, H.H., "Manual for kit of factor-referenced cognitive tests," *ETS*, 1976.

[114] Kozhevnikov, M., and Hegarty, M., "A dissociation between object manipulation spatial ability and spatial orientation ability," *Memory & Cognition*, Vol.29, No.5, Jul. 2001, pp.745−756. <DOI: 10.3758/BF03200477>

[115] Hunt, E., Pellegrino, J.W., Frick, R.W., Farr, S.A., and Alderton, D., "The ability to reason about movement in the visual field," *Intelligence*, Vol.12, No.1, Jan. 1988, pp.77−100. <DOI: 10.1016/0160-2896(88)90024-4>

[116] D'Oliveira, T.C., "Dynamic spatial ability: an exploratory analysis and a confirmatory study," *The*

International Journal of Aviation Psychology, Vol.14, No.1, Feb. 2004, pp.19−38.
<DOI: 10.1207/s15327108ijap1401_2>

[117] Pan, D., Zhang, Y., Li, Z., and Tian, Z., "Association of individual characteristics with teleoperation performance," *Aerospace Medicine and Human Performance*, Vol.87, No.9, Sep. 2016, pp.772−780. <DOI: 10.3357/AMHP.4557.2016>

[118] Ito, S., Sakano, Y., Fujino, K., and Ando, H., "Remote controlled construction equipment by using high-resolution stereoscopic 3D images," *Journal of Japan Society of Civil Engineers, Ser. F3 (Civil Engineering Informatics)*, Vol.73, No.1, Jan. 2017, pp.15−24. <DOI: 10.2208/jscejcei.73.15>

[119] Menchaca-Brandan, M.A., Liu, A.M., Oman, C.M., and Natapoff, A., "Influence of perspective-taking and mental rotation abilities in space teleoperation," in: *2007 2nd ACM/IEEE International Conference on Human-Robot Interaction*, Arlington, VA, USA, Mar. 2007, pp.271−278. <DOI: 10.1145/1228716.1228753>

[120] DeJong, B.P., Colgate, J.E., and Peshkin, M.A., "Improving teleoperation: reducing mental rotations and translations," in: *IEEE International Conference on Robotics and Automation, 2004. Proceedings*, New Orleans, LA, USA, May 2004, pp.3708−3714. <DOI: 10.1109/ROBOT.2004.1308838>

[121] Long, L.O., Gomer, J.A., Moore, K.S., and Pagano, C.C., "Investigating the relationship between visual spatial abilities and robot operation during direct line of sight and teleoperation," in: *Proceedings of the Human Factors and Ergonomics Society Annual Meeting*, Vol.53, No.18, Oct. 2009, pp.1437−1441. <DOI: 10.1518/107118109X12524443347797>

[122] Long, L.O., Gomer, J.A., Wong, J.T., and Pagano, C.C., "Visual spatial abilities in uninhabited ground vehicle task performance during teleoperation and direct line of sight," *Presence*, Vol.20, No.5, Oct. 2011, pp.466−479. <DOI: 10.1162/PRES_a_00066>

[123] Pan, D., Zhang, Y., Li, Z., and Tian, Z., "Effects of cognitive characteristics and information format on teleoperation performance: a cognitive fit perspective," *International Journal of Industrial Ergonomics*, Vol.84, Jul. 2021, 103157. <DOI: 10.1016/j.ergon.2021.103157>

[124] Vessey, I., "Cognitive fit: a theory-based analysis of the graphs versus tables literature," *Decision Science*, Vol.22, No.2, Mar. 1991, pp.219−240. <DOI: 10.1111/j.1540-5915.1991.tb00344.x>

[125] Nakagomi, J., Hikizu, M., Kamiya, Y., and Seki, H., "Improvement of the operation performance of the remote controlled robot (in Japanese)," in: *Proceedings of The Japan Society for Precision Engineering Semestrial Meeting*, Sep. 2011, pp.401−402.

[126] Salthouse, T.A., "Adult age differences in integrative spatial ability," *Psychology and Aging*, Vol.2, No.3, Oct. 1987, pp.254−260. <DOI: 10.1037/0882-7974.2.3.254>

[127] Newcombe, N., Bandura, M.M., and Taylor, D.G., "Sex differences in spatial ability and spatial activities," *Sex Roles*, Vol.9, Mar. 1983, pp.377−386. <DOI: 10.1007/BF00289672>

[128] Lawton, C.A., "Gender differences in way-finding strategies: Relationship to spatial ability and spatial anxiety," *Sex Roles*, Vol.30, Jun. 1994, pp.765−779.

[129] Ohnhaus, E.E., and Adler, R., "Methodological problems in the measurement of pain: a comparison between the verbal rating scale and the visual analogue scale," *Pain*, Vol.1, No.4, Dec. 1975, pp.379−384. <DOI: 10.1016/0304-3959(75)90075-5>

[130] Carlsson, A.M., "Assessment of the chronic pain. I. Aspects of the reliability and validity of the visual analogue scale," *Pain*, Vol.16, No.1, May 1983, pp.87−101. <DOI: 10.1016/0304-3959(83)90088-X>

[131] Price, D.D., McGrath, P.A., Rafii, A., and Buckingham, B., "The validation of visual analogue scales as ratio scale measures for chronic and experimental pain," *Pain*, Vol.17, No.1, Sep. 1983, pp.45−56. <DOI: 10.1016/0304-3959(83)90126-4>

[132] Karwowski, W., "The human world of fuzziness, human entropy and general fuzzy systems theory," *Journal of Japan Society for Fuzzy Theory and Systems*, Vol.4, No.5, Oct. 1992, pp.825−841.

<DOI: 10.3156/jfuzzy.4.5_825>

[133] Komori, M., Terakawa, T., and Yasuda, I., "Experimental investigation of operability in six-DOF gesture-based operation using a lower limb and comparison with that in an upper limb," *IEEE Access*, Vol.8, Jun. 2020, pp.118262−118272. <DOI: 10.1109/ACCESS.2020.3002954>

[134] Zadeh, L.A., "Fuzzy sets," *Information and Control*, Vol.8, No.3, Jun. 1965, pp.338−353. <DOI: 10.1142/9789814261302_0021>

[135] Dubois, D., and Prade, H., "Fuzzy sets, probability and measurement," *European Journal of Operational Research*, Vol.40, No.2, May 1989, pp.135−154. <DOI: 10.1016/0377-2217(89)90326-3>

[136] Smithson, M., "Applications of fuzzy set concepts to behavioral sciences," *Mathematical Social Sciences*, Vol.2, No.3, Apr. 1982, pp.257−274.

[137] Takagi, T., and Sugeno, M., "Fuzzy identification of systems and its applications to modeling and control," *IEEE Transactions on Systems, Man, and Cybernetics*, SMC-15, No.1, Jan.−Feb. 1985, pp.116−132. <DOI: 10.1109/TSMC.1985.6313399>

[138] Uehara, K., and Hirota, K., "Fuzzy inference: basic methods and their extensions (part 1) (in Japanese)," *Journal of Japan Society for Fuzzy Theory and Intelligent Informatics*, Vol.28, No.4, Aug. 2016, pp.107−112. <DOI: 10.3156/jsoft.28.4_107>

[139] Matsuda, D., Uemura, K., Sakata, N., and Nishida, S., "'Toe input' using wearable projector and depth camera (<Special issue> Real World Imaging) (in Japanese)," *Transactions of the Virtual Reality Society of Japan*, Vol.17, No.3, Sep. 2012, pp.161−169. <DOI: 10.18974/tvrsj.17.3_161>

[140] Fukahori, K., Sakamoto, D., and Igarashi, T., "Exploring subtle foot plantar-based gestures using sock-style pressure sensors (in Japanese)," *Computer Software*, Vol.33, No.2, Apr. 2016, pp.116−124. <DOI: 10.11309/jssst.33.2_116>

[141] Yamamoto, T., Tsukamoto, M., and Yoshihisa, T., "Foot-Step input method for operating information devices while jogging," in: *2008 International Symposium on Application and Internet*, Turku, Finland, Jul. 2008, pp.173−176. <DOI: 10.1109/SAINT.2008.97>

[142] Alexander, J., Han, T., Judd, W., Irani, P., and Subramanian, S., "Putting your best foot forward: investigating real-world mapping for footed-based gestures," in: *CHI 2012*, Austin, Texas, USA, May 2012, pp.1229−1238. <DOI: 10.1145/2207676.2208575>

[143] Saunders, W., and Vogel, D., "Tap-kick-click: foot interaction for a standing desk," in: *DIS' 2016 Proceedings of the 2016 ACM Conference on Designing Interactive Systems*, Brisbane, Australia, Jun. 2016, pp.323−333. <DOI: 10.1145/2901790.2901815>

[144] Scott, J., Dearman, D., Yatani, K., Truong, K.N., "Sensing foot gestures from the pocket," in: *UIST '10 Proceedings of the 23nd Annual ACM Symposium on User Interface Software and Technology*, New York City, NY, USA, Oct. 2010, pp.199−208. <DOI: 10.1145/1866029.1866063>

[145] Komori, M., and Miyauchi, H., "Position operation method by leg motion and characteristics of leg motion during operation (in Japanese)," *Journal of Japan Society for Design Engineering*, Vol.53, No.7, Jul. 2018, pp.511−526. <DOI: 10.14953/jjsde.2017.2773>

[146] Kume, Y., and Inoue, A., "Feasibility of feet-operated pointing device (in Japanese)," *The Journal of The Institute of Image Information and Television Engineers*, Vol.54, No.6, Jun. 2000, pp.871−874. <DOI: 10.3169/itej.54.871>

[147] Kamakura, N., Ohmura, M., Ishii, H., Mitsuboshi, F., and Miura, Y., "Positional patterns for prehension in normal hands (in Japanese)," *The Japanese Journal of Rehabilitation Medicine*, Vol.15, No.2, Jun. 1978, pp.65−82. <DOI: 10.2490/jjrm1963.15.65>

[148] Yasuda, N., Murata, S., and Murata, J., "Relationship between hand function and finger muscle strength, sensation and reaction time in frail elderly women (in Japanese)," *Rigakuryoho Kagaku*, Vol.25, No.3, Jul. 2010, pp.469−472. <DOI: 10.1589/rika.25.469>

[149] Ito, H., "Tsukamite no dousakinoukaiseki: junnougata hand no approach nitsuite, [The functional analysis of grasping hands: about the adaptable hand approach] (in Japanese)," *Biomechanisms*, Vol.3, Nov. 1975, pp.145−154. <DOI: 10.3951/biomechanisms.3.145>

[150] Komori, M., Kobayashi, K., and Tashiro, T., "Method of position command generation by index finger motion to mitigate influence of unintentional finger movements during operation," *Precision Engineering*, Vol.53, Jul. 2018, pp.96−106. <DOI: 10.1016/J.PRECISIONENG.2018.03.003>

[151] Kabe, N., Kurosawa, K., Nishida, Y., Kishida, A., Kobayashi, S., Tanaka, Y., Makizako, H., Masuda, Y., and Watanabe, M., "The study of relationship between toe and dynamic postural control (in Japanese)," *Rigakuryoho Kagaku*, Vol.17, No.3, Aug. 2002, pp.199−204. <DOI: 10.1589/rika.17.199>

[152] Handa, S., Horiuchi, K., and Aoki, K., "A study on the measurement of toes grasping strength and effect of standing postural control," *The Japanese Journal of Ergonomics*, Vol.40, No.3, Jun. 2004, pp.139−147. <DOI: 10.5100/jje.40.139>

[153] Joseph, J., "Range of movement of the great toe in men," *The Journal of Bone and Joint Surgery. British volume*, Vol.36-B, No.3, Aug. 1954, pp.450−457. <DOI: 10.1302/0301-620X.36B3.450>

[154] Allen, R.H., and Gross, M.T., "Toe flexors strength and passive extension range of motion of the first metatarsophalangeal joint in individuals with plantar fasciitis," *Journal of Orthopaedic & Sports Physical Therapy*, Vol.33, No.8, Aug. 2003, pp.468−478. <DOI: 10.2519/jospt.2003.33.8.468>

[155] Ahn, T.K., Kitaoka, H.B., Luo, Z.P., and An, K.N., "Kinematics and contact characteristics of the first metatarsophalangeal joint," *Foot & Ankle International*, Vol.18, No.3, Mar. 1997, pp.170−174. <DOI: 10.1177/107110079701800310>

[156] Boschert, J., Hink, R.F., and Deecke, L., "Finger movement versus toe movement-related potentials: further evidence for supplementary motor area (SMA) participation prior to voluntary action," *Experimental Brain Research*, Vol.52, No.1, Sep. 1983, pp.73−80. <DOI: 10.1007/BF00237151>

[157] Pfurtscheller, G., Flotzinger, D., and Neuper, C., "Differentiation between finger, toe and tongue movement in man based on 40 Hz EEG," *Electroencephalography and Clinical Neurophysiology*, Vol.90, No.6, Jun. 1994, pp.456−460. <DOI: 10.1016/0013-4694(94)90137-6>

[158] Kai, Y., Murata, S., and Tanaka, S., "Comparison of foot-gripping strength and quadriceps femoris muscle strength of the dominant foot and non-dominant foot (in Japanese)," *Rigakuryoho Kagaku*, Vol.22, No.3, Aug. 2007, pp.365−368. <DOI: 10.1589/rika.22.365>

[159] Fukuda, I., and Kobayashi, R., "The effect of the toes-grip training in healthy young adults (in Japanese)," *Physical Therapy Japan*, Vol.35, No.5, Aug. 2008, pp.261−266. <DOI: 10.15063/rigaku.KJ00005028753>

[160] Soma, M., Igarasi, T., Kudou, W., Nakae, H., and Abiko, T., "Influence of foot-gripping strength training to Functional Reach Test and maximal step length, walking ability in healthy adults (in Japanese)," *Japanese Journal of Health Promotion and Physical Therapy*, Vol.2, No.2, Jan. 2012, pp.59−63. <DOI: 10.9759/hppt.2.59>

[161] Sun, D., Fekete, G., Mei, Q., and Gu, Y., "The effect of walking speed on the foot inter-segment kinematics, ground reaction forces and lower limb joint moments," *PeerJ*, Vol.6, No.4, Aug. 2018, e5517. <DOI: 10.7717/peerj.5517>

[162] Tanaka, N., Ueda, T., Nakao, M., Sato, T., Minato, K., Yoshida, M., and Kouketsu, K., "Evaluation of kinematic characteristics of the foot thumb for the development of a new input device (in Japanese)," *Transactions of Japanese Society for Medical Biological Engineering*, Vol.43, No.4, 2005, pp.790−794. <DOI: 10.11239/jsmbe.43.790>

[163] Arakawa, H., Ishii, N., and Okuyama, S., "Soku kansetsu sokushi no kin [Foot's joints and toes' muscles], Puro ga oshieru kinnikunoshikumi hataraki perfect jiten: all color [The perfect encyclopedia of mechanism and work of muscle taught by professional: all color] (in Japanese)," *Natsume*, 1st ed., 2012,

pp.166−176.

[164]Kapandji, I.A., "Sokubu [foot part], in Physiologie articulaire, schemas commentes de mecanique humaine: anatomie fonctionnelle II [Joint physiology, commented diagrams of human mechanics: functional anatomy II] (in Japanese)," *Ishiyaku Publishers*, *Inc.*, 6th ed., 2010, pp.208−228.

[165]Ridge, S.T., Myer, J.W., Olsen, M.T., Jurgensmeier, K., and Johnson, A.W., "Reliability of doming and toe flexion testing to quantify foot muscle strength," *Journal of Foot and Ankle Research*, Vol.10, No.55, Dec. 2017. <DOI: 10.1186/s13047-017-0237-y >

[166]Murata, S., Kai, Y., Tanaka, S., and Yamasaki, S., "Development of a strain gauge based foot-gripping force meter (in Japanese)," *Rigakuryoho Kagaku*, Vol.21, No.4, 2006, pp.363−367.
<DOI: 10.1589/rika.21.363>

[167]Mita, T., Yamashita, K., Koyama, H., and Kawasumi, M., "Evaluation of walking characteristics obtained by the measurement device of MP joint range of motion (in Japanese)," *LIFE2016*, 2016, pp.663−666.

[168]Fujii, N., and Moriwaki, T., "A study on motion measurement of fingers based on image analysis (in Japanese)," *Japanese Journal of Ergonomics*, Vol.27, No.3, Jun. 1991, pp.151−157.
<DOI: 10.5100/JJE.27.151>

[169]Isaji, S., Takano, M., and Sasaki, K., "Development of a measurement system for manipulative motion of human fingers (in Japanese)," *Journal of the Japan Society for Precision Engineering*, Vol.64, No.8, 1998, pp.1127−1131. <DOI: 10.2493/JJSPE.64.1127>

[170]Terado, T., and Fujiwara, O., "A method for recognizing state of finger flexure and extension," *IEEJ Transactions on Electronics, Information and Systems*, Vol.124, No.12, 2004, pp.2414−2420.
<DOI: 10.1541/ieejeiss.124.2414>

[171]Lee, K.S., and Jung, M.C., "Flexion and extension angles of resting fingers and wrist," *International Journal of Occupational Safety and Ergonomics*, Vol.20, No.1, 2014, pp.91−101.
<DOI: 10.1080/10803548.2014.11077038>

[172]Yonemoto, K., Ishigami, S., and Kondo, T., "Kansetsu kadouikihyouji narabini sokuteihou [Joint movement range indication and measurement method] (in Japanese)," *The Japanese Journal of Rehabilitation Medicine*, Vol.32, No.4, Apr. 1995, pp.207−217. <DOI: 10.2490/jjrm1963.32.207>

List of Publications

Chapter 2 consists of:

Yao, Q., Terakawa, T., Morita, Y., and Komori, M., "Mobile parallel manipulator consisting of two nonholonomic carts and their path planning," *Journal of Advanced Mechanical Design, Systems, and Manufacturing*, accepted.

Chapter 3 consists of:

Yao, Q., Terakawa, T., Komori, M., Fujita, H., and Yasuda, I., "Effect of viewpoint change on robot hand operation by gesture- and button-based methods," *Journal of Robotics and Mechatronics*, Vol.34, No.6, Dec. 2022, pp.1411−1423. <DOI: 10.20965/jrm.2022.p1411>

Chapter 4 consists of:

Yao, Q., Komori, M., Terakawa, T., Higashide, R., and Watanabe, T., "Experimental evaluation of the flexion and extension movement characteristics of toes in a position operation task and a comparison with fingers," *Precision Engineering*, Vol.64, Jul. 2022, pp.288−299.
<DOI: 10.1016/j.precisioneng.2020.04.006>